# 12. SITE 769[1]

Shipboard Scientific Party[2]

## HOLE 769A

**Date occupied:** 14 December 1988

**Date departed:** 15 December 1988

**Time on hole:** 16 hr, 15 min

**Position:** 08°47.14′N, 121°13.16′E

**Bottom felt (rig floor; m, drill-pipe measurement):** 3656.1

**Distance between rig floor and sea level, m):** 11.30

**Water depth (drill-pipe measurement from sea level, m):** 3644.8

**Total depth (rig floor; m):** 3721.50

**Penetration (m):** 65.40

**Number of cores (including cores with no recovery):** 7

**Total length of cored section (m):** 65.40

**Total core recovered (m):** 68.48

**Core recovery (%):** 105.1

**Oldest sediment cored:**
Depth (mbsf): 65.40
Nature: nannofossil marl
Age: Pleistocene
Measured velocity (km/s): not available (see text)

## HOLE 769B

**Date occupied:** 15 December 1988

**Date departed:** 17 December 1988

**Time on hole:** 1 day, 18 hr, 15 min

**Position:** 08°47.12′N, 121°17.68′E

**Bottom felt (rig floor; m, drill-pipe measurement):** 3654.9

**Distance between rig floor and sea level, m):** 11.30

**Water depth (drill-pipe measurement from sea level, m):** 3643.6

**Total depth (rig floor; m):** 3945.10

**Penetration (m):** 290.20

**Number of cores (including cores with no recovery):** 32

**Total length of cored section (m):** 290.2

**Total core recovered (m):** 281.63

**Core recovery (%):** 97.0

**Oldest sediment cored:**
Depth (mbsf): 278.45
Nature: clay with silty layers
Age: late early Miocene
Measured velocity (km/s): 1.58

**Hard rock:**
Depth (mbsf): 290.2
Nature: coarse tuff and lapillistone
Age: late early Miocene
Measured velocity (km/s): 4.46

## HOLE 769C

**Date occupied:** 17 December 1988

**Date departed:** 18 December 1988

**Time on hole:** 1 day, 18 hr, 15 min

**Position:** 08°47.12′N, 121°17.69′E

**Bottom felt (rig floor; m, drill-pipe measurement):** 3654.9

**Distance between rig floor and sea level, m):** 11.30

**Water depth (drill-pipe measurement from sea level, m):** 3643.6

**Total depth (rig floor; m):** 4031.8

**Penetration (m):** 376.90

**Number of cores (including cores with no recovery):** 12

**Total length of cored section (m):** 115.80

**Total core recovered (m):** 51.6

**Core recovery (%):** 44.6

**Oldest sediment cored:**
Depth (mbsf): 278.45
Nature: clay with silty layers
Age: late early Miocene
Measured velocity (km/s): N/A

**Hard rock:**
Depth (mbsf): 376.90
Nature: coarse tuff and lapillistone
Age: late early Miocene
Measured velocity (km/s): 3.17

**Principal results:** The upper 102 m of Site 769 (8°47′N, 121°17′E; water depth, 3644 mbsl; Table 1) are upper Pliocene to Holocene, thin- to thick-bedded nannofossil marl with foraminifers, interpreted as a mixture of pelagic biogenic carbonate sediment and hemipelagic clay. Minor ash layers are present in this section. From 102 to 278 mbsf (lower middle Miocene to upper Pliocene) the section is mainly clay, with minor marls and silts. The lowest part of the section is brown clay, which is very water rich and significantly weaker than the section above. Underlying the clay is a massive, unstratified dark green coarse tuff and lapillistone of andesitic to basaltic composition, with no intermixed or interbedded sedimentary material. Volcanic glass makes up over 70% of the material in the tuff and fine lapillistone. The glass is highly vesicular but rarely pumiceous. The tuff is not dated, but from superposition it is of late early Miocene age or older.

The paleomagnetic stratigraphy is well defined from the surface to the Gilbert Epoch and shows an excellent and remarkably continuous record from the Gilbert through Chron 11. Precise correlations can be made between Holes 769A and 769B by means of the susceptibility record and inclination measurements in the cores of block faults, which is in excellent agreement with the seismic record.

The major increase in carbonate content of the cores in Sites 768 and 769 occurs at about 2.4 Ma and indicates a rapid drop in the

[1] Rangin, C., Silver, E., von Breymann, M. T., et al., 1990. *Proc. ODP, Init. Repts.*, 124: College Station, TX (Ocean Drilling Program).

[2] Shipboard Scientific Party is as given in the list of participants preceding the contents.

**Table 1. Coring summary, Site 769.**

| Core no. | Date (Dec. 1988) | Time (UTC) | Depth (mbsf) | Cored (m) | Recovered (m) | Recovery (%) |
|---|---|---|---|---|---|---|
| 124-769A- | | | | | | |
| 1H | 14 | 1545 | 0–8.4 | 8.4 | 8.37 | 99.6 |
| 2H | 14 | 1705 | 8.4–17.9 | 9.5 | 10.09 | 106.2 |
| 3H | 14 | 1750 | 17.9–27.4 | 9.5 | 9.98 | 105.0 |
| 4H | 14 | 1840 | 27.4–36.9 | 9.5 | 9.67 | 102.0 |
| 5H | 14 | 1925 | 36.9–46.4 | 9.5 | 10.24 | 107.8 |
| 6H | 14 | 2015 | 46.4–55.9 | 9.5 | 10.04 | 105.7 |
| 7H | 14 | 2105 | 55.9–65.4 | 9.5 | 10.09 | 106.2 |
| Coring totals | | | | 65.4 | 68.48 | 104.7 |
| 124-769B- | | | | | | |
| 1H | 15 | 0100 | 0–5.4 | 5.4 | 5.39 | 99.8 |
| 2H | 15 | 0200 | 5.4–14.9 | 9.5 | 9.98 | 105.0 |
| 3H | 15 | 0240 | 14.9–24.4 | 9.5 | 9.81 | 103.0 |
| 4H | 15 | 0325 | 24.4–33.9 | 9.5 | 10.06 | 105.9 |
| 5H | 15 | 0405 | 33.9–43.4 | 9.5 | 9.96 | 105.0 |
| 6H | 15 | 0445 | 43.4–52.9 | 9.5 | 9.97 | 105.0 |
| 7H | 15 | 0540 | 52.9–62.4 | 9.5 | 9.97 | 105.0 |
| 8H | 15 | 0625 | 62.4–71.9 | 9.5 | 9.98 | 105.0 |
| 9H | 15 | 0710 | 71.9–81.4 | 9.5 | 9.95 | 105.0 |
| 10H | 15 | 0800 | 81.4–90.9 | 9.5 | 10.01 | 105.3 |
| 11H | 15 | 0845 | 90.9–100.4 | 9.5 | 9.98 | 105.0 |
| 12H | 15 | 0935 | 100.4–109.9 | 9.5 | 6.61 | 69.6 |
| 13H | 15 | 1155 | 109.9–119.4 | 9.5 | 9.76 | 103.0 |
| 14H | 15 | 1415 | 119.4–128.9 | 9.5 | 10.00 | 105.2 |
| 15H | 15 | 1505 | 128.9–138.4 | 9.5 | 9.91 | 104.0 |
| 16H | 15 | 1601 | 138.4–147.9 | 9.5 | 9.93 | 104.0 |
| 17H | 15 | 1715 | 147.9–157.4 | 9.5 | 9.72 | 102.0 |
| 18H | 15 | 1810 | 157.4–166.9 | 9.5 | 9.98 | 105.0 |
| 19H | 15 | 1915 | 166.9–173.3 | 6.4 | 6.32 | 98.7 |
| 20H | 15 | 2135 | 173.3–182.8 | 9.5 | 10.00 | 105.2 |
| 21H | 15 | 2250 | 182.8–192.3 | 9.5 | 9.25 | 97.3 |
| 22H | 15 | 2350 | 192.3–201.8 | 9.5 | 9.10 | 95.8 |
| 23H | 16 | 0050 | 201.8–211.3 | 9.5 | 9.85 | 103.0 |
| 24H | 16 | 0155 | 211.3–220.8 | 9.5 | 9.39 | 98.8 |
| 25X | 16 | 0255 | 220.8–230.4 | 9.6 | 9.73 | 101.0 |
| 26X | 16 | 0345 | 230.4–240.1 | 9.7 | 8.20 | 84.5 |
| 27X | 16 | 0445 | 240.1–249.7 | 9.6 | 9.20 | 95.8 |
| 28X | 16 | 0515 | 249.7–259.4 | 9.7 | 9.50 | 97.9 |
| 29X | 16 | 0600 | 259.4–269.0 | 9.6 | 6.95 | 72.4 |
| 30X | 16 | 0645 | 269.0–278.7 | 9.7 | 9.88 | 102.0 |
| 31X | 16 | 0810 | 278.7–283.2 | 4.5 | 2.70 | 60.0 |
| 32X | 16 | 1050 | 283.2–290.2 | 7.0 | 0.59 | 8.4 |
| Coring totals | | | | 290.2 | 281.63 | 97.0 |
| 124-769C- | | | | | | |
| 1R | 17 | 0730 | 261.1–270.8 | 9.7 | 1.90 | 19.6 |
| 2R | 17 | 0835 | 270.8–280.5 | 9.7 | 7.67 | 79.1 |
| 3R | 17 | 1015 | 280.5–290.2 | 9.7 | 3.00 | 30.9 |
| 4R | 17 | 1230 | 290.2–299.7 | 9.5 | 5.44 | 57.2 |
| 5R | 17 | 1430 | 299.7–309.3 | 9.6 | 5.79 | 60.3 |
| 6R | 17 | 1615 | 309.3–319.0 | 9.7 | 2.18 | 22.5 |
| 7R | 17 | 1845 | 319.0–328.6 | 9.6 | 1.48 | 15.4 |
| 8R | 17 | 2035 | 328.6–338.2 | 9.6 | 7.37 | 76.8 |
| 9R | 17 | 2230 | 338.2–347.9 | 9.7 | 4.19 | 43.2 |
| 10R | 18 | 0005 | 347.9–357.6 | 9.7 | 2.68 | 27.6 |
| 11R | 18 | 0230 | 357.6–367.2 | 9.6 | 3.49 | 36.3 |
| 12R | 18 | 0435 | 367.2–376.9 | 9.7 | 6.17 | 63.6 |
| Coring totals | | | | 115.8 | 51.36 | 44.4 |

Note: Depths are drill-pipe measurements corrected to sea level.

carbonate-compensation depth (CCD). The rapid increase in carbonate accumulation is coincident with the onset of Northern Hemisphere glaciation at about 2.4 Ma, implying that the influence of expanded Northern Hemisphere ice sheets was felt in the tropics. In addition, increased carbonate preservation in the Sulu Sea beginning at about 2.4 Ma indicates that global lowering of the sea level may have been at least partially responsible for the drop in the CCD. Alternatively, the low carbonate and high CCD in the late Miocene and early Pliocene may be the result of the closing off of the basin because of collisions.

The eruption of the tuffs and lapillistones corresponds closely in time with the opening of the Sulu Sea in the late early Miocene. The pyroclastic rocks at Site 768 are about the same age as the tuffs in Site 769, but their gross compositions are different (rhyolitic vs. andesitic). We are not sure, therefore, of the parentage of the Site 768 pyroclastic rocks. The overlying sections differ in the lack of turbidite input to Site 769.

## BACKGROUND AND OBJECTIVES

### Background

The Cagayan Ridge is 120 km wide, separating the Sulu Sea into two distinct sub-basins (Fig. 1). The ridge is covered locally by reef carbonates (Meander Reefs, Cagayan Islands) and Quaternary volcanic rocks (Cagayan de Sulu Island). Morphologically, its northern flank has a smooth slope that resulted from blanketing by a thick pile of Neogene sediments, whereas its southern flank is steep. Discontinuous southeast-facing normal fault scarps apparently control this morphology. Individual scarps are over 500 m in relief, producing a cumulative relief of 500–1000 m above the deep (4000 m) southeast Sulu Basin (Rangin and Silver, this volume). Sediments infilling this basin abut the base of the first scarps, preventing confident seismic stratigraphic correlations between ridge and basin.

This positive area is characterized by a gravity anomaly of approximately 80 mgal (Watts, 1975), in contrast with the higher anomalies that characterize active island arcs of the region (commonly reaching values in excess of 200 mgal), including the Sulu Ridge (125 mgal). The Cagayan anomaly is comparable in intensity to those found in remnant arcs, such as the Parece–Vela Ridge (60–90 mgal), and slightly greater than that of the Reed Bank–North Palawan epicontinental platform (40–50 mgal).

The Cagayan Ridge basement is considered to be volcanic in origin (Hamilton, 1979; Holloway, 1981), and an early to early middle Miocene age was proposed for the cessation of volcanism (Holloway, 1981; Kudrass et al., 1985). The assumed early to middle Miocene age was subsequently supported by a dredged andesite in the central part of the ridge (Kudrass et al., 1985), dated 14.7 Ma (by K/Ar). Andesites, basalts, and tuffs were recently dredged from the southeast flank of the ridge (Kudrass et al., this volume) supporting the volcanic origin of the ridge.

Extension of this volcanic ridge onshore in Sabah is possible but not obvious (see Rangin and Silver, this volume). Northeast-

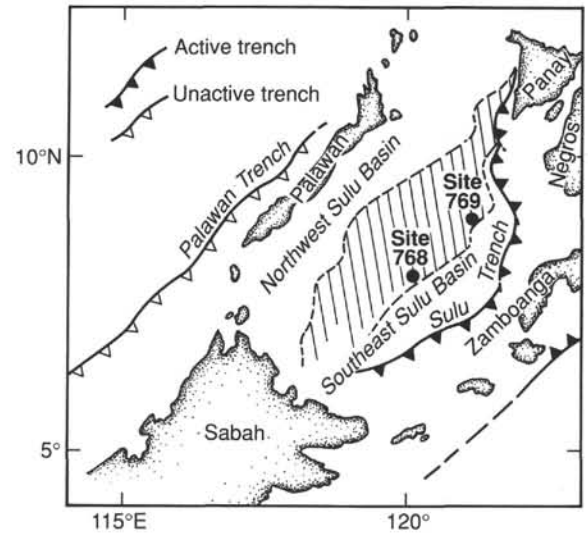


Figure 1. Regional setting of the Sulu Sea–Cagayan Ridge region, showing the location of Sites 768 and 769.

ward correlations with the volcanic sequences known in the Philippine Mobile Belt are also very difficult, because the volcanic ridge pinches out approaching the Negros Trench and the Panay collision zone. Consequently, the Cagayan Ridge appears as a volcanic edifice, not clearly connected with other island-arc sequences present around the Sulu Basin. Understanding the paleobathymetry of the sediments deposited on that ridge can help to decipher the rifting and post-rifting history of the Sulu Basin. The Cagayan Ridge was interpreted (Hamilton, 1979; Holloway, 1981; Karig, 1983) as related to the opening of the Sulu Sea. It can be considered as coeval with the opening of this small oceanic basin or as the remnant volcanic arc for the Sulu Ridge.

### Objectives

Drilling on top of one of the tilted fault blocks of the Cagayan Ridge was designed to answer several questions. One was the Neogene evolution of the restricted paleoenvironment of the Sulu Sea in a position that has been protected from terrigenous turbidite input. The Neogene stratigraphy was expected to record the fluctuation of the CCD recorded on the ridge. We hoped (1) to use the magnetostratigraphic record for precise dating of sedimentation rates and/or high biogenic productivity periods; (2) to determine if the ridge was tectonically stable enough to record sea-level stand changes through the Neogene; and (3) to investigate the possibility that shallow-water carbonates, dredged at depths in excess of 3000 m along the ridge (Kudrass et al., this volume), are the result of subsidence caused by intra-arc rifting.

A major objective of Site 769 was to study Pleistocene glacial/interglacial changes recorded by fluctuations in the nature of Sulu Sea Deep Water. Because of its shallow-silled configuration, the Sulu Sea is currently dysaerobic and isothermal below the thermocline (Exon et al., 1985; Frische and Quadfasel, this volume). Neogene glacial/interglacial sea-level fluctuations would have periodically enhanced the isolation of the basin from the surrounding basins, and may have significantly changed its deep-water properties.

A second objective, which will be pursued in shore-based studies, was to add further documentation on the Pleistocene paleoceanographic and paleoclimatic variability in this region. A previous study of piston cores in the Sulu Sea found that planktonic foraminifers and their stable isotopic compositions have preserved a record of significant late Pleistocene/Holocene oceanographic and climatic changes (Linsley et al., 1985). Oceanographic conditions in the Sulu Sea and surrounding basins are strongly influenced at the present by the quasipermanent Indonesian low-pressure system. This low-pressure system is important because of its effect on western Pacific climate as well as its role in the Southern Oscillation (SO). The large increase in land area that resulted from the emergence of the shallow-shelf areas in the Malay-Indonesian region during glacial low stands of sea level has been proposed as a driving force in causing Pleistocene variability in the Indonesian low-pressure system (Quinn, 1974; Bowler et al., 1976; Webster and Streten, 1978). A sedimentary record showing a continuous and high accumulation rate would allow detailed studies of Neogene climatic and oceanographic variability in this climatically important area.

The third major objective was to date the cessation of volcanism on the ridge precisely. We planned to investigate if the cessation was related to the collision of the ridge with the Palawan Block, or if it was the consequence of back-arc rifting of the Sulu Sea and related isolation of the Cagayan Ridge from the Sulu Arc. We also hoped to determine if the thick pyroclastic rocks, drilled in the Sulu Sea at Site 768, were related to this volcanism, and if the Cagayan Ridge was active during the eruption of these pyroclastic rocks.

The fourth objective was to determine the petrology, chemistry, and radioisotope ratios of the flows expected at the base of the hole. The location of the site at the ridge/basin boundary indicates a transition with Sulu Sea basement.

### Site Selection

Site 769 is located in the eastern part of the ridge and along its southeast flank. It was chosen because of its position as an isolated high, protected from the terrigenous influx coming from the top of the ridge. A small SeaBeam map of the site area indicates that the site is located southeast of a high, trending northeast at 45°, that could be interpreted as a submarine volcano blanketed by sediments. Double advanced hydraulic piston (APC) coring in the uppermost part of the section was planned followed by extended core barrel (XCB) and rotary core barrel (RCB) coring.

## OPERATIONS

Site 769 is located about 47 nmi north of Site 768, on the Cagayan Ridge. Nine hours of surveying were required before a positioning beacon was launched at 0700 (UTC), 14 December 1988.

### Hole 769A

The "mud-line" core established water depth at 3644.8 mbsl, and seven APC cores were then taken through the requested interval of double APC coverage (Table 1). Cores 124-769A-2H to -7H were oriented with the magnetic multishot. At total depth, a heat flow measurement with the water sampling/temperature/pressure (WSTP) probe was performed with excellent results.

The bit was then pulled above the seafloor for the deeper APC/XCB penetration.

### Hole 769B

Oriented coring began with the seafloor core, and continuous APC coring reached 221 mbsf before full-stroke penetration was lost. Successful temperature probe runs were made at 65 and 119 mbsf.

Coring with the XCB then proceeded through clayey sediment to 279 mbsf, where unexpectedly hard drilling was encountered. Two short cores, totaling 11.5 m, were taken in siliceous volcanic sediments before coring ended. The material was much too hard for the XCB coring system. A round trip was made for the RCB coring system.

### Hole 769C

Hole 769C was drilled, without coring, to 261 mbsf, where continuous RCB coring began. Coring then continued to a total depth of 376.9 mbsf, where the scientific objectives of the site were declared to be fulfilled. The drill string was recovered, and the ship was underway for Zamboanga at 1145 (UTC), 18 December 1988.

## LITHOSTRATIGRAPHY

### Sedimentary Units

The holes drilled at Site 769 penetrated 376.9 m of sedimentary and volcaniclastic strata. The section can be divided into three lithologic units (Table 2 and Fig. 2) on the basis of visual description and smear slide analysis of the recovered cores. Unit I is formed by hemipelagic to pelagic marls deposited above the CCD, Unit II is dominantly hemipelagic clays with only a few calcareous layers, and Unit III consists of coarse volcaniclastic rocks. Figure 3 shows variations in relative abundance vs. depth for several key sediment components that are indicators of varying provenance within the sequence.

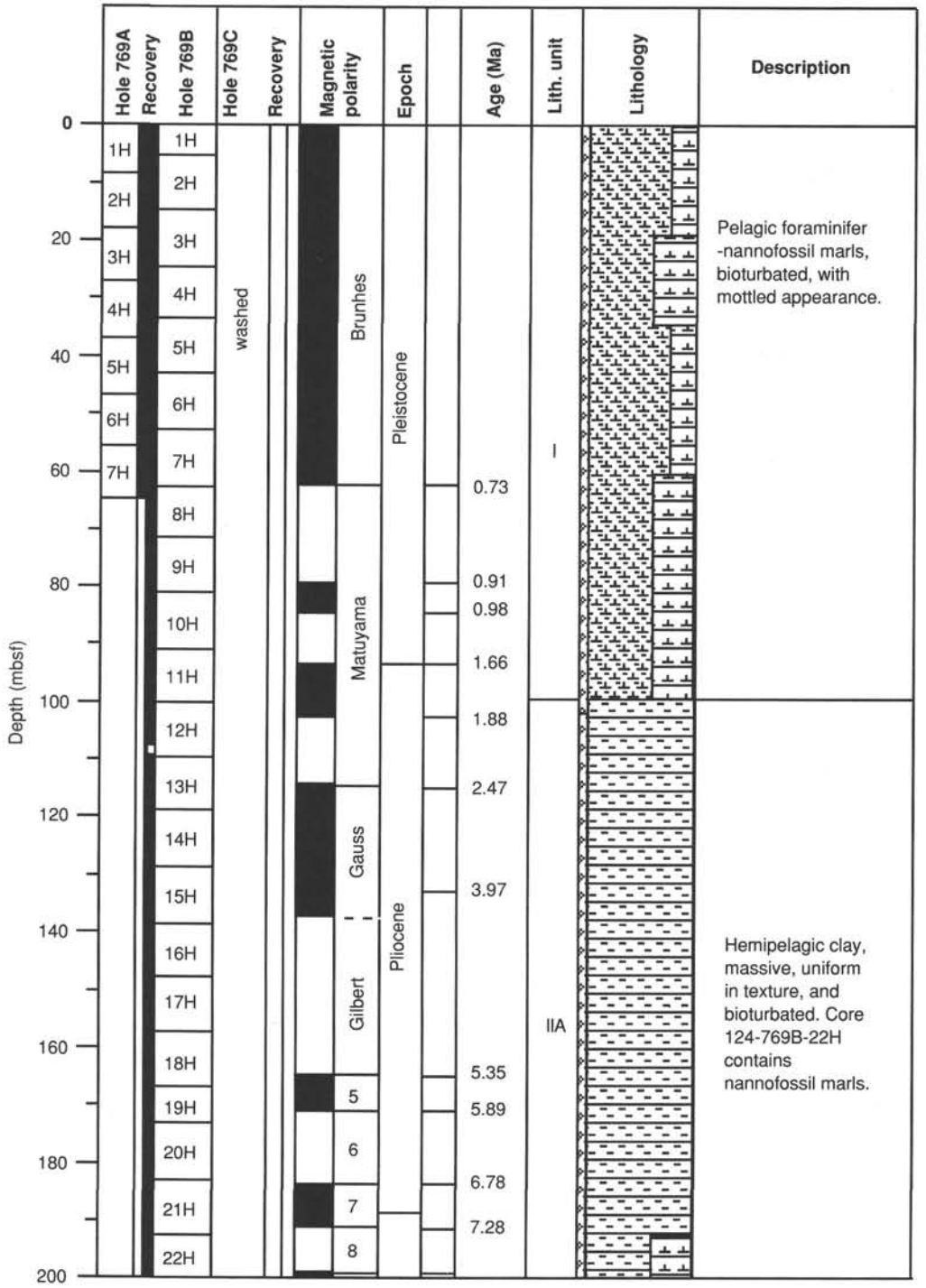


Figure 2. Graphic log of lithologic variations and units at Site 769.

### *Unit I*

Depth: 0–102.15 mbsf
Interval: Cores 124-769A-1H through -7H and Core 124-769B-1H through Section 124-769B-12H-2
Thickness: 102.15 m
Age: late Pliocene to Holocene

The dominant lithology in Unit I consists of thin- to thick-bedded nannofossil marl with foraminifers and foraminiferal nannofossil marl. The marl is interpreted as a mixture of pelagic biogenic carbonate sediment and hemipelagic clay. Minor thin beds of volcanic ash and turbidites of foraminiferal ooze are also present within the unit.

The marl is gray to greenish gray in color and is bioturbated throughout, with faint laminations preserved in places. Bioturbation is expressed by dark gray mottling and by 2–3-mm-thick burrows that are filled by ash. The marl contains clay, abundant nannofossils and planktonic foraminifers, scattered benthic foraminifers, volcanic glass, and varying amounts of siliceous biogenic material (spicules, diatoms, and radiolarians).

In the upper part of the unit (Cores 124-769B-1H to -7H), some thin-to-thick, upward-fining beds of foraminifer ooze are

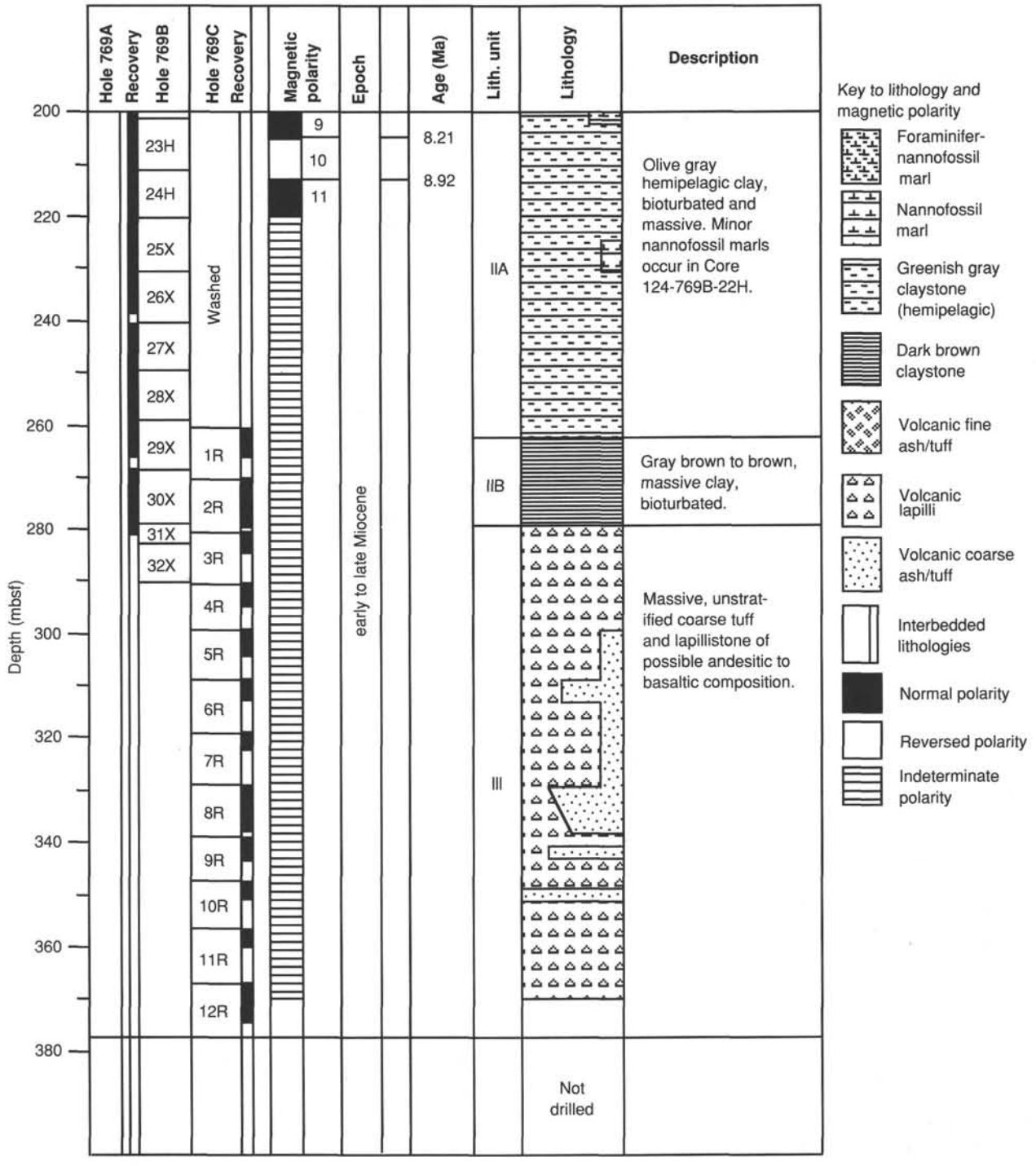


Figure 2 (continued).

**Table 2. Lithologic units, Site 769.**

| Unit | Subunit | Depth (mbsf) | Thickness (m) | Age |
|---|---|---|---|---|
| I | | 0–102.15 | 102.15 | late Pliocene to Holocene |
| II | | 102.15–278.45 | 176.30 | late early Miocene to late Pliocene |
| | IIA | 102.15–262.35 | 160.20 | middle(?) Miocene to late Pliocene |
| | IIB | 262.35–278.45 | 16.10 | late early to middle(?) Miocene |
| III | | 278.45–376.99 | 8.45 | late early Miocene(?) |

present. A bivalve shell lag with echinoid spines appears at some of the basal contacts. The lower-bounding contacts of these layers are sharp. The upper limits are transitional with the marl. These layers are interpreted as turbiditic deposits.

In the lower part of the unit (Cores 124-769B-8H to -12H), very thin, somewhat indurated, dark green layers are present. The layers show a high proportion of clay minerals and are probably of diagenetic origin.

Beginning in Core 124-769B-6H, pale olive gray to greenish brown patches are disseminated throughout the marls. Some of the patches, which are round to subangular in shape, have a

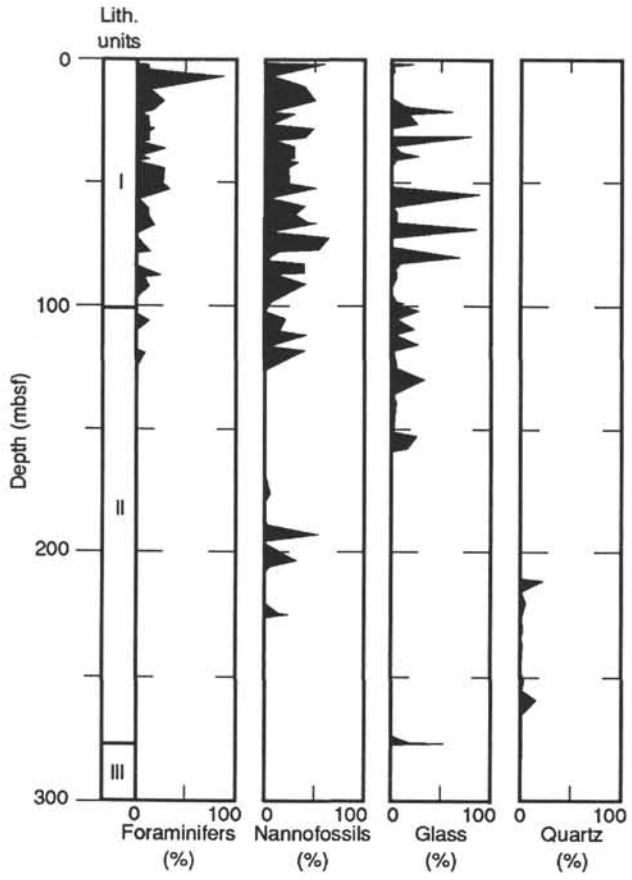


Figure 3. Abundance plot of variation with depth for several sediment components in the sedimentary sequence (Units I and II) in Hole 769B. Data are derived from shipboard smear slide analyses of all rock types present in the section.

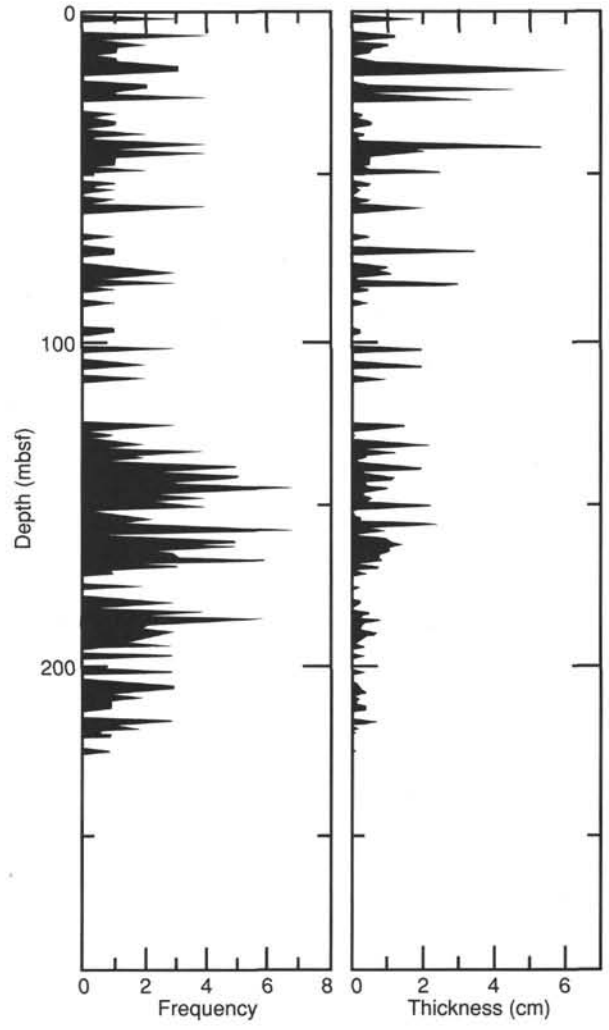


Figure 4. Plot of ash layer frequency and thickness per meter vs. depth in Unit I and II, Hole 769B. Thickness and frequency increase above 225 mbsf and reach a maximum around 150 mbsf in the upper part of Unit II. The frequency of ash layers is fairly constant throughout Unit I, but thickness increases from the Unit I/II boundary to the top of Unit I.

well-defined boundary with the surrounding deposits. Contrasting with the indistinct mottling of the surrounding marls, these patches show lighter 2-mm-thick elongated burrows (*Planolites*?). Others show ill-defined boundaries with an additional dark gray rim. Diatoms, radiolarians, and marine organic matter are found in rather high abundance within these patches. The origin of these features is unclear at present. They may be clasts introduced during slumping of strata, further evidence for which is presented below. However, some of the patches have more diffuse margins, and they could be the result of bioturbation.

Volcanic ash is present throughout the unit as layers, patches, or burrow infillings. The fresher ash layers are grayish brown, light gray, and black, but the altered ones are grayish green. A slight decrease in the frequency of ash layers per meter is observed from 60 mbsf to the bottom of the unit (Fig. 4). Layers of fine to coarse ash range from thin beds to thick laminae. Most layers exhibit sharp bases, normal grading, and gradational tops, and they contain little admixed nonvolcanic material; they are interpreted as airfall deposits. A few thin beds show sharp and in some cases scoured basal contacts and laminated upper portions mixed with foraminifers and nannofossils. These beds represent reworked ash probably deposited by turbidity currents.

Ash layers in the top 25 mbsf (down through Core 124-769B-3H) are dominantly vitric-crystal to crystal-vitric ash (Fig. 5) consisting mainly of glass, plagioclase, hornblende, and minor lithic fragments, opaques, and clay. From 25 to 60 mbsf (Core 124-769B-4H through -7H), crystal-lithic and altered ashes are common with very few crystal-vitric ashes. Crystal-lithic ashes are made up mostly of volcanic lithic fragments and plagioclase with minor hornblende and pyroxene. The altered ashes, which appear as grayish green thin laminae, are composed mainly of clayey materials and minor plagioclase, hornblende, pyroxene, and opaques. Vitric ashes, which are composed mainly of glass and plagioclase with minor hornblende, pyroxene, and biotite, are present between 60 and 85 mbsf (Core 124-769B-8H through Section 124-769B-10H-1). Crystal-lithic and altered ashes also are present in this interval and become dominant toward the base of the unit (102.5 mbsf).

The deposits of Unit I show significant soft-sediment deformation, which affects parts of the section from about 15 mbsf to the bottom of the unit. The deformation is commonly expressed as (1) slightly to steeply inclined lithologic contacts, (2) convolute lamination, and (3) possible water escape structures. Folds that affect up to several meters of section and appear to have gently inclined axial surfaces are present in Sections 124-769B-3H-2 (Fig. 6) and 124-769B-10H-5 (see core photographs at the back of the book). These features imply that episodic small-scale slumping has affected significant portions of Unit I, but much of the section nevertheless remains intact.

The marl of Unit I is interpreted as a mixture of hemipelagic clay and pelagic biogenic sediment, with only a minor proportion of redeposited biogenic sediment originating from shal-

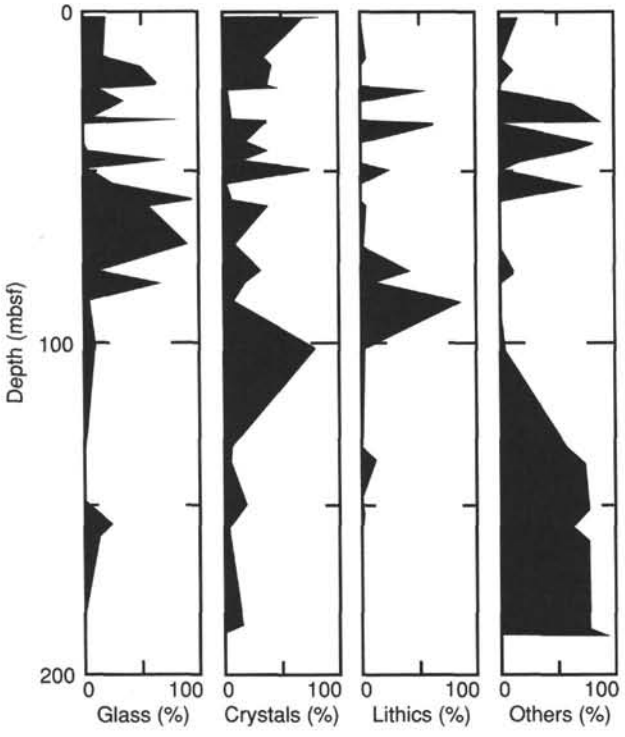


Figure 5. Abundance plot vs. depth for ash layer components in Units I and II, Site 769. From 280 mbsf to the uppermost part of Unit II, the "Others" component (mostly clay minerals and zeolite derived from altered volcanic rocks) is dominant. In the lower part of Unit I, crystal-lithic and vitric-lithic ash are dominant. The upper part of Unit I shows an irregular distribution of the components, except above 15 mbsf where crystal ash dominates.

lower depths. Intermittent small-scale slumping points to deposition on a sloping surface (similar to the present depositional surface). The slumping could have been triggered solely by the instability of water-rich sediment accumulating on a slope, or it could indicate possible synsedimentary tectonic activity.

### *Unit II*

Depth: 102.15–278.45 mbsf
Interval: Sections 124-769B-12H-2 through 124-769B-30X-7
Thickness: 176.30 m
Age: late early Miocene to late Pliocene

Unit II consists primarily of hemipelagic clay. On the basis of a color change from grayish green to brown, we have distinguished two subunits.

### *Subunit IIA*

Depth: 102.15–262.35 mbsf
Interval: Sections 124-769B-12H-2 through 124-769B-29X-2
Thickness: 160.20 m
Age: middle(?) Miocene to late Pliocene

Subunit IIA is composed mainly of clay with a carbonate content typically less than 1%. Minor rock types include marl, calcareous clay, and silty clay. The clay is dark greenish gray to greenish gray in color. At the base of the subunit, it shows a transitional color change toward olive gray and grayish brown (Cores 124-769B-27X to -29X). The clay is present in thick, ill-defined beds with common gray and green mottles throughout caused by bioturbation. It is composed mainly of clay minerals, with small amounts of feldspar, rock fragments, quartz, plant

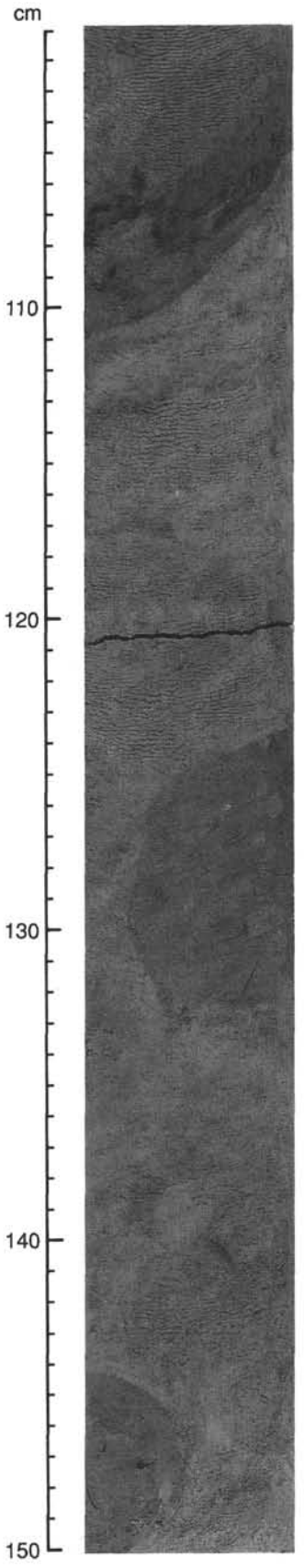


Figure 6. Slump fold in marl beds in Unit I (Section 124-769B-3H-2, 101–150 cm).

debris, hornblende, pyroxene, biotite, and opaques. Dispersed small green-brown patches with a higher amount of nannofossils (*Discoaster*) are also present in the sequence.

In the lower part of the subunit (Cores 124-769B-26X to -29X), dolomite (or rhodochrosite?) is present in small light brownish nodules or is dispersed in the sediment as silt-size crystals. The texture and composition of the olive gray and grayish brown clay does not differ from the greenish gray clay.

Marl is interlayered with the greenish gray clay in the upper part of the succession (Cores 124-769B-12H to -14H) and as thin to thick layers in Cores 124-769B-18H, -22H, and -23H. The marl is greenish gray in color with mottling caused by bioturbation, and the boundaries of the beds are diffuse. It consists of clay with nannofossils, foraminifers, radiolarians, and sponge spicules, and it has carbonate contents that range from 14% to 45% (see "Sediment Inorganic Geochemistry" section, this chapter).

Light greenish gray calcareous clay appears as thin to thick beds in Cores 124-769B-24H and -25X. The clay differs from the marl in its lower carbonate content (1%–7%), which results from a lower abundance of nannofossils. One such bed has a sharp base and transitional top, whereas others have diffuse boundaries.

Thin- to thick-bedded, dark greenish gray silty clay is present in Cores 124-769B-12H to -14H. It is mottled because of bioturbation. The silty clay is composed of clay minerals, variable amounts of glass and feldspar, sponge spicules, radiolarians, and scattered nannofossils.

Dark greenish gray to dusky green, thin to thick laminations and burrow fills are dispersed above Section 124-769B-25X-2. The laminae, where undisturbed by bioturbation, exhibit sharp bases and gradational tops; they consist mainly of greenish clay minerals with minor glass, plagioclase, opaques, hornblende, and pyroxene. Their appearance within the thick beds of hemipelagic clay, the sharp bases and gradational tops, and the absence of contamination by biogenic material indicate that these might be altered fine airfall ash layers. The frequency of altered ash layers has its peak at ~140–160 mbsf (Section 124-769B-16H-2 through Core 124-769B-18H; Fig. 4). Compared with Unit I, the ash layers in Unit II are thinner but more frequent.

The clay in Subunit IIA is interpreted as hemipelagic in origin. The upper part of the subunit is a zone of interbedded clay and marl, representing a transition from the mixed clay and pelagic carbonate sediment of Unit I to the mostly carbonate-free clay of Unit II (Cores 124-769B-12H to -14H). Some of the rare interbedded marl and calcareous clay layers in the remainder of the unit may be turbidites, but most of them are probably pelagic in origin. The portion of Subunit IIA recovered by oriented hydraulic piston cores (Cores 124-769B-12H through -24H) shows bedding surfaces that are fairly undisturbed by coring.

Beginning with Core 124-769B-16H (140 mbsf), the section shows a gradually increasing southwestward dip that reaches 19°–27° in Cores 124-769B-20H to -24H. Paleomagnetic data indicate that this dip results from progressive tilting of the section rather than from slumping (see "Paleomagnetics" section, this chapter). This tilting can be related to syndepositional rotation of small fault-bounded blocks above a bedding-parallel detachment surface that is close to the base of Unit II (see "Seismic Stratigraphy" section, this chapter). Minor downdip (eastward) movement on this gently sloping surface may have been a response to gravitational stresses.

### *Subunit IIB*

Depth: 262.35–278.45 m
Interval: Sections 124-769B-29X-2 through 124-769B-30X-CC
Thickness: 16.10 m
Age: late early to middle(?) Miocene

Subunit IIB consists of grayish brown to brown, massive clay with very rare silty layers. There is no evidence of bedding except for thin laminae in Section 124-769B-30X-3. The clay is composed of clay minerals with <5% silt-size plagioclase, biotite, hornblende, opaques, and quartz. Small (1–2 mm) manganese nodules are common in Core 124-769B-30X. The silty layers consist of quartz, plagioclase, and glass. The clay is interpreted as pelagic or hemipelagic in origin, with slow sedimentation indicated by the scarcity of silt-size grains and the presence of manganese micronodules.

### *Unit III*

Depth: 278.45–376.9 m
Interval: Section 124-769B-29X-2 through Core 124-769C-12R
Thickness: 98.45 m
Age: late early Miocene(?)

The lower 98.45 m of section penetrated at Site 769 is assigned to Unit III. It consists of massive, unstratified dark green coarse tuff and lapillistone of andesitic to basaltic composition, with no intermixed or interbedded sedimentary material. Since no fossils were found in this unit, its age can only be constrained to late early Miocene or older, given the age of the lower part of the overlying Unit II. The apparent contact with the brown clay of Unit II is sharp, but it may be disturbed by drilling.

Lapillistone is the dominant lithology in Unit III, but vertical gradations between lapillistone and coarse tuff are common. The mean grain size of both rock types is commonly close to the 2-mm grain size, which is defined as the boundary between these rock types. Therefore, changes from lapillistone (Fig. 7) to coarse tuff (Fig. 8) in most cases represent rather subtle shifts in grain size. Both reverse and normal grading are present over intervals of several decimeters to several meters. Sorting in the lapillistone and coarse tuff is moderate to poor, with scattered large lapilli to blocks (up to 20 cm diameter) suspended in much finer-grained lapillistone or coarse tuff (Fig. 9). The deposits are entirely grain supported, with no interstitial silt or clay-size clastic matrix. Lamination and stratification are virtually absent, and no sharp grain-size boundaries are found within individual pieces of the core. Abrupt changes in grain size and texture are observed in some cases between adjacent core pieces in this interval of generally poor recovery, but these may be a result of the loss of an intervening section during coring. We found no criteria for defining discrete depositional units (beds) within the entire interval of Unit III.

The major constituents of the tuff and lapillistone are volcanic glass, lesser aphanitic lithic fragments, and very minor free crystals. The glass fragments make up over 70% of the coarse tuff and fine lapillistone and also appear as coarser lapilli in the lower part of the unit. The glass is green to very pale green and moderately to highly vesicular, but it is only very rarely pumiceous. Most glass fragments are aphyric, but some have up to 10% phenocrysts of plagioclase or olivine. The shape of the glass fragments is commonly very irregular, with embayed or scalloped margins that were probably formed during eruptive fragmentation; there is little evidence for breakage, abrasion, or rounding of the clasts. Some of the vesicular clasts have very angular margins formed by broken vesicle walls, but these are less common than the unbroken clasts.

Gray volcanic lithic fragments make up a small proportion of the fine lapilli and ash particles, but form all of the blocks and most of the coarse lapilli in the unit. In the lower part of Unit III, coarse glassy lapilli are also present. The lithic fragments are aphanitic, slightly (Fig. 10) to moderately vesicular (Fig. 11), and commonly porphyritic, with up to 15% phenocrysts. Plagioclase and olivine in varying proportions are the dominant phenocrysts, and glomeroporphyritic aggregates of

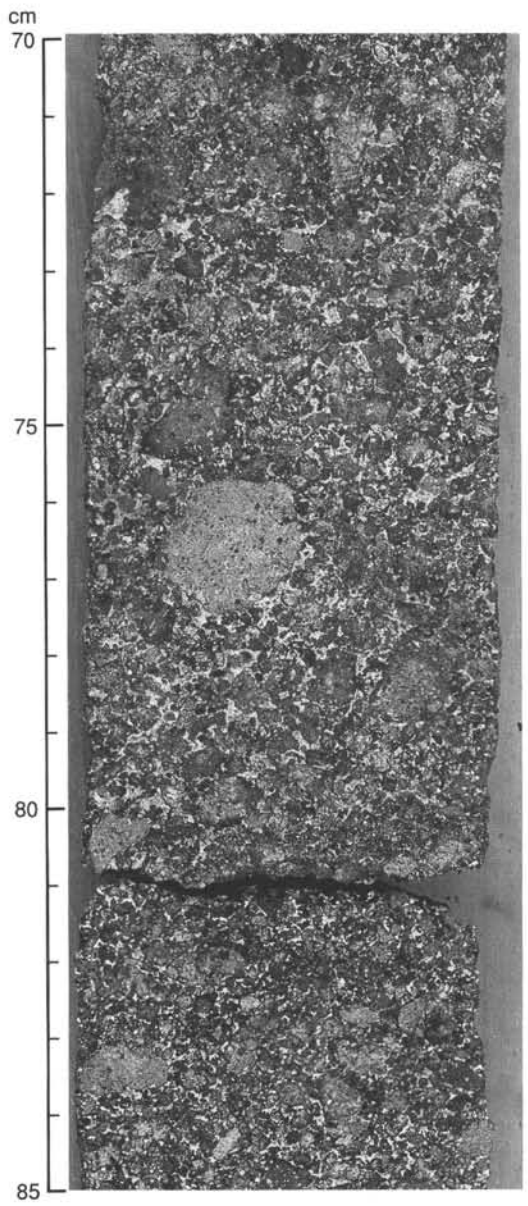


Figure 7. Lapillistone in Unit III (Section 124-769C-8R-6, 70–85 cm). Note the variations in clast size and the white chalcedony cement.

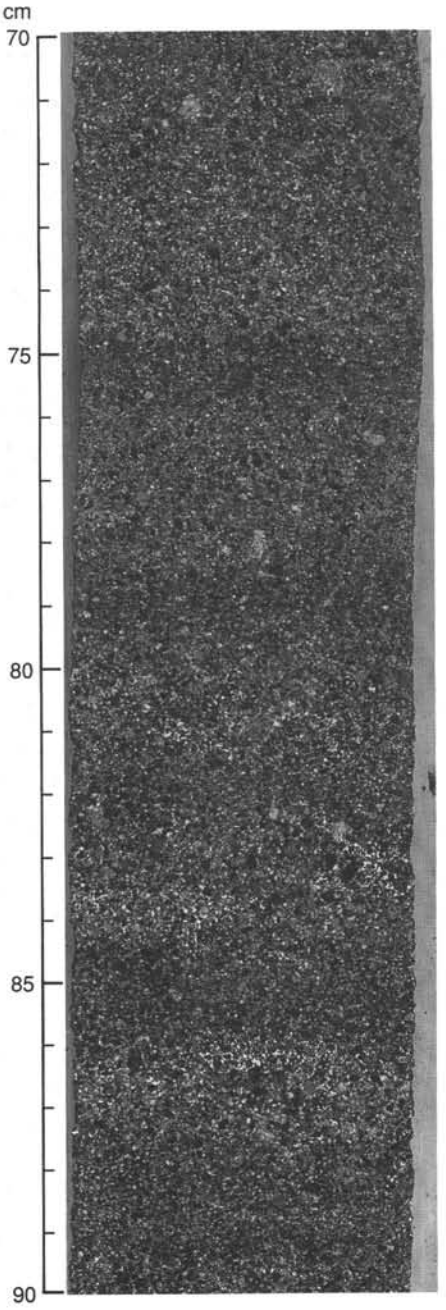


Figure 8. Crudely layered coarse tuff in Unit III (Section 124-769C-5R-1, 70–90 cm).

plagioclase are common. Pyroxene is present in very minor amounts, and hornblende is very rare. These clasts have angular, subangular, or subrounded shapes (Fig. 12).

Some of the lithic coarse lapilli and blocks in the upper part of the unit are rounded with chilled margins and may be volcanic bombs (Fig. 13). In other cases, small dense lithic fragments are completely enclosed in larger vesicular glass fragments and, therefore, must have been incorporated within the glassy magma as accidental fragments during eruption. Very rare lithic clasts have been highly altered to a reddish brown color; this alteration is confined to individual clasts intermixed with similar but unaltered lithic clasts. This implies that the reddish clasts were altered by subaerial weathering before incorporation within the deposit. However, the vast majority of the lithic clasts show only postdepositional diagenetic alteration.

The final primary component of the coarse tuff and lapillistone consists of free crystals of plagioclase, olivine, and rare pyroxene, which make up only a few percent of the deposit.

The following observations indicate that the pyroclastic rocks of Unit III accumulated very rapidly on the flanks of a volcano as the result of a single eruptive/depositional cycle: (1) the clast composition is very uniform throughout the unit; (2) no interbedded or intermixed nonvolcanic sediment is present; (3) no stratification or bedding surfaces have been found within the sequence; and (4) the pyroclast shapes show no evidence of abrasion or rounding, and few show evidence of breakage during transport.

Given the high vesicularity of the dominant glassy ash and lapilli, it is likely that these particles formed by explosive fragmentation of a volatile-rich, vesiculating magma. Fisher and Schmincke (1984, p. 97) note that there are few published descriptions of pyroclastic glass shards of intermediate composition, but those observed are clearly distinct from the bubble-

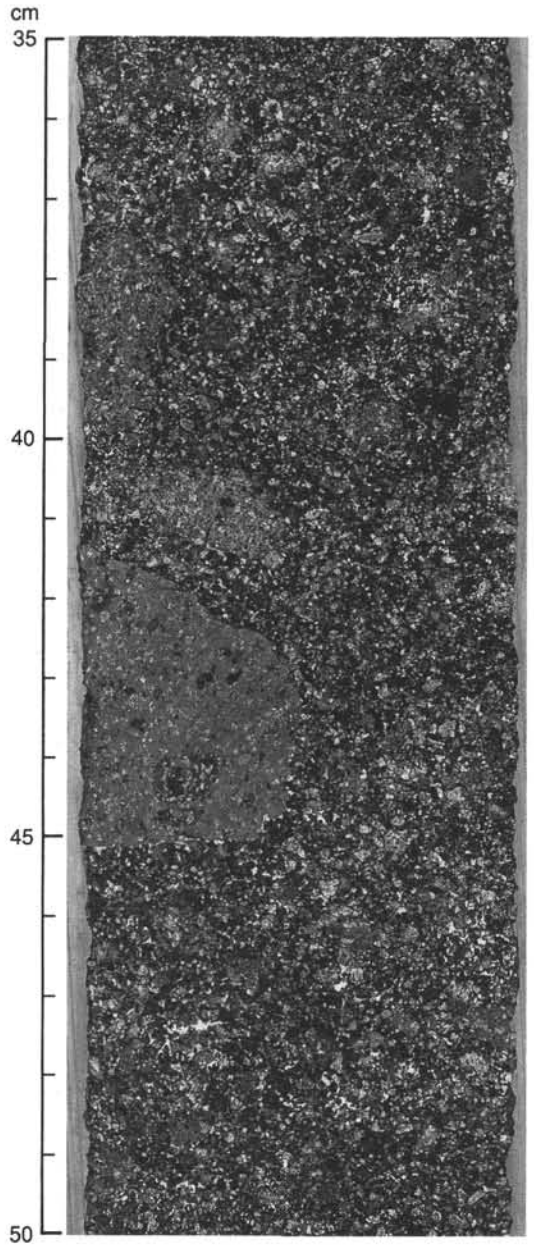


Figure 9. Large lapilli suspended in coarse tuff in Unit III (Section 124-769C-8R-5, 35–50 cm).

wall shards and pumice lumps typical of silicic pyroclastic eruptions. The andesitic shards have irregular lumpy forms with some botryoidal surfaces, and they commonly contain ovoid or spherical vesicles; the glass fragments in Unit III correspond closely to this description.

In submarine eruptions, explosive vesiculation is progressively inhibited with increasing depth because of the increasing water pressure. Fisher (1984) asserted that the maximum depth for such explosive eruptions rarely exceeds 1000 m for silicic and volatile-rich mafic alkalic magmas. Therefore, we propose that the pyroclastic material in Unit III was erupted from a shallow submarine or subaerial vent and not in a deep-marine setting.

The mode and depth of deposition of Unit III remain as significant questions. The observations cited above are most consistent with an origin as a near-vent, fall-out deposit of pyroclastic eruptions, conceivably with syneruptive rolling and slid-

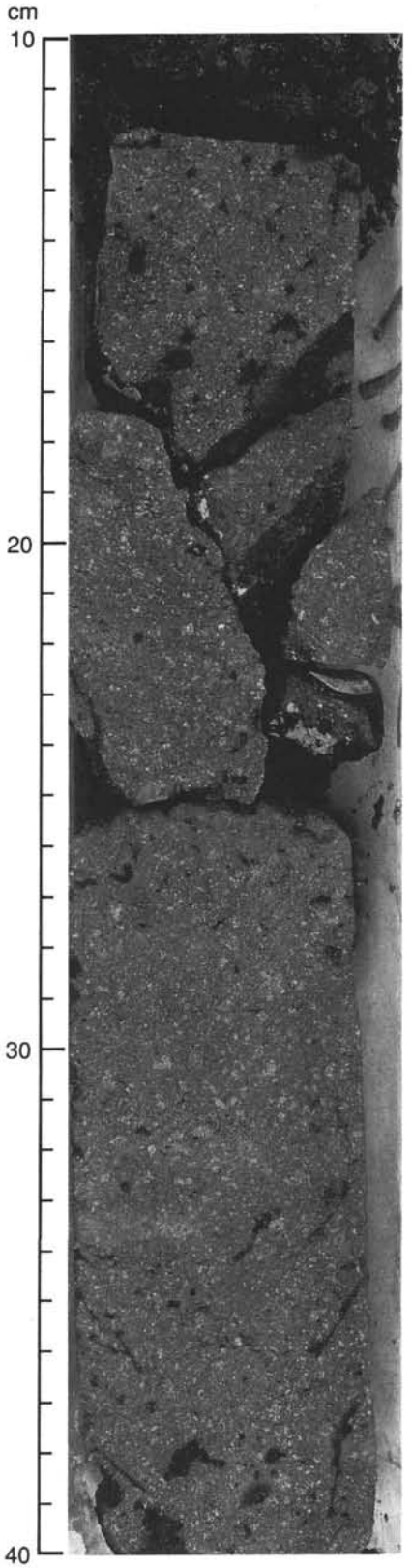


Figure 10. Slightly vesicular lithic block in lapillistone of Unit III (Section 124-769B-31X-CC, 10–40 cm). Block is porphyritic, with plagioclase phenocrysts.

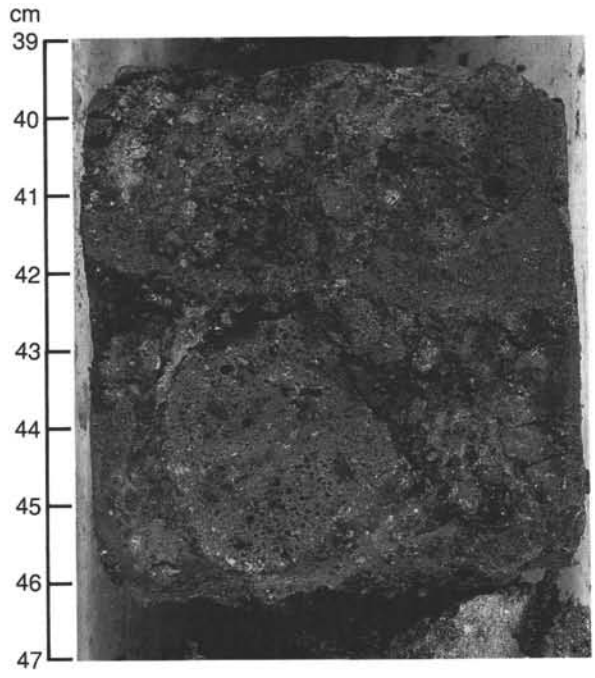


Figure 11. Moderately vesicular lithic fragments in lapillistone of Unit III (Section 124-769B-32X-CC, 39–47 cm).

ing of pyroclasts down the subaerial or submarine flanks of the volcano. Alternatively, the unit could represent a series of very thick, massive pyroclastic flows that swept down the flanks of the volcano during eruptions. If so, the boundaries of these flow units are not preserved in the cores.

Since only rare lithic clasts show any evidence of subaerial weathering, the pyroclastic material probably accumulated in a submarine setting. If the near-vent interpretation is correct, then Unit III accumulated at a depth shallower than 1000 m on the upper flank of a submarine volcano. If, on the other hand, it was deposited by pyroclastic flows, then the site of deposition could have been substantially deeper, and the vent could have been either subaerial or shallow submarine.

The coarse tuff and lapillistone of Unit III are cemented by several generations of void-filling cement with very consistent textural relationships. The earliest cement is a dark green, even clay layer that coats the exterior surface of all grains and lines vesicles within both glassy and lithic fragments. The second cement phase is clear chalcedony with a botryoidal, radial-fibrous habit. It partially fills the intergranular voids that remained after precipitation of the clay cement and also lines vesicles in the smaller clasts. In some of the large vesicular lapilli and bombs, the chalcedony cement is absent in the vesicles or is restricted to isolated botryoidal clusters overlying the green clay cement. The latest cement consists of milky white zeolites that fill the centers of most original intergranular voids. The crystal habit of the zeolite cement varies from radial fibrous to coarse anhedral single crystals, indicating that more than one zeolite mineral is present. The relative proportions of the cements varies through the unit; the layer of early green clay cement is very thin in the upper part, but it becomes much thicker in the lower part of the unit.

## Clay Mineralogy

The mineralogy of the >2-$\mu$m size fraction of 27 samples from Site 769 was investigated by X-ray diffraction (XRD) techniques described in the "Explanatory Notes" section (this volume). The data are reported in Table 3.

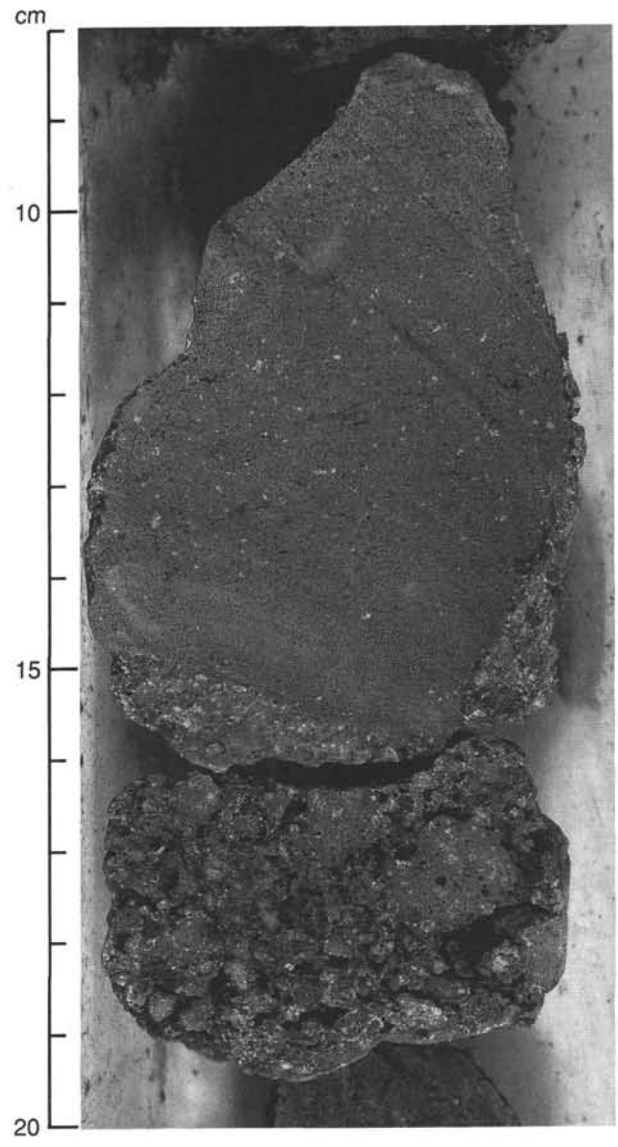


Figure 12. Angular lithic block in lapillistone of Unit III (Section 124-769B-32X-CC, 8–20 cm). Block is slightly vesicular.

### *Smectite*

Smectite is abundant in the cores from Site 769 (Fig. 14). The data are slightly noisy, but there is a tendency for smectite abundance to decrease with increasing depth in Unit I (0–102.15 mbsf). Smectite abundances range from 50% to 60% near the top of the unit, decreasing to below 45% near the bottom.

In Subunit IIA, smectite continues to be variable within a range from 40% to 60%, with the possibility of an increase with depth. In Subunit IIB, however, smectite abundance climbs sharply to >80% at the base.

No measurements were made on Unit III.

### *Illite*

Illite is common throughout Units I and IIA at Site 769 (Fig. 14), averaging around 30% and ranging from 20% to 40%. No trends with depth appear until 230 mbsf, where a steep decline in the abundance of illite begins which continues into Unit IIB. The illite abundance at the base of Unit IIB is below 10%. This

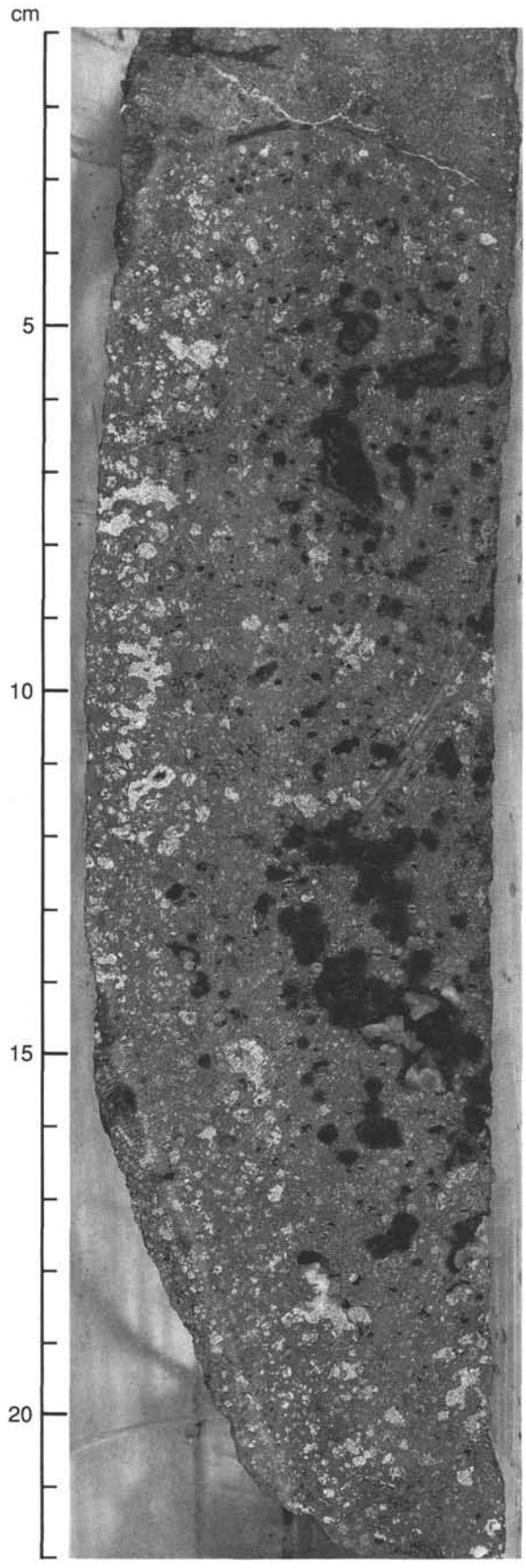


Figure 13. Highly vesicular volcanic block with chilled margin (probably a volcanic bomb) from lapillistone in Unit III (Section 124-769C-4R-2, 1–22 cm).

**Table 3. Clay mineral data, Site 769.**

| Core, section, interval (cm) | Depth (mbsf) | Smectite (wt%) | Illite (wt%) | Kaolinite (wt%) | Chlorite (wt%) | Continentality index |
|---|---|---|---|---|---|---|
| 124-769B- | | | | | | |
| 1H-3, 100–106 | 4 | 50.68 | 27.03 | 0 | 22.29 | 0.30 |
| 2H-1, 50–56 | 5.9 | 58.60 | 15.70 | 12.85 | 12.85 | 0.17 |
| 3H-1, 46–52 | 15.36 | 56.24 | 23.40 | 0 | 20.35 | 0.25 |
| 5H-1, 50–56 | 34.4 | 36.75 | 42.76 | 0 | 20.49 | 0.43 |
| 7H-1, 50–56 | 53.4 | 60.87 | 20.87 | 0 | 18.26 | 0.22 |
| 8H-1, 50–56 | 62.9 | 39.30 | 32.75 | 13.97 | 13.98 | 0.34 |
| 9H-1, 54–60 | 72.44 | 44.39 | 27.96 | 0 | 27.65 | 0.35 |
| 12H-1, 50–56 | 100.9 | 38.14 | 29.66 | 0 | 32.20 | 0.42 |
| 13H-1, 50–56 | 110.4 | 33.08 | 36.76 | 13.31 | 16.85 | 0.42 |
| 14H-1, 120–126 | 120.6 | 50.00 | 21.62 | 11.64 | 16.74 | 0.25 |
| 15H-1, 50–56 | 129.4 | 48.21 | 25.00 | 0 | 26.79 | 0.32 |
| 16H-1, 50–56 | 138.9 | 46.47 | 21.77 | 16.84 | 14.92 | 0.25 |
| 17H-1, 95–101 | 148.85 | 35.80 | 30.15 | 0 | 34.05 | 0.45 |
| 18H-1, 55–61 | 157.95 | 42.28 | 28.37 | 15.64 | 13.71 | 0.30 |
| 19H-1, 50–56 | 167.4 | 41.33 | 34.19 | 0 | 24.48 | 0.38 |
| 20H-1, 80–86 | 174.1 | 52.79 | 24.48 | 0 | 22.73 | 0.28 |
| 21H-2, 100–106 | 185.3 | 49.66 | 33.79 | 16.55 | 0 | 0.23 |
| 22H-1, 50–56 | 192.8 | 59.88 | 23.95 | 16.17 | 0 | 0.15 |
| 24H-1, 54–60 | 211.84 | 50.29 | 35.60 | 17.11 | 0 | 0.23 |
| 25X-2, 50–56 | 222.8 | 62.76 | 26.35 | 0 | 10.89 | 0.20 |
| 26X-1, 50–56 | 230.9 | 43.21 | 39.51 | 8.98 | 8.30 | 0.32 |
| 27X-1, 50–56 | 240.6 | 42.56 | 38.37 | 9.12 | 9.95 | 0.33 |
| 28X-1, 50–56 | 250.2 | 50.28 | 30.89 | 18.83 | 0 | 0.21 |
| 29X-1, 50–56 | 259.9 | 55.19 | 28.22 | 5.93 | 10.66 | 0.23 |
| 30X-2, 64–70 | 271.14 | 85.71 | 8.16 | 0 | 6.13 | 0.07 |
| 124-769C- | | | | | | |
| 1R-1, 116–122 | 262.26 | 66.09 | 19.23 | 7.34 | 7.34 | 0.15 |
| 2R-1, 60–66 | 271.4 | 80.77 | 9.79 | 0 | 9.44 | 0.09 |

rapid decline corresponds exactly to the steep increase in smectite discussed above.

### *Kaolinite*

Kaolinite is close to its detection limit at Site 769 (Fig. 14). Frequent zero values for the kaolinite abundance indicate the difficulty in discriminating between kaolinite and chlorite at these low levels. Kaolinite ranges from 5% to 15% in these samples with only the higher values reported here. Kaolinite does not appear to be a useful indicator of provenance at Site 769, although its generally low abundance demonstrates that the products of intense tropical weathering are not abundant anywhere at this site.

### *Chlorite*

Chlorite is somewhat more abundant than kaolinite at Site 769 (Fig. 14), but higher abundances generally occur when kaolinite has been assigned a value of zero and the entire area of the 7Å diffraction has been assigned to chlorite, reflecting the difficulty in assigning the area of this peak by the techniques used in this study (see "Explanatory Notes" chapter, this volume). Chlorite averages around 10% in most of the samples from Site 769, although the very low values in Unit IIB are real and reflect a decline in both kaolinite and chlorite.

### *"Continentality" Index*

The continentality index used in these studies is the logarithm of the ratio of the sums of the abundance of smectite, illite, and chlorite to the abundance of smectite. It reflects the influence of clay minerals associated with the weathering of continental igneous (illite) and metamorphic (chlorite) rocks compared with the abundance of smectite, which represents the weathering of basic and intermediate igneous rocks.

The "continentality" of the sediments at Site 769 is low ($<0.5$) and trends toward even lower values in Subunit IIB (Fig. 15). At other sites in the Celebes and Sulu seas, "continentality" has risen in some parts above 1.0, showing the strong influence of nearby continental masses on the sedimentation at these sites. This continental influence is much weaker at Site 769, re-

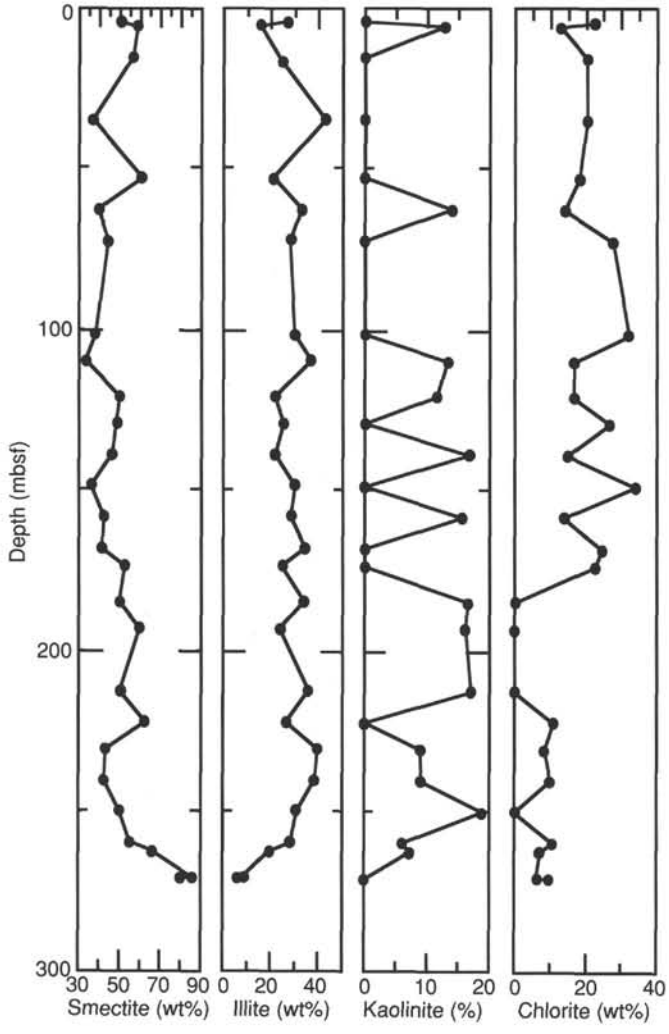


Figure 14. Abundance of smectite, illite, kaolinite, and chlorite in the <2-μm size fraction, Site 769.

flecting the elevated position that protected it from turbidity currents derived from the basin margins.

## Igneous Clast Petrology

At Site 769, igneous rocks are present from 278.45 mbsf to the bottom of the hole as clasts in coarse volcaniclastic rocks that consist of lapillistone and coarse tuff. Volcanic glass is the dominant clastic component of the lapillistone and tuff. Lithic fragments of fine-grained and hypocrystalline rocks and crystals occur in lesser amounts. Lithic fragments up to 20 cm in size compose the coarser lapilli. The poorly sorted lapillistone that is present in the upper 15 m contains some coarse lithic fragments with the structural features of volcanic bombs.

Fresh, homogeneous rock samples of a size sufficient for chemical analysis were taken from coarse lithic fragments in the lapillistone. Samples for chemical analysis could not be obtained from the clasts of volcanic glass because of their small sizes, the advanced alteration at their borders, and the difficulty in isolating them from their extensive siliceous cementation.

Seven samples of coarse lithic fragments in lapillistone were selected for petrographic studies and chemical analyses on board ship. Although they are a minor component, they can be considered as crystallized equivalents of vitric clasts or as representative of co-magmatic rocks. In fact, the hydroclastic and pyroclastic origin of the volcanic debris and the poor reworking indicate that the materials were originated by single eruptive events from a proximal volcanic vent.

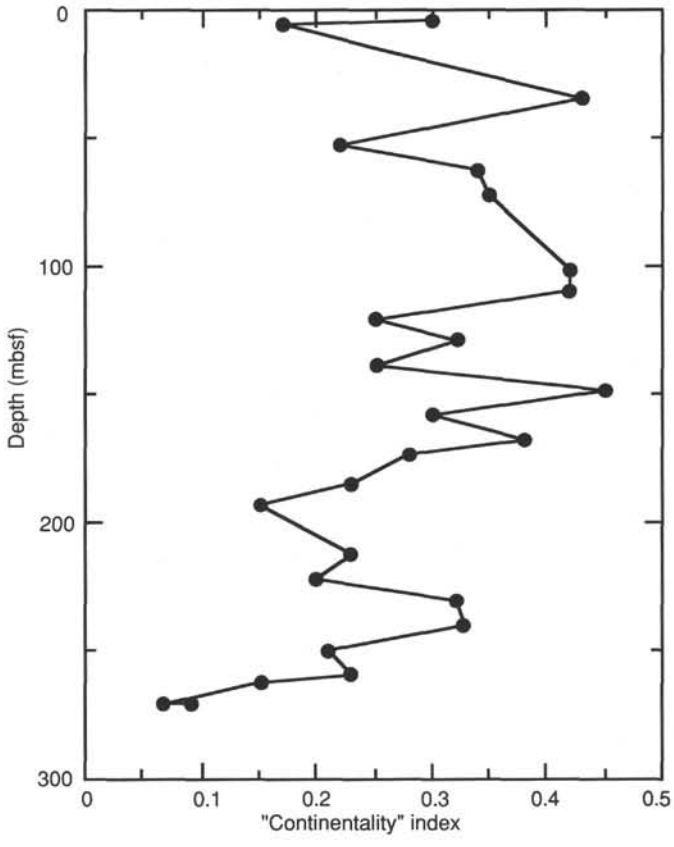


Figure 15. "Continentality" index, Site 769.

Samples were analyzed for major and trace elements by X-ray fluorescence (XRF) with the analytical procedure described in the "Explanatory Notes" chapter (this volume). Petrography of the analyzed samples is summarized in Table 4, and the results of XRF analyses are reported in Tables 5 and 6.

## Discussion

The sediments at Site 769 contain a suite of clay minerals that appear to be dominantly hemipelagic. The general absence of turbidites in the cores (see above) and the low value of the "continentality" index indicate that continental margin turbidites are unimportant to sedimentation at Site 769. The very high smectite and very low illite contents in Subunit IIB imply that it may be derived by local weathering or by alteration of material from the waning stages of the eruption that deposited the coarse volcaniclastic sediments of Unit III.

## Depositional Environment and Processes

Site 769 is located on the flank of the Cagayan Ridge at 3644 mbsl water depth, nearly 800 m shallower than Site 768. Three major phases of sedimentation in this part of the Sulu Sea can be recognized. The earliest phase is late early Miocene or older and consists of at least 98 m of coarse volcaniclastic rocks (Unit III). This unit is overlain by 176 m of clay with rare silt and marl, which ranges in age from late early Miocene to late Pliocene (Unit II). The lowest 16 m of this clay (Subunit IIB) is brown, contains a sparse fauna of poorly preserved radiolarians and rare manganese nodules, and may be pelagic in origin. It grades up through 10 m to greenish gray hemipelagic clay (Subunit IIA), which dominates the sequence up to 102 mbsf. The

**Table 4. Petrographic data on volcanic rocks, Site 769.**

| Core, section, interval (cm) | Phenocrysts Ol | Pl | Cpx | Opx | Mt | Gdm | Amg | Total | Sec | Groundmass texture |
|---|---|---|---|---|---|---|---|---|---|---|
| 124-769B- | | | | | | | | | | |
| 31X-CC, 37-39 | 4 | 27 | 3 | 0 | 2 | 60 | 4 | 100 | 16 | intersertal-hyalopilitic |
| 32X-CC, 12-13 | 1 | 5 | 3 | 0 | 0 | 75 | 16 | 100 | 1 | intersertal |
| 124-769C- | | | | | | | | | | |
| 3R-2, 41-43 | 4 | 25 | 6 | 0 | 0 | 60 | 5 | 100 | 19 | intersertal |
| 4R-5, 9-12 | 8 | 15 | 1 | 0 | Tr | 72 | 4 | 100 | 25 | intersertal |
| 5R-5, 25-26 | 0 | 30 | 6 | 0 | 3 | 60 | 1 | 100 | 2 | hyalopilitic |
| 7R-1, 105-110 | 2 | 30 | 10 | Tr | 4 | 52 | 2 | 100 | 2 | hyalopilitic-pilotaxitic |
| 9R-3, 121-122 | 1 | 25 | 6 | 8 | 4 | 54 | 2 | 100 | 1 | hyalopilitic |
| 9R-4, 45-46 | 5 | 35 | 8 | Tr | 3 | 48 | 1 | 100 | 4 | hyalopilitic |

Note: Ol = olivine, Pl = plagioclase, Cpx = clinopyroxene, Opx = orthopyroxene, Mt = magnetite, Gdm = groundmass, Amg = amygdules, Sec = secondary minerals, and Tr = trace.

**Table 5. Major element composition and CIPW norms of volcanic rocks, Site 769.**

| Core, section, interval (cm) | $SiO_2$ | $TiO_2$ | $Al_2O_3$ | $Fe_2O_3$ | MnO | MgO | CaO | $Na_2O$ | $K_2O$ | $P_2O_5$ | Total | LOI | Mg# | Qz | Or | Ab | An | Di | Hy | Ol | Ap | Il | Mt | Total |
|---|---|---|---|---|---|---|---|---|---|---|---|---|---|---|---|---|---|---|---|---|---|---|---|---|
| 124-769B- | | | | | | | | | | | | | | | | | | | | | | | | |
| 31X-CC, 26-29 | 52.90 | 0.95 | 18.28 | 8.13 | 0.12 | 4.14 | 7.91 | 3.43 | 2.70 | 0.37 | 98.93 | 2.51 | 54 | 0 | 15.95 | 29.02 | 26.51 | 8.03 | 10.98 | 3.46 | 0.88 | 1.80 | 1.62 | 98.25 |
| 124-769C- | | | | | | | | | | | | | | | | | | | | | | | | |
| [a]3R-2, 41-43 | 50.60 | 0.62 | 17.60 | 9.47 | 0.12 | 7.50 | 10.15 | 2.30 | 0.62 | 0.40 | 99.38 | 2.05 | 65 | 0.32 | 3.66 | 19.46 | 35.87 | 9.24 | 26.02 | 0 | 0.95 | 1.18 | 1.88 | 98.58 |
| [a]4R-5, 9-15 | 51.25 | 1.15 | 18.20 | 9.25 | 0.14 | 5.12 | 8.87 | 2.98 | 1.86 | 0.38 | 99.20 | 1.83 | 56 | 0 | 10.99 | 25.21 | 30.79 | 8.35 | 15.17 | 3.10 | 0.90 | 2.18 | 1.87 | 98.56 |
| [a]5R-5, 22-25 | 55.35 | 0.98 | 18.85 | 7.50 | 0.14 | 3.60 | 7.60 | 3.50 | 1.62 | 0.30 | 99.44 | 1.21 | 52 | 5.16 | 9.57 | 29.61 | 30.94 | 3.74 | 15.72 | 0 | 0.71 | 1.86 | 1.49 | 98.80 |
| [a]7R-1, 108-112 | 56.50 | 0.89 | 17.70 | 7.73 | 0.15 | 3.90 | 7.97 | 3.03 | 1.25 | 0.26 | 99.38 | 1.21 | 54 | 9.33 | 7.39 | 25.64 | 31.00 | 5.32 | 16.21 | 0 | 0.62 | 1.69 | 1.54 | 98.74 |
| 9R-3, 116-120 | 58.39 | 0.90 | 16.70 | 7.71 | 0.15 | 3.26 | 7.15 | 3.38 | 1.61 | 0.23 | 99.48 | 1.14 | 49 | 10.78 | 9.51 | 28.60 | 25.64 | 6.48 | 14.02 | 0 | 0.54 | 1.71 | 1.53 | 98.81 |
| [a]9R-4, 46-49 | 52.85 | 0.96 | 19.50 | 7.42 | 0.15 | 4.15 | 8.65 | 3.20 | 1.85 | 0.43 | 99.16 | 1.14 | 56 | 1.26 | 10.93 | 27.08 | 33.38 | 5.23 | 16.35 | 0 | 1.02 | 1.82 | 1.47 | 98.54 |

Note: Major element compositions are given in wt% oxide. LOI = loss on ignition.
[a] On-board samples reanalyzed at the University of Udine, Italy.

**Table 6. Trace element composition of the volcanic rocks from Site 769.**

| Core, section, interval (cm) | Nb | Zr | Y | Sr | Rb | Zn | Cu | Ni | Cr | V | Ce | Ba | Ti | Ti/Zr | Ti/V | Ce/Zr | Y/Zr | K | K/Rb |
|---|---|---|---|---|---|---|---|---|---|---|---|---|---|---|---|---|---|---|---|
| 124-769B- | | | | | | | | | | | | | | | | | | | |
| 31X-CC, 26-29 | 9 | 112 | 34 | 261 | 37 | 71 | 34 | 19 | 23 | 291 | 30 | 225 | 5695 | 51 | 20 | 0.27 | 0.30 | 22414 | 606 |
| 32X-CC, 9-12 | 22 | 89 | 41 | 283 | 15 | 90 | 62 | 54 | 62 | 338 | 33 | 211 | 6654 | 75 | 20 | 0.37 | 0.46 | 9962 | 664 |
| 124-769C- | | | | | | | | | | | | | | | | | | | |
| 3R-2, 41-43 | 4 | 51 | 26 | 368 | 11 | 110 | 50 | 70 | 49 | 248 | 16 | 63 | 3537 | 69 | 14 | 0.31 | 0.51 | 5230 | 475 |
| 4R-5, 9-15 | 20 | 94 | 33 | 306 | 35 | 79 | 31 | 60 | 178 | 377 | 39 | 229 | 6834 | 73 | 18 | 0.41 | 0.35 | 15524 | 444 |
| 5R-5, 22-25 | 10 | 124 | 33 | 291 | 15 | 71 | 41 | 21 | 24 | 295 | 26 | 225 | 5755 | 46 | 20 | 0.21 | 0.27 | 13946 | 930 |
| 7R-1, 108-112 | 14 | 106 | 27 | 293 | 30 | 68 | 45 | 21 | 49 | 236 | 35 | 217 | 5216 | 49 | 22 | 0.33 | 0.25 | 10460 | 349 |
| 9R-3, 116-120 | 10 | 110 | 33 | 259 | 36 | 66 | 34 | 9 | 26 | 267 | 33 | 187 | 5395 | 49 | 20 | 0.30 | 0.30 | 13365 | 371 |
| 9R-4, 46-49 | 14 | 119 | 32 | 323 | 16 | 69 | 32 | 28 | 43 | 276 | 38 | 196 | 5635 | 47 | 20 | 0.32 | 0.27 | 15607 | 975 |

Note: Trace element composition given in parts per million (ppm).

clay sequence accumulated below the CCD. The upper Pliocene to Holocene sequence is composed of hemipelagic and pelagic foraminifer-nannofossil marls.

The coarse volcaniclastic deposits in Unit III are unstratified and very uniform in composition (dominantly glassy pyroclasts) and lack intermixed sediment as well, so we infer that deposition was a direct result of processes associated with explosive pyroclastic eruptions. We have interpreted the unit as shallow-water (<1 km), near-vent, fall-out deposits, or as possible deeper water deposits of pyroclastic flows. A problematic aspect of the first interpretation is the fact that Unit III is overlain by hemipelagic or pelagic brown clay lacking in biogenic carbonate (Subunit IIB), which therefore must have accumulated at depths below the CCD.

Although the recovered contact between the two units may be disturbed by the coring process, there is no lithologic evidence for a gradual transition between the two units; rather, an abrupt change in lithology takes place. If the shallow-water interpretation of the pyroclastic rocks is correct, this abrupt contact represents considerable deepening of Site 769 between the deposition of Units II and III. Because of the lack of age controls for Unit III, the time period between the cessation of volcanic activity and the deposition of the brown clay is not known, and the possibility of a significant hiatus separating the deposition of the two units cannot be ruled out.

The superposition of brown clay on the pyroclastic strata of Unit III is more easily explained if the latter are interpreted as deep-water deposits of eruption-generated pyroclastic flows. The

expected sharp boundaries between flow units are not evident in the cores, but this could be attributed to poor recovery in this unit (<50%). The coarse grain size and absence of a clay-rich matrix require transport to have occurred as high-density laminar mass flows rather than as debris flows or turbidity currents. Such laminar flows would be expected to produce segregation of grains by size to produce features such as the normal and reverse grading that are observed in Unit III (Fisher and Schmincke, 1984, p. 198). However, subaqueous pyroclastic flows typically consist of a lower massive to poorly bedded flow unit and an upper sequence of thin graded ash beds (Fisher, 1984). If the tuff and lapillistone of Unit III were deposited as pyroclastic flows, they either lacked these upper fine-grained intervals, or the intervals are present but were not recovered in the cores, perhaps a result of the lesser induration related to the difference in grain size. In this scenario, the abrupt transition from pyroclastic rocks to brown clay could reflect a simple cessation of volcanic activity, resulting in mantling of the deep-water pyroclastic deposits by pelagic brown clay. If this were the case, the absence of eroded epiclastic volcanic debris within the brown clay would indicate that the volcanic source was submarine and therefore not subjected to erosion after volcanic activity ceased.

The brown clay of Subunit IIB grades up into the greenish gray clay of Subunit IIA. The change in color may be associated with an increase in sedimentation rate. The greenish gray clay beds are considered to be hemipelagic deposits that include small amounts of silt (both terrigenous and volcanic in origin). The carbonate content of the greenish gray clay is variable: small numbers of nannofossils are commonly present, becoming a major component in some beds. A turbiditic origin is possible for some of the thicker beds of marl, but much of this carbonate is probably pelagic in origin (principally the nannofossil *Discoaster*). This implies that the sediment accumulated not far below the CCD.

The transition from the Pliocene hemipelagic clay to the late Pliocene foraminifer and nannofossil marl involved a gradual influx of planktonic calcareous biogenic material. The transition occurred over approximately 0.3 Ma, compared with 0.7 Ma at Site 768. The first appearance of marl composed of pelagic carbonate material is in Section 124-769B-14H-4. The noncalcareous clays were totally replaced by marl beginning with Section 124-769B-12H-4. Paleomagnetic stratigraphy dates the bottom of this transition at approximately 2.4 Ma (see "Paleomagnetics" section, this chapter), the same age as observed at Site 768.

Renewal of explosive volcanic activity in the area may be indicated by the presence of numerous thin laminae to thin beds of dark green clay in the sequence above Core 124-769B-25X (223 mbsf, Unit II), which are interpreted as highly altered airfall ash. If this interpretation is correct, ash deposition began in late middle Miocene time (NN9). This volcanic activity peaked in the early Pliocene, as shown by the maximum in frequency of ash layers between 140 and 160 mbsf (Fig. 4). The lowest unequivocal fresh ash in the section is in Core 124-769B-12H (101.27 mbsf) and is late Pliocene in age (NN18). Ash deposition continued into Pleistocene to Holocene time.

## Petrography

The analyzed lithic fragments consist of highly porphyritic, hypocrystalline, and hypohyaline rocks with different mineral assemblages and modes. Given the presence of a glassy component in the groundmass, the lithologic types have been classified according to Ewart (1982), with $SiO_2$ contents as the discriminant. The identified rocks include basalt, basaltic andesite, and andesite and have been distinguished in the following petrographic types:

1. Moderately plagioclase-olivine-clinopyroxene phyric basalt (Sample 124-769B-32X-CC, 12 cm). Phenocrysts consist of plagioclase (5% vol), clinopyroxene (3%), and altered olivine (1%). Plagioclase (about $An_{70-85}$) is present in isolated laths and glomerophyric aggregates up to 2 mm in size, and clinopyroxene (optically augite) appears mainly in aggregates of prisms up to 1 mm in size. Olivine is mostly euhedral and sometimes intergrown with clinopyroxene. The groundmass is hypocrystalline and consists of an intersertal aggregate of plagioclase, clinopyroxene, and Fe-Ti oxide microliths with glassy mesostasis. Vesicles are abundant (16%), 0.1–2 mm in size, and filled with green clays and scarce chalcedony. Alteration is slight, as shown by preservation of glass in the groundmass. Olivine is completely replaced by clays and iron hydroxides.

2. Highly plagioclase-olivine-clinopyroxene phyric basalt (Samples 124-769C-3R-2, 41 cm, and 124-769C-4R-5, 9 cm). Phenocrysts consist of plagioclase (12%–25%), olivine (6%–8%), and clinopyroxene (1%–6%). Plagioclase (about $An_{65-90}$) is partly glomerophyric and 0.2–2 mm in size. Olivine is euhedral to subhedral, 0.1–2 mm in size, and completely altered. In Sample 124-769C-4R-5, 9 cm, the olivine shows embayed outlines and includes magnetite euhedrals. In Sample 124-769C-4R-5, 9 cm, it is sometimes included within clinopyroxene. Clinopyroxene (augite) is in prisms 0.2–2 mm in size. Groundmass is intersertal and consists mainly of plagioclase (30%–33%) and clinopyroxene (12%–20%) with 10%–15% mesostasis of altered glass. Accessory Fe-Ti oxides and apatite are present. Vesicles are less than 1 mm, 4%–5% in volume, with clay filling. Alteration is moderate. Olivine, glassy mesostasis, and (incipient) plagioclase are replaced by clays, iron oxides, and scarce calcite.

3. Highly plagioclase-olivine-clinopyroxene phyric basaltic andesite (Samples 124-769B-31X-CC, 37 cm, and 124-769C-9R-4, 45 cm). Phenocrysts consist of plagioclase (27%–35%), clinopyroxene (8%–3%), altered olivine (4%–5%), magnetite (2%–3%), and orthopyroxene (<1% in Sample 124-769C-9R-4, 45 cm). Plagioclase is often glomerophyric, 0.3–4 mm in size, and shows strong oscillatory zoning ($An_{35-80}$). Clinopyroxene (augite) is present in prisms 0.3–1 mm. The orthopyroxene in Sample 124-769C-9R-4, 45 cm, is a pale yellow hypersthene present either as prisms up to 0.5 mm in size or as corroded crystals with epitaxial overgrowth of augite. Groundmass is hyalopilitic to intersertal and consists of plagioclase, clinopyroxene, Fe-Ti oxides, and reddish brown altered glass. Sparse vesicles (1%–4%), less than 0.5 mm, are filled with clays and chalcedony. Alteration is slight to moderate and affects olivine (pseudomorphed by clays), calcite, iron hydroxides, and glassy mesostasis, which is oxidized and partly replaced by clays.

4. Highly plagioclase-clinopyroxene phyric andesite (Sample 124-769C-5R-5, 25 cm). Plagioclase phenocrysts (30%) are isolated or glomerophyric, up to 4 mm in size, with sieve texture or inclusion-free and strong oscillatory zoning ($An_{45-85}$). Clinopyroxene phenocrysts (6%) consist of prisms of brownish augite 0.3–2 mm in size. Magnetite forms small granular phenocrysts, sometimes included within augite. Groundmass texture is hyalopilitic. Crystals are small laths of plagioclase, clinopyroxene microliths and minor granular Fe-Ti oxides, and acicular apatite. Mesostasis consists of reddish brown slightly oxidized glass. Sparse vesicles, 0.5 mm in size, are filled with clays.

5. Highly plagioclase-clinopyroxene-olivine-orthopyroxene augite phyric andesite (Samples 124-769C-7R-1, 105 cm, and 124-769C-9R-3, 121 cm). The phenocryst mineral assemblage includes plagioclase (25%–30%), augite (6%–10%), altered olivine (1%–2%), hypersthene (<1%–8%), and magnetite (4%). Clusters of plagioclase, augite, hypersthene, and magnetite are present in Sample 124-769C-9R-3, 121 cm. Plagioclase is mostly glomerophyric, 0.3–3 mm in size, with typical sieve texture and

strong oscillatory zoning ($An_{40-80}$). Augite forms pale green prisms, 0.3–2 mm in size. Hypersthene appears either as isolated prisms up to 0.8 mm in size or as corroded crystals epitaxially overgrown by augite. Groundmass is dominantly glassy, with hyalopilitic to pilotaxitic texture. Crystalline phases are plagioclase, clinopyroxene, and minor magnetite and apatite. Sparse vesicles, spherical or pipe-shaped, are filled with clays. Alteration is shown mostly by replacement of olivine with clays and iron hydroxides. Glass shows slight oxidation.

### *Geochemistry*

The major element chemistry shows that the basaltic rocks are olivine-normative with subalkaline (moderately phyric basalt) and subalkaline to slightly alkaline (highly phyric basalt) tendencies, according to Irvine and Baragar (1971). One basaltic andesite is olivine-normative with an alkaline tendency (Sample 124-769B-31X-CC, 26 cm), whereas the other two are quartz-normative and subalkalic (Fig. 16). The andesites are subalkalic and contain 3%–10% normative quartz. Total alkalis show poor correlation relative to $SiO_2$ (Fig. 16) from the basaltic to the andesitic rocks. Since the rocks are fairly fresh, the contents of these elements should indicate primary abundances. $K_2O$ is variable and significantly higher relative to silica in the basalts (except in Sample 124-769C-3R-2, 41 cm) and in the basaltic andesites rather than in the andesites (Fig. 16). One basaltic andesite (Sample 124-769B-31X-CC, 26 cm) in particular has a remarkable distinctly higher $K_2O/SiO_2$ ratio relative to the other rocks.

In variation diagrams against $FeO_{tot}/MgO$ ratios, considered as the fractionation index, the high enrichment of $SiO_2$ relative to $FeO_{tot}/MgO$ is observed (Fig. 17). This behavior characterizes the fractionation of calc-alkaline rocks, $FeO_{tot}$ shows a marked negative correlation with $FeO_{tot}/MgO$, and $TiO_2$ has a slight negative correlation with $FeO_{tot}/MgO$ (Fig. 17). Both are characteristic of the fractionation trend of calc-alkaline rocks (Miyashiro, 1974).

Minor element chemistry (Table 6) is characterized by rather high abundances of hygromagmatophile elements Rb, Sr, and Ba and of incompatible elements, particularly Nb and Zr in all lithotypes. Values of these elements are in the range of the calc-alkaline, basalt-andesite series (Ewart, 1979). A comparison of some trace elements with typical abundances in calc-alkaline basalt and andesite (Jakes and Gill, 1970; Jakes and White, 1972) shows higher K/Rb values, which mainly reflect a tendency toward a potassium-rich composition, particularly for the basalt and basaltic andesite lithotypes.

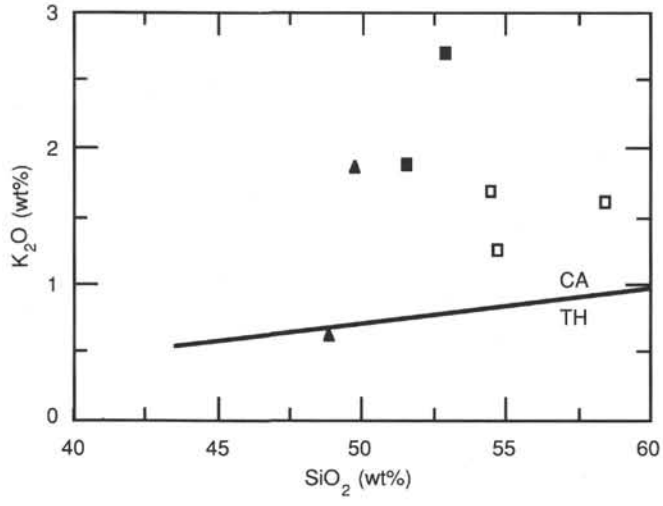


Figure 16. $K_2O$-silica diagram for Site 769 volcanic rocks. The boundaries between the calc-alkaline (CA) and island-arc tholeiitic (IAT) series are after Jakes and Gill (1970). Filled triangle = basalt, filled square = basaltic andesite, and open square = andesite.

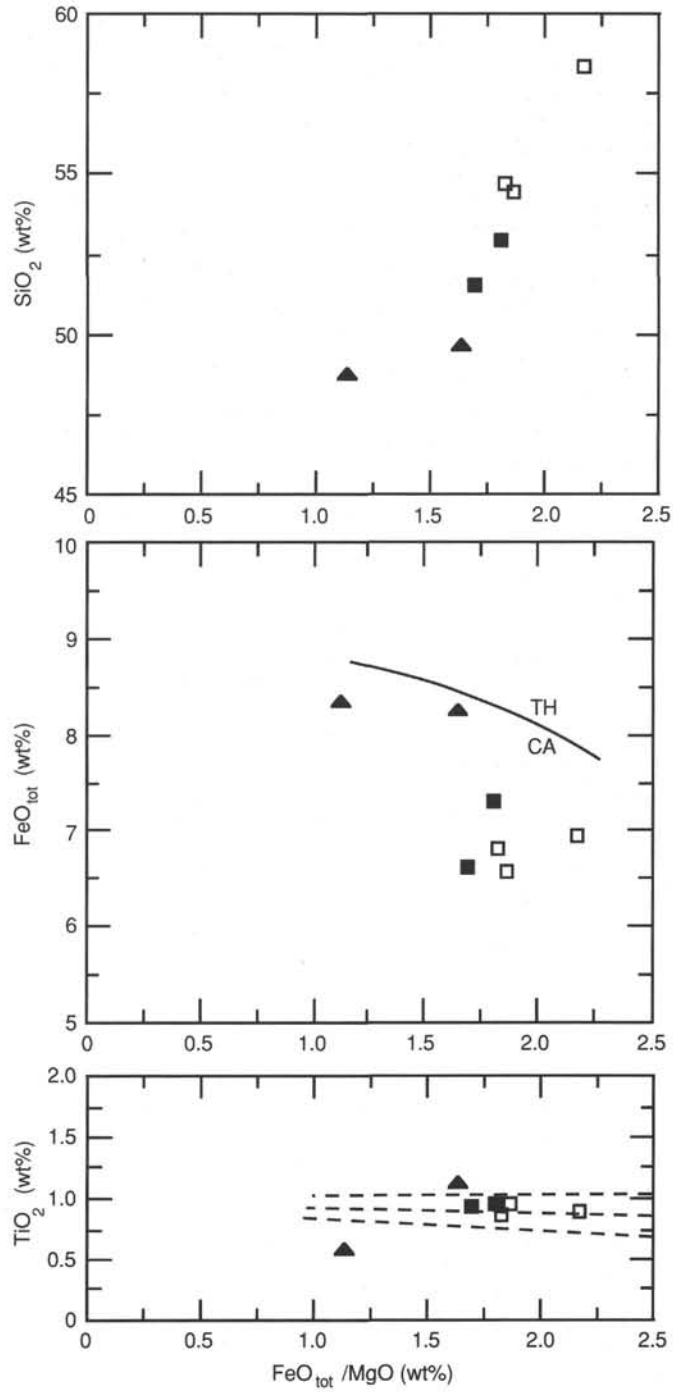


Figure 17. Variations of $SiO_2$, $FeO_{tot}$, and $TiO_2$ vs. $FeO_{tot}/MgO$ for Site 769 volcanic rocks. The boundary between the tholeiitic (TH) and calc-alkaline (CA) series in the $FeO_{tot}$ vs. $FeO_{tot}/MgO$ diagram, and typical trends of calc-alkaline rocks (dotted lines) in the $TiO_2$ vs. $FeO_{tot}/MgO$ diagram are after Miyashiro (1974). See Figure 16 for an explanation of the symbols.

### *Conclusions*

The igneous rocks that are in the coarse volcaniclastic rocks from the lower section of Site 769 include basalt, basaltic andes-

ite, and andesite, which display the typical petrographic features of calc-alkaline (orogenic) rocks, notably high abundances of phenocrysts and the appearance of hypersthene in andesitic lithotypes. Geochemical analysis shows that the rocks are fairly homogeneous in serial character. They are calc-alkaline with a tendency toward a K-rich composition in the basalt and basaltic andesite lithotypes.

The presence of these calc-alkaline lithic fragments in the coarse volcaniclastic rocks is not sufficient to characterize, in petrographical and geochemical features, the volcanism to which they are related, because the composition of the dominant glassy clasts is not known. The appearance of andesite typical of the hypersthenic series of evolved orogenic volcanism indicates a prevalent calc-alkaline character of the volcanism.

### Comparison of Sites 768 and 769

The stratigraphy of Sites 768 and 769 are compared in Figure 18. The oldest material drilled at Site 769 is a sequence of coarse volcaniclastic rocks. These are considered likely to be proximal pyroclastic deposits that formed on the submarine flanks of subaerial or shallow submarine volcanic vent, although it is possible that the material was redeposited in deeper water. They are andesitic to basaltic in composition. In contrast, the pyroclastic deposits of apparently similar age at Site 768 (Unit IV) are interpreted as flows of redeposited pumiceous pyroclastic material that is dominantly rhyolitic to dacitic in composition. Both sites, therefore, record somewhat different products of the explosive arc volcanism that occurred during early Miocene time.

The late early Miocene to late Pliocene sedimentary record at Site 769 is condensed in relation to Site 768. The 526-m-thick sequence in Unit II of Site 768 is equivalent in age to only 176 m of sediment in Unit II at Site 769. The hemipelagic clays that form the bulk of this interval at Site 769 are similar in appearance and composition to the hemipelagic clays that are between the silty turbidites at Site 768. These silty turbidites of terrigenous clastic detritus are absent from the sequence at Site 769, and this accounts for the difference in the thickness of this interval between the two sites. The absence of terrigenous turbidites at Site 769 indicates that the site was isolated from the area of deposition of turbidites, possibly because it was located on a ridge above the basin floor, as it is at the present day.

Currently, the CCD is at about 4800 m in the Sulu Sea, and the carbonate lysocline is between 3800 and 4000 m (Linsley et al., 1985). This is 200 m deeper than the CCD calculated by Berger et al. (1976) for the western Pacific, and substantially deeper than the CCD of the South China Sea, which currently lies at approximately 4000 m (Rottman, 1979). The Sulu Sea is presently isothermal below the thermocline with a temperature of 10°C. The shallow depth (420 m) of the deepest sill controlling water exchange between the South China and Sulu seas explains the anomalous deep-water temperature of the Sulu Sea.

Van Riel (1943) observed that the Sulu Sea Deep Water has the same physical properties as the water entering from the South China Sea over this sill; he concluded, therefore, that deep water in the Sulu Sea is replenished by throughflow of water over this sill. This conclusion has been supported by recent work in the area (Frische and Quadfasel, this volume). The present abnormally warm bottom waters of the Sulu Sea basin result in much better carbonate preservation than in the adjacent Pacific Ocean or South China Sea (Valencia, 1973; Exon et al., 1981).

The upper Pliocene to Holocene sequences at the two sites are very similar and differ only in the total thickness of pelagic and hemipelagic marl (Figs. 18 and 19). The calcareous sequence at Site 769 is about 20 m thinner, most likely a result of the lack of significant turbidite deposition or of disturbance in the section caused by slumping.

At Sites 768 and 769, pelagic carbonate became a major sediment component after its beginning at about 2.4 Ma, apparently as a result of a deepening of the CCD in the basin. A concurrent climatic and oceanographic development at 2.4 Ma was the initiation of moderate-sized ice sheets in the Northern Hemisphere at the Gauss-Matuyama transition (Backman, 1979; Shackleton et al., 1984; Zimmerman et al., 1985). This finding is based primarily on percent $CaCO_3$ records from Deep Sea Drilling Project (DSDP) Site 552 in the North Atlantic.

Uniformly high carbonate values preserved in the early Pliocene suddenly yielded to periodically lower values as a result of the influx of ice-rafted continental debris. Furthermore, an abrupt increase in $\delta^{18}O$ values at 2.4 Ma partially reflects the growth of continental ice sheets. Confirmation that 2.4 Ma was the age of onset of ice rafting has come from subsequent coring by DSDP and the Ocean Drilling Program (ODP) across the subpolar North Atlantic and in the Labrador and Norwegian seas (Ruddiman, Kidd, Thomas, et al., 1986; Eldholm, Thiede, et al., 1987; Srivastava, Arthur, et al., 1987).

The coincidence of a rapid increase in carbonate accumulation with the onset of the Northern Hemisphere glaciation at about 2.4 Ma implies that the influence of expanded Northern Hemisphere ice sheets was felt in the tropics. In addition, the correspondence between increased carbonate preservation in the Sulu Sea (deepening CCD) and the increase in global ice volume indicates that a global lowering of the sea level may have been partially responsible for shoaling the sill depth in the Sulu Sea and elevating the bottom-water temperatures, rather than strictly local tectonic adjustments of sill depth.

The Sulu Arc was volcanically active during the late Pleistocene, so a consequent uplift of the arc could have helped limit deep-water exchange in the Sulu Sea and led to a warming of deep water. Although these preliminary findings do not rule out productivity changes and increased carbonate flux, they do suggest that the increase in carbonate deposition in the Sulu Sea at 2.4 Ma was related to sea-level fluctuations brought about by the inception of Northern Hemisphere glaciation.

## BIOSTRATIGRAPHY

### Summary

Three holes were drilled at Site 769, located on the southeastern edge of the Cagayan Ridge. This site was mainly chosen to obtain a good hemipelagic upper Neogene sequence for paleoenvironmental studies. Hole 769A was drilled down to 65.4 mbsf. This sequence was repeated in Hole 769B, which then was drilled down to 290.2 mbsf. In Core 124-769B-30X, brown clays overlie andesitic pyroclastic rocks. Hole 769C was washed down to 261.1 mbsf and then drilled to a total depth of 376.9 mbsf.

The sedimentary sequence recovered at Site 769 ranges in age from Pleistocene to late early Miocene. The Quaternary sediments are rich in well-preserved calcareous micro- and nannofossils. Diatoms and radiolarians are present mainly within the surface sediments. However, siliceous microfossils are common within olive green marls intercalated as layers or patches. These marls also show low levels of organic matter of marine origin (see "Organic Geochemistry" section, this chapter). These layers might represent periods of upwelling and reduced bottom oxygenation.

Signs of calcite dissolution can be observed around the Pliocene/Pleistocene boundary and increase with depth. The lower Pliocene sediments are almost barren of foraminifers and nannofossils. The upper to upper lower Miocene is represented by slightly calcareous claystones, deposited close to or below the CCD. Foraminifers are few and poorly preserved, whereas nannofossils are still abundant within certain levels. The assemblages consist predominantly of discoasters, whereas the less-resistant coccoliths are dissolved.

The oldest sediments dated by nannofossils are upper middle Miocene (Zones NN9–NN8?) at a depth of 230 mbsf. This age

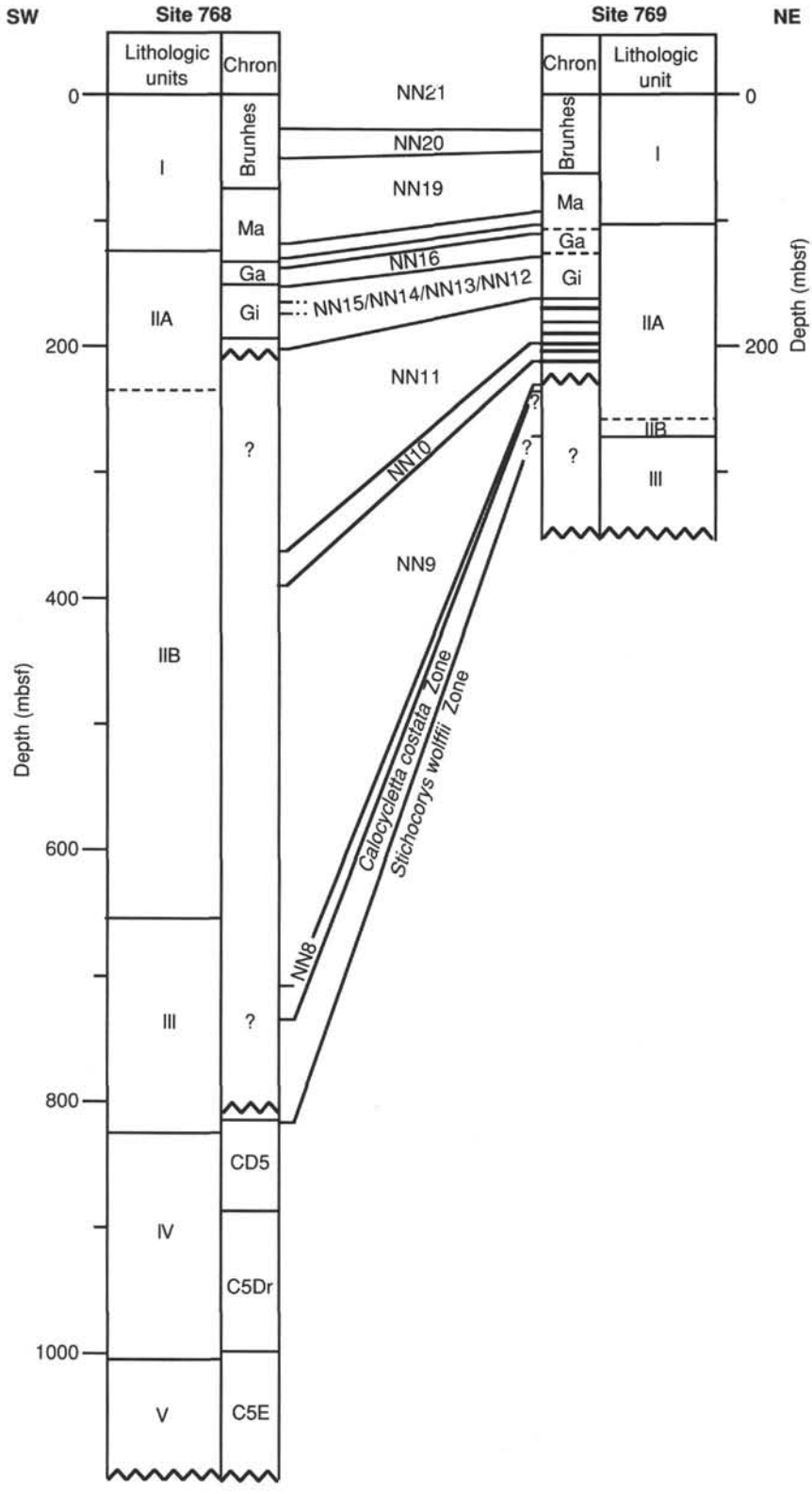


Figure 18. Biostratigraphic, magnetostratigraphic, and lithologic correlation of Sites 768 and 769 sedimentary successions in the Sulu Sea. Nannofossil Zones NN21 (upper Pleistocene) through NN8 (middle Miocene) and radiolarian zones *Calocycletta costata* and *Stichocorys wolffii* (upper lower Miocene) are represented.

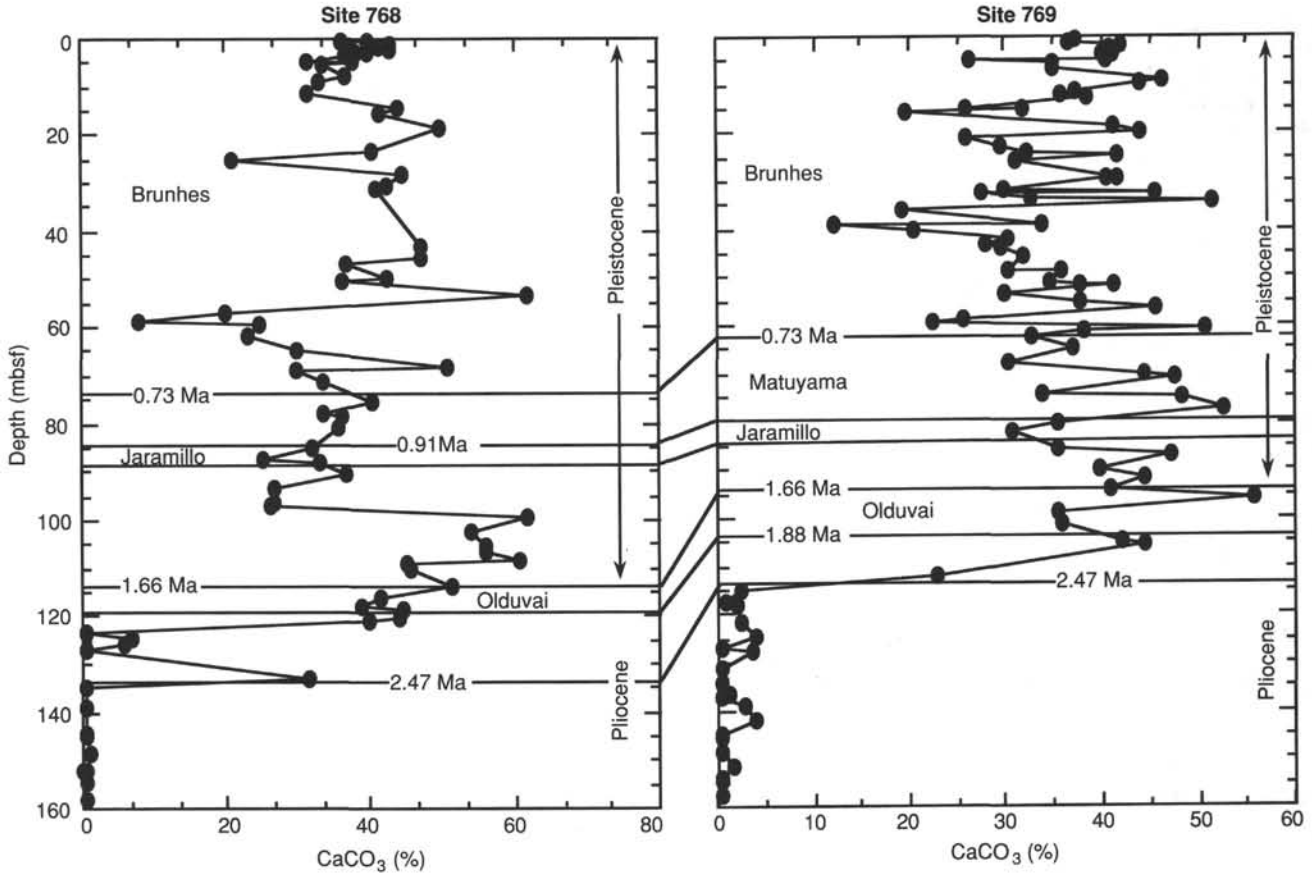


Figure 19. Plot of carbonate vs. depth for Unit I and the upper part of Unit II, Site 769, compared with the equivalent interval at Site 768. Paleomagnetic datum levels and the position of the Pliocene/Pleistocene boundary are also shown. Note the rapid increase in carbonate content just above the Pliocene/Pleistocene boundary.

is confirmed by foraminifers (N14) and by radiolarians found at 240 mbsf (*Diartus petterssoni* Zone). The sediments at 269 mbsf, above the pyroclastic rocks, were dated by radiolarians as upper lower Miocene (probably *Stichocorys wolffii* Zone).

The biostratigraphic results show that time-equivalent sequences were drilled at Sites 768 and 769. However, there is little terrigenous input during the Miocene at Site 769, which caused a more condensed section. Figure 18 shows biostratigraphic and magnetostratigraphic datums correlated between Sites 768 and 769 in the Sulu Sea, as compared with the main lithologic units.

## Nannofossils

Quaternary sediments were recovered at Site 769 from Core 124-769A-1H to Sample 124-769B-10H-CC (0–91.7 mbsf). The sediments consist predominantly of marls with volcanic ashes. They are rich in well-preserved nannofossils.

Zone NN21 was determined from Core 124-769B-1H to Sample 124-769B-3H-5, 40–41 cm (21.3 mbsf), underlain by Zone NN20 from Section 124-769B-3H-5 to Sample 124-769B-5H-1, 30–31 cm (37.2 mbsf).

The LO of *Pseudoemiliania lacunosa* was observed in Sample 124-769B-5H-3, 30–31 cm, indicating the top of Zone NN19. Its base was determined in Sample 124-769B-11H-1, 30–31 cm (91.2 mbsf), with the LO of *Discoaster brouweri*. We recognized the acme zone of the small *Gephyrocapsa*, which falls together with the Jaramillo paleomagnetic event (Gartner, 1977), at the base of Core 124-769A-9H at about 81.0 mbsf. The same biostratigraphic intervals were determined in Hole 769B, drilled with a lateral offset of 25 m.

The nannoplankton assemblages of the Quaternary are dominated by *Gephyrocapsa oceanica, Gephyrocapsa* sp., *Umbilicosphaera sibogae*, and *Helicosphaera carteri. Pseudoemiliania lacunosa* is very rare within the uppermost part of Zone NN19. We observed an increase of *Pontosphaera pacifica* and *Discolithina japonica* in Zone NN19 and the upper Pliocene, which is known from other areas.

The Pliocene/Pleistocene boundary at Site 769 is determined by the LO of *Discoaster brouweri* in Sample 124-769B-11H-1, 30–31 cm (at about 91.2 mbsf). At the same time we observed the disappearance of *Coccolithus pelagicus.*

A precise subdivision of the Pliocene is not possible because of carbonate dissolution mainly within the lower Pliocene. Zone NN18 was determined from Samples 124-769B-11H-1, 30–31 cm, to 124-769B-12H-3, 125–126 cm (about 91.2–104.6 mbsf). The interval around the Pliocene/Pleistocene boundary is characterized by stronger dissolution, including the presence of abundant, very small coccoliths.

Zone NN17 was determined from Samples 124-769B-12H-4, 38–39 cm (105.2 mbsf), to 124-769B-13H-1, 60–61 cm. *Discoaster pentaradiatus* is very rare within the upper part of this zone. Zone NN16, of late Pliocene age, is present from Samples 124-769B-13H-1, 60–61 cm (110.5 mbsf), to 124-769B-14H-5, 40–41 cm. *Discoaster surculus* is rare. The sediments contain variable amounts of volcanic ash, and dissolution increases with depth. The upper Pliocene nannoplankton assemblages are dominated by very small coccoliths. Discoasters are generally abundant.

The lower Pliocene (NN12–NN15) was recognized from Samples 124-769B-14H-6, 80–81 cm (127.7 mbsf), to 124-769B-18H-

CC (166.9 mbsf) by the presence of *Sphenolithus abies* and small *Reticulofenestra pseudoumbilica*. Below this level nannofossils are absent because of dissolution. The lowermost Pliocene (Zone NN12) was determined only in Section 124-769B-18H-4. The assemblage consists of the following species: *Amaurolithus delicatus, Discoaster brouweri, Discoaster pentaradiatus, Discoaster* cf. *pentaradiatus, Discoaster surculus, Sphenolithus abies*, and *Reticulofenestra pseudoumbilica*. As observed at other Leg 124 sites, *Reticulofenestra pseudoumbilica* is generally few to rare and of small size. Nannofossils within this sample are common, but they are poorly preserved because of overgrowth.

The Miocene/Pliocene boundary (Zones NN11/NN12) lies between Section 124-769B-18H-5 and the top of Core 124-769B-19H and coincides with the base of the Gilbert paleomagnetic event, at about 165.0 mbsf. Nannoplankton Zone NN11 was recognized from the top of Core 124-769A-19H to Sample 124-769B-22H-3, 112–113 cm (166.9–196.5 mbsf), by the presence of *Discoaster quinqueramus*. Discoasters are generally common, but the less-resistant coccoliths are dissolved. The sediments consist predominantly of clay with a very low carbonate content deposited close to the CCD.

Nannoplankton Zone NN10, of the upper Miocene, was encountered from Samples 124-769B-22H-4, 80 cm, to 124-769B-23H-CC, underlain by middle Miocene Zone NN9 from Samples 124-769B-24H-2, 33–34 cm (213.1 mbsf), to at least 124-769B-25X-3, 63–64 cm (213.1–224.4 mbsf). Samples 124-769B-25X-4, 97–98 cm, to 124-769B-25H-4, 97–98 cm, belong to Zone NN8.

Nannofossils are absent from Cores 124-769B-26X to -30X because of carbonate dissolution. The andesitic pyroclastic rocks were encountered in the core catcher of Core 124-769B-30X (278.5 mbsf). No nannofossils were found in the brown clays overlying the pyroclastic rocks in Hole 769C.

## Foraminifers

At Site 769, foraminifers are abundant in the marls from the upper part of the sedimentary sequence throughout Hole 769A and in Cores 124-769B-1H through -11H in Hole 769B. Cores 124-769B-12H through -14H show increasing signs of dissolution. The gray clays in Core 124-769B-15H and in deeper cores are interpreted to have been deposited below the CCD. Only a few levels in Cores 124-769B-21H through -25X contain some carbonate, yielding poorly preserved foraminiferal faunas showing signs of severe dissolution. Carbonate-rich turbidites are found in Cores 124-769B-15H through -26X, but most of these are recrystallized.

The sediments from Hole 769A contain rich foraminiferal faunas that belong to Zone N22. In Hole 769B, the LO of *Globigerinoides obliquus* in Sample 124-769B-11H-4, 57–61 cm, approximately marks the Pliocene/Pleistocene boundary. The change in coiling direction in *Globorotalia menardii*, which is used here to mark the lower boundary of N22, is found at a depth of 105 mbsf. Sample 124-769B-12H-4, 79–84 cm, is the first sample containing right-coiling *G. menardii*. The presence of *Globigerinoides fistulosus* in Sample 124-769B-14X-1, 134–136 cm, indicates a N21 age.

Foraminifers are rare in Cores 124-769B-15H through -25X (130–230 mbsf). The gray clays, which make up most of this part of the section, contain rare arenaceous foraminifers only. Some carbonate-rich turbidites are present, but only one contained foraminifers (Sample 124-769B-18H-4, 117–119 cm). The poorly preserved faunas show an early Pliocene age (N19/N20), on the basis of the co-occurrence of *Sphaeroidinella dehiscens* and *Globoquadrina altispira*. Faunas from rare carbonate-bearing levels in Cores 124-769B-21H through -25X show strong signs of dissolution. *Sphaeroidinellopsis* spp. constitute the bulk of these faunas. Sample 124-769B-21H-CC probably belongs to upper Miocene Zone N17, given the presence of *Globorotalia plesiotumida*, whereas the dissolution-resistant *Globorotalia tumida* is absent. *Globigerina nepenthes* is present in samples from Cores 124-769B-22H and -24H, whereas *Neogloboquadrina acostaensis* is absent, which gives N15–N16 as an age (late middle or early late Miocene). The co-occurrence of *G. nepenthes* with *Globorotalia siakensis* in Sample 124-769B-25X-4, 94–96 cm, places that sample in Zone N14.

Calcareous foraminifers are absent in the deeper cores from Hole 769B as well as in Hole 769C. The grey clays in Cores 124-769B-26X through -28X contain rare fragments of arenaceous foraminifers only (230–260 mbsf). The brown clays in Cores 124-769B-29X and -30X and in Cores 124-769C-1R and -2R (260–278 mbsf) are barren of foraminifers, as are the pyroclastic deposits below the brown clays.

## Diatoms

The preservation of diatoms is, in general, poor in sediments collected at Site 769, as it was with Sites 768 and 767. Usable diatom assemblages were recovered to a greater depth and age at Site 769 than at previous sites. Diatoms are abundant in the Holocene brown muds encountered in the upper 60–80 cm of Cores 124-769A-1H and 124-769B-1H. Below this level, diatoms are generally rare and show signs of strong dissolution. This profile compares precisely with that seen in Sites 767 and 768. Diatoms are found sporadically down to Core 124-769B-12H (109.9 mbsf). These occurrences are mostly in thin, olive green sediment "pods" that contain higher marine-derived organic carbon and lower carbonate than the matrix sediments. These sediments may be related to periods of higher productivity.

Contrary to diatom-bearing samples from Sites 767 and 768, Site 769 samples contained few benthic diatoms. In the previous sites, a large percentage of shelf-derived material is present, whereas on the bathymetric high at Site 769, input of biogenic material has been more strongly dominated by pelagic processes.

Diatoms representing the *Pseudoeunotia doliolus* Zone were found in abundance at the top of Cores 124-769A-1H and 124-769B-1H. The *P. doliolus* Zone is found down to Sample 124-769A-7H-3, 96–98 cm (59.9 mbsf), although definition of the boundary between the *P. doliolus* and the *Nitzschia reinholdii* Zones is difficult because of the incomplete preservation of the assemblage. The *N. reinholdii* Zone is present in Samples 124-769A-7H-CC (bottom of hole, 65.4 mbsf) and 124-769B-7H-CC (62.4 mbsf), as indicated by the presence of *N. reinholdii*.

The core catcher of Core 124-769B-11H contains a moderately preserved diatom assemblage including *Pseudoeunotia doliolus* and *Rhizosolenia praebergonii*. The co-occurrence of these species indicates that this sample lies between the upper part of the Olduvai paleomagnetic event and just above that event (Burckle, 1977; Burckle and Trainer, 1979; Barron, 1985a, 1985b). However, paleomagnetic and nannofossil datums indicate a slightly older age for this sample. Either *P. doliolus* ranges lower in the section in this region or this core-catcher sample includes some contamination from higher in Core 124-769B-11H. The base of Core 124-769B-11H is more likely in the *Rhizosolenia praebergonii* Zone.

Biostratigraphic application of diatom assemblages is not possible below this level on the basis of shipboard analyses. All samples evaluated below the levels discussed above are barren of diatom remains, with one exception. Fragments of *Ethmodiscus* sp., which is of little use in biostratigraphy, are found accompanying common radiolarians and sponge spicules and rare silicoflagellates and ebridians in the >44-μm fraction of certain samples from Core 124-769B-25X, preserved by replacement of the biogenic silica by pyrite.

### Radiolarians

Radiolarians are abundant at the sediment-water interface, but they show a rapid degradation with depth, as with the diatoms. Late Neogene radiolarians were not studied in detail on board. Samples from 100 mbsf (Core 124-769B-12H) to 227 mbsf (Section 124-769B-25X-6) are effectively barren of radiolarians. Several samples in the lower part of Core 124-769B-25X, which are in the green clays, contain an assemblage of radiolarians entirely replaced by pyrite. Fine detail on the skeletons is preserved, including delicate lattice structures and spines. An upper middle Miocene assemblage is found in these samples. Radiolarians identified include *Diartus petterssoni, Didymocyrtis laticonus, Anthocyrtidium ehrenbergi, Lamprocyclas maritalis, Pterocanium audax*, and *Cyrtocapsella japonica* of the *Diartus petterssoni* Zone. Radiolarians preserved in this manner are found in only a few samples in this interval; most samples are barren.

Radiolarians are absent in the greenish pelagic clays in Cores 124-769B-26X down to -29X. A gradational color change, from dominantly green clay to reddish brown clay, is noted in Core 124-769B-29X. Radiolarians are not found in most of this core, but a poorly preserved assemblage was recovered from the core catcher (269.0 mbsf). *Stichocorys wolffii* is the most common radiolarian in the assemblage. Present in very low numbers are *Stichocorys delmontensis, Didymocyrtis violina, Calocycletta virginis*, and *Lithopera baueri*(?). The co-occurrence of *S. wolffii* and *D. violina* define an upper lower Miocene succession. We did not find *Calocycletta costata*, suggesting that the assemblage is within the *S. wolffii* Zone; however, poor preservation and low abundance makes an unconvincing argument for zonal boundary definition based on negative evidence. A similar assemblage was found in Sample 124-769C-2R-4, 47–49 cm (275.8 mbsf). Considerable drilling disturbance in this core makes an exact depth below seafloor uncertain.

Radiolarians are rare and very poorly preserved below this level in Holes 769B and 769C. The remains of radiolarians were found overlying pyroclastic rocks by only a few centimeters in Samples 124-769B-30X-CC (278.7 mbsf) and 124-769C-3R-1, 5–7 cm (~280.5 mbsf). These fossils are too poorly preserved for positive identification, but forms tentatively identified include *S. wolffii, C. virginis*, and the heavily silicified *Theochorys spongoconum*(?), all of which are present in the assemblage found 9.7 m above. Holes 769B and 769C ended in pyroclastic sediments, which are barren of fossils. The radiolarian assemblage found overlying pyroclastic rocks at Site 769 is about the same age as that found overlying a pyroclastic sequence at Site 768.

### Ichthyoliths

Icthyolityhs are present in the grey clays in Hole 769B (Cores 124-769B-15H through -28X; 130–260 mbsf). However, they are very rare. Even large core-catcher samples (20 $cm^3$ or more) yielded less than 15 specimens. The Cenozoic "triangle with triangular projection" was found in most samples. Otherwise, biostratigraphic markers are absent.

## PALEOMAGNETICS

### Overview

The quality of paleomagnetic data collected at Site 769 was generally good in APC cores. We recognized all the widely accepted magnetic reversal boundaries above the bottom of the upper part of the Réunion Subchron, and below the bottom of the Cochiti Subchron, down to the top of the Chron 11. Poor recovery in several cores and slumped beds in other cores made the chron assignment difficult between the Réunion and Cochiti subchrons. Results indicate that the sedimentary column in Cores 124-769B-1H to -24H has accumulated since 9.4 Ma, with a few breaks in deposition.

Magnetic susceptibility measurements at Site 769 were divided into four distinctive magnetic susceptibility units on the basis of the character of the curve. Hole 769A was drilled to take samples for detailed paleoclimatic and paleomagnetic studies. Correlation of the susceptibility data from Hole 769A with data from Hole 769B shows intervals in each hole that are not represented in the other.

### Magnetostratigraphy

To establish the magnetostratigraphy of Site 769, the remanent magnetization of all the archive halves of APC cores was measured at 10-cm intervals, with a 2G-Enterprise pass-through rock magnetometer. Measurements were made at natural remanent magnetization (NRM) and after at least one step of alternating field (AF) demagnetization at 10, 15, or 20 mT. One section of each core was demagnetized and measured progressively at 5, 10, 15, and 20 mT to determine an appropriate demagnetization level for other sections within a particular core. Magnetic directions and intensities after demagnetization are shown in Figure 20. The declination values were corrected with core orientation data obtained with the multishot core orientation tool. Because orientation data were not available in the first core, declinations from the core were corrected to align with those of the following cores.

The paleomagnetic records in Holes 769A and 769B were fairly good, except for intervals with scattered magnetic directions seen about 90 mbsf and 125 mbsf. The first seven magnetic reversals were identified as reversals above the upper part of Réunion Subchron. The Cobb Mountain Subchron seen at the last two sites was not observed because of the disturbed beds that occurred from 2 m below the Jaramillo Subchron to 3 m above the Olduvai Subchron. The short subchron that we saw in Site 768 above the Jaramillo Subchron was again observed in this site (Fig. 21); we discuss it below.

From 107 to 131 mbsf, the chron assignment is difficult because of several cores with poor recovery and also because of scattered directions caused by slumped beds. The reversal at 114.5 mbsf is assigned to the Gauss/Matuyama Chron boundary, and the reversal at 117.5 mbsf is assigned to the top of the Kaena Subchron. Other possible correlations are discussed below. From the bottom of the Cochiti Subchron, the quality of magnetic records was much improved throughout the rest of the APC cores. In this portion, we recognized 26 magnetic reversals, which are readily correlated with reversals from the bottom of the Cochiti Subchron to the top of Chron 11. The depths and ages of identified reversals are shown in Table 7. The ages of the reversals are from Berggren et al. (1985). The ages of the Réunion Subchrons are taken from Harland et al. (1982).

Three correlations are possible for the normal interval from 114.5 to 117.5 mbsf, namely, one of three separate normal periods in the Gauss Chron. This normal interval cannot be the oldest normal part of the Gauss Chron because there is another normal portion from 121 to 124 mbsf, although it is not bounded by clear reversals on both top and bottom. Of the remaining possibilities, we have assigned this normal interval to the latest one, because (1) an abrupt carbonate increase at about 120 mbsf is correlated with the same event observed at the Gauss/Matuyama Chron boundary in Site 768, and (2) the NN16/NN17 boundary (2.45 Ma) was determined at 110.5 mbsf, which is just above the 121-mbsf boundary.

An age-vs.-depth plot determined from this chron assignment is shown in Figure 22. In addition to the disturbed zone from 107 to 131 mbsf, the points in the figure can be represented by three line segments: (1) from the seafloor to the bottom of the Jaramillo Subchron, (2) from the bottom of the Co-

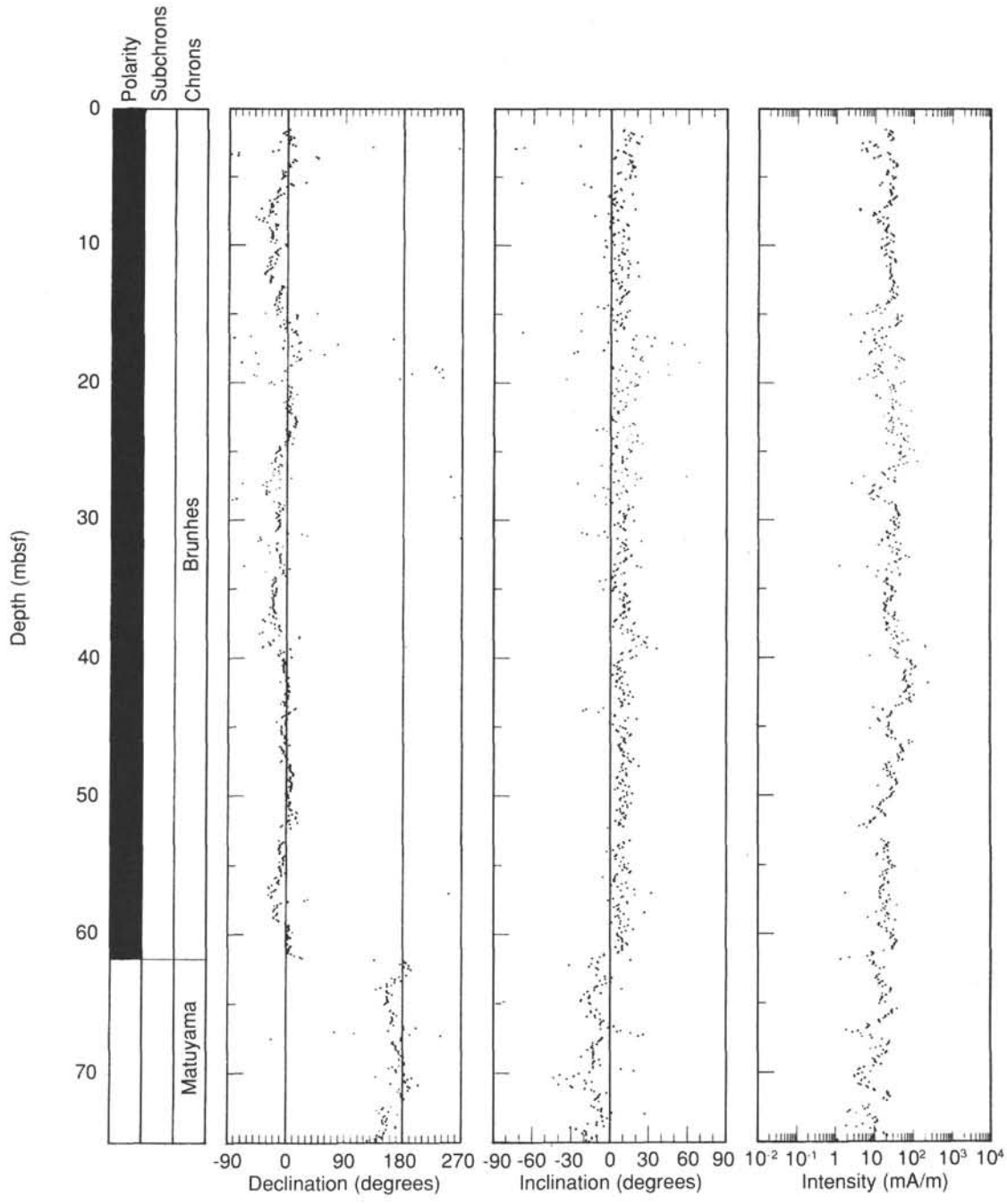


Figure 20. Magnetostratigraphic plot of declination, inclination, and intensity for Cores 124-769B-1H to -24H. The declinations are corrected by core orientation data.

chiti Subchron to the top of the reversal subchron in Chron 5, and (3) from the top of the reversal subchron in Chron 5 to the top of Chron 11. These intervals yield sedimentation rates of 87, 23, and 12 m/m.y., respectively.

The position of the "post-Jaramillo" short subchron at this site coincides well with the one in Site 768. Figure 23 compares the reversal depth between Sites 768 and 769 around the short subchron. The linearity from the short subchron to the bottom of the Jaramillo Subchron indicates a constant sedimentation rate throughout the duration. The age of the top of the short subchron is then calculated to be 0.86 Ma. The bottom of the short subchron in this site is not as clear as the one in Site 768 (Fig. 21). Taking the position from which the intermediate direction begins, the length of the subchron is 60 cm; but, taking a position of complete reversal, it is only 30 cm. The values yield durations of 8,000 and 4,000 yr, respectively. This reversal was not observed in Site 767. The depth expected for Site 767 is about the boundary of Cores 124-767B-6H and -7H. It would be in the core catcher of the 124-767B-6H or in the disturbed portion between these cores.

In the XCB cores, the magnetic directions were highly scattered. The rotary operation of the XCB cutting shoe creates frequent biscuit structures. It is, however, very difficult to identify each biscuit when the cores are split with wire. The scatter of the magnetic inclination in these cores is attributed to inappropriate sampling position.

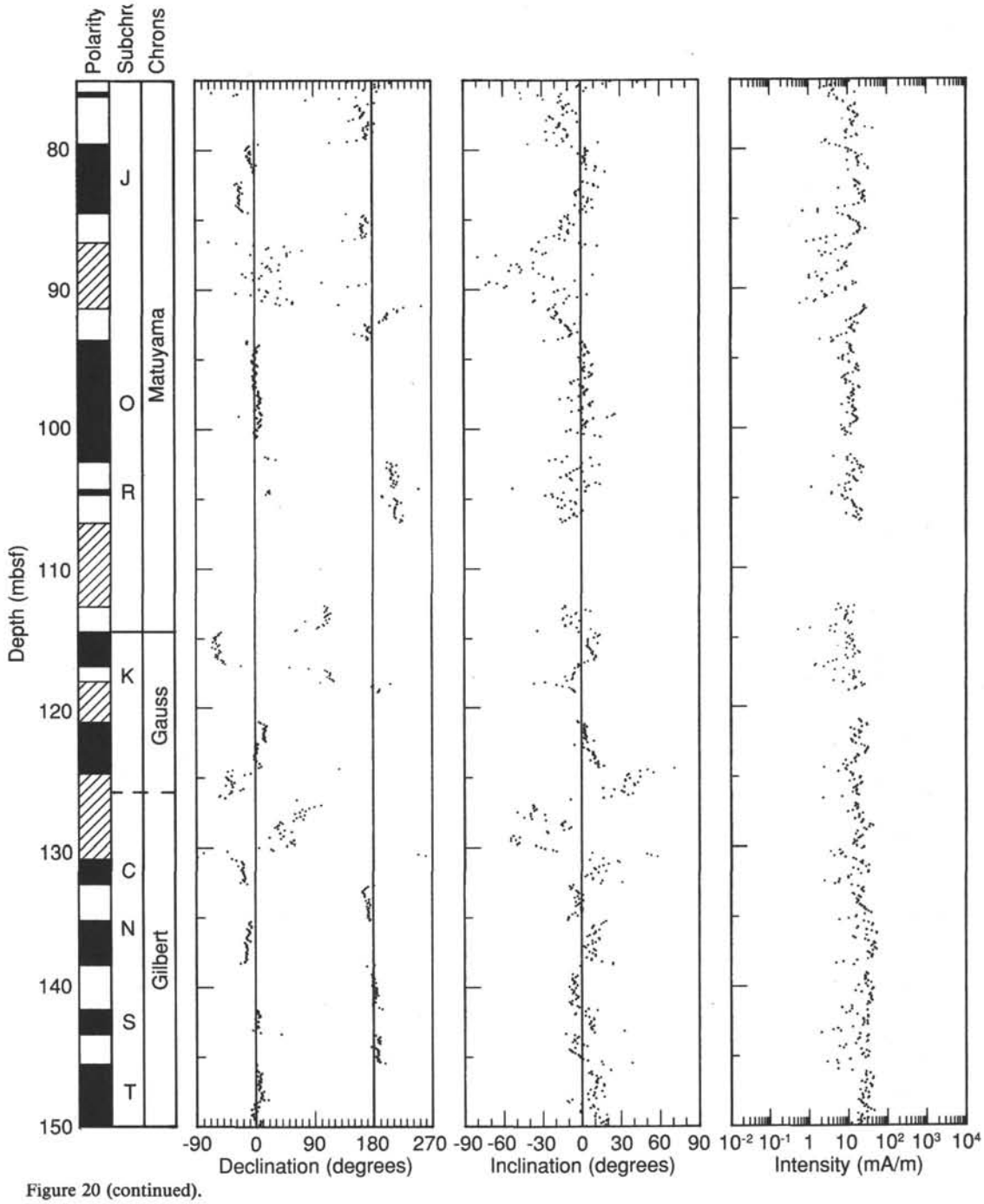


Figure 20 (continued).

## Inclination Change

The magnetic inclinations at the bottom of the APC section (205–220 mbsf) are clearly different from the inclinations at the top of the section, that is, inclinations are negative in normal polarity at the bottom. Figure 24 shows the mean inclination of every 100 measurements. At the bottom of this section, we observed tilting of the bedding plane. We measured some of the bedding planes in Cores 124-769B-20H to -23H. The mean tilt direction and angle were 227° and 21°, respectively. These values would produce an apparent tilt of 15° to the south in magnetic inclination measurements. The inclination change observed is consistent with the tilting, as seen in Figure 24. Most of the tilting happened over a 2-m.y. period from 5 to 7 Ma.

## Magnetic Susceptibility

Magnetic susceptibility plots for Site 769 are shown in Figure 25. Four major susceptibility units are identified at Site 769 within the sediment column cored:

1. Susceptibility Unit 1 extends from the seafloor to 100 mbsf. This unit has average susceptibility values of $90 \times 10^{-6}$ cgs, with three main pulses of higher susceptibility occurring from 13 to 36 mbsf, from 36 to 50 mbsf, and from 73 to 100 mbsf. The pulses have average magnetic susceptibility values ranging from $110 \times 10^{-6}$ cgs to $240 \times 10^{-6}$ cgs, with a highly variable nature to the curve, and peak values of up to $1320 \times 10^{-6}$ cgs.

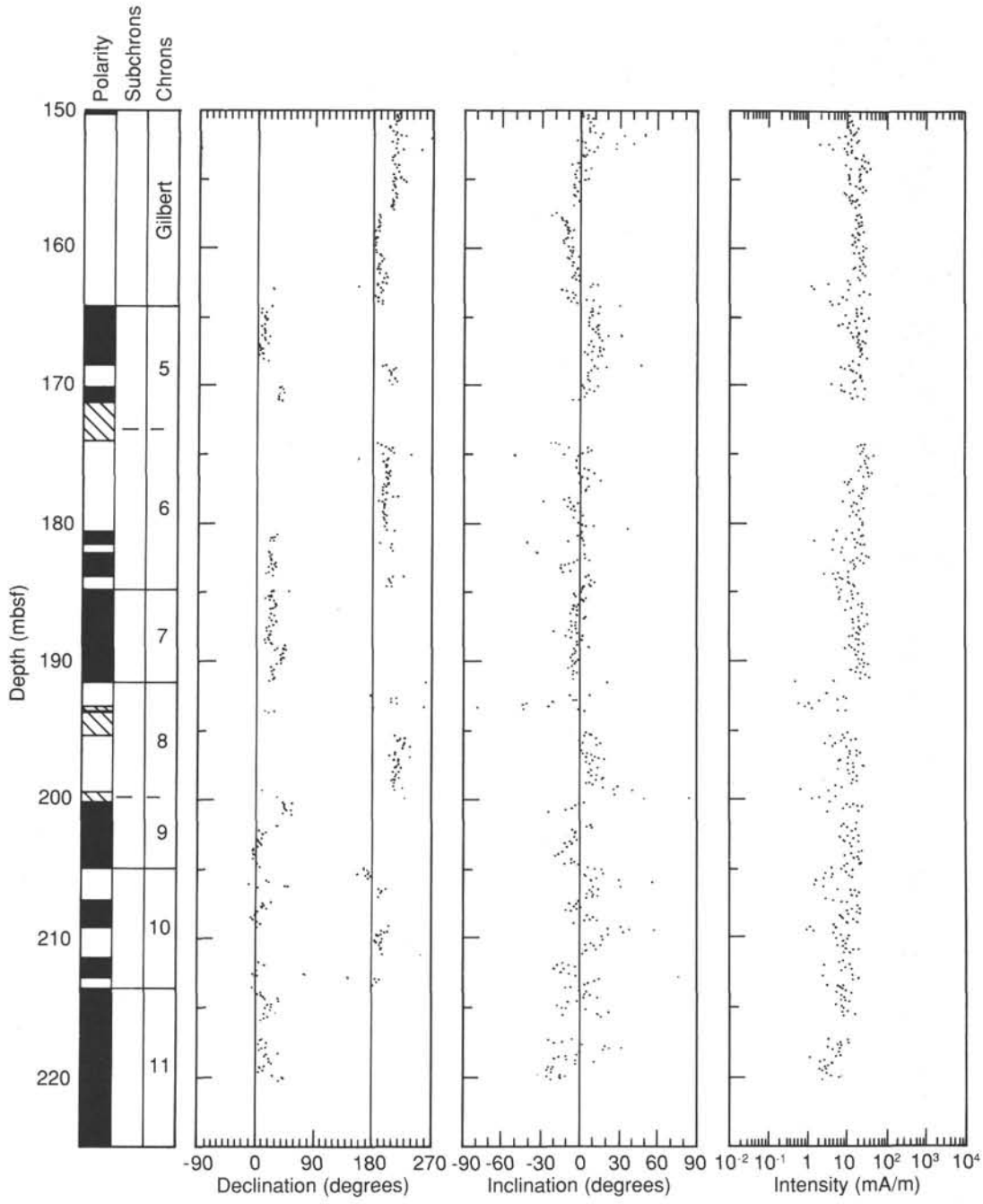


Figure 20 (continued).

2. Within Susceptibility Unit 2, susceptibility values increase from average values of 50 $\times$ $10^{-6}$ cgs at 100 mbsf, to 180 $\times$ $10^{-6}$ cgs at 140 mbsf, and then decrease to 50 $\times$ $10^{-6}$ cgs at the base of Susceptibility Unit 2. Overprinted on this first order curve are several thin layers of higher susceptibility with values of up to 130 $\times$ $10^{-6}$ cgs above those of the underlying curve.

3. Susceptibility Unit 3 extends from 238 to 265 mbsf. This unit is transitional from lower values in Unit 2 above to much higher values in Susceptibility Unit 4 below. Average magnetic susceptibility values range from 50 $\times$ $10^{-6}$ cgs at the top of the unit to 230 $\times$ $10^{-6}$ cgs at the base with small amounts of variability.

4. Pyroclastic sediments dominate Susceptibility Unit 4. This lithology produces generally high, variable, susceptibility values. Susceptibility values average 400 $\times$ $10^{-6}$ cgs, with peaks of up to 1050 $\times$ $10^{-6}$ cgs.

Magnetic susceptibility logs were used to provide an accurate correlation of Holes 769A and 769B. Relative spacing of susceptibility peaks and general trends observed within the susceptibility logs were used for correlation purposes with excellent results. Absolute peak heights were not used since these can be quite variable for corresponding peaks. The results of this correlation are shown in Figure 26, with lines connecting the correlatable positions on each log.

Good correlation occurs down to 15.8 mbsf in each hole. Hole 769B exhibits a condensed section from 15.8 to 18.2 mbsf, which corresponds to the interval from 15.8 to 19.3 mbsf in

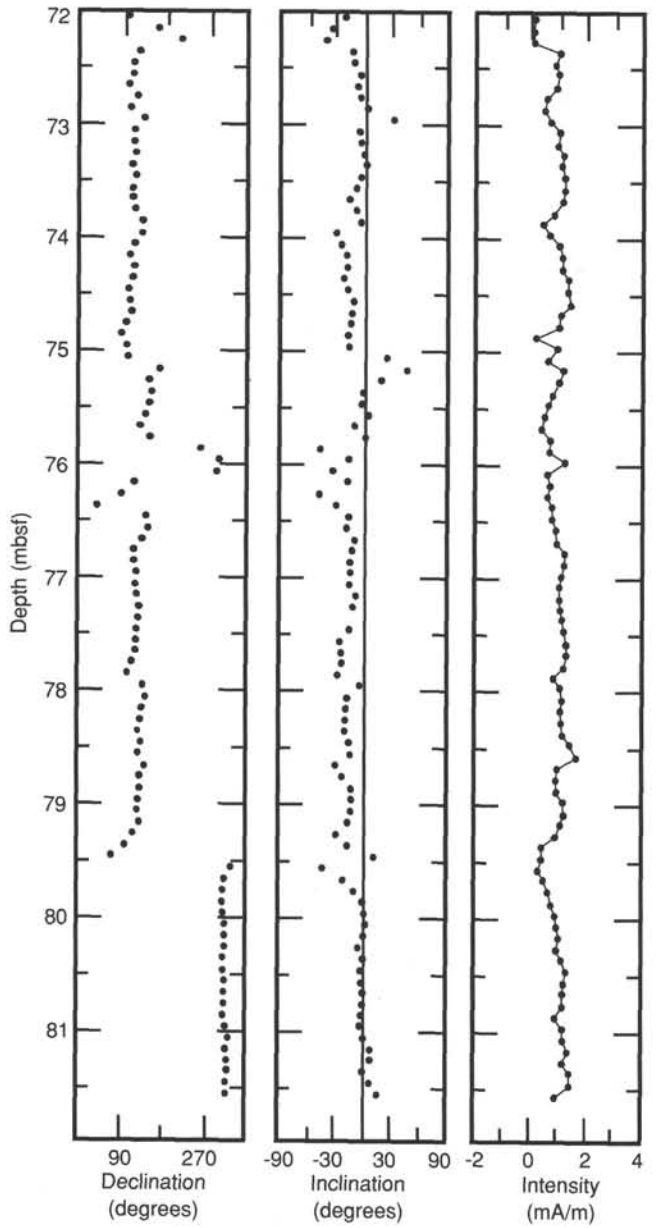


Figure 21. Magnetostratigraphic plot of declination, inclination, and intensity for Core 124-769B-9H.

Hole 769A. Hole 769A is expanded by 3.1 m more than Hole 769B over the equivalent intervals from 19.3 to 56.4 mbsf in Hole 769A, and from 18.2 to 52.2 mbsf in Hole 769B. There is a large discrepancy of 3.8 m between the two logs over the equivalent intervals from 56.4 to 56.6 mbsf in Hole 769A and from 52.2 to 56.2 mbsf in Hole 769B. Visual core descriptions of the interval in Hole 769B indicate a possible slump that does not appear in Hole 769A. Below 56.6 mbsf in Hole 769A and 56.2 mbsf in Hole 769B, there is a close, although slightly offset, correspondence of the susceptibility log.

## SEDIMENT ACCUMULATION RATES

Sediment accumulation rates were determined at Site 769 using magnetostratigraphy and biostratigraphy. The time scale of Berggren et al. (1985a, 1985b) was used for correlation of the magneto- and biostratigraphic zones. Calcareous nannoplankton zones are described in Martini (1971), and radiolarian zones are defined by Riedel and Sanfilippo (1978).

**Table 7. Reversal ages and depths, Holes 769A and 769B.**

| Chron/subchron | Age (m.y.) | Depth (mbsf) 769B | Depth (mbsf) 769A |
|---|---|---|---|
| Brunhes | | | |
| | 0.73 | 61.8 | 62.4 |
| (???) | | 75.8 | |
| | | 76.1–76.4 | |
| MATUYAMA Jaramillo | 0.91 | 79.5 | |
| | 0.98 | 84.5 | |
| MATUYAMA Olduvai | 1.66 | 93.6 | |
| | 1.88 | 102.3 | |
| MATUYAMA Réunion 2 | 2.01 | 104.3 | |
| | 2.04 | 104.7 | |
| MATUYAMA Réunion 1 | 2.12 | | |
| | 2.14 | | |
| | 2.47 | 114.5 | |
| GAUSS Kaena | 2.92 | 117.0 | |
| | 2.99 | | |
| GAUSS Mammoth | 3.08 | | |
| | 3.18 | | |
| | 3.40 | | |
| GILBERT Cochiti | 3.88 | | |
| | 3.97 | 132.6 | |
| GILBERT Nunivak | 4.10 | 135.2 | |
| | 4.24 | 138.3 | |
| GILBERT Sidufjall | 4.40 | 141.6 | |
| | 4.47 | 143.4 | |
| GILBERT Thvera | 4.57 | 145.5 | |
| | 4.77 | 150.3 | |
| | 5.35 | 164.2 | |
| Chron 5 (N) | | | |
| R-subchron | 5.53 | 168.5 | |
| | 5.68 | 170.1 | |
| | 5.89 | 171.2–174.0 | |
| Chron 6 (R) | | | |
| N-subchron | 6.37 | 180.6 | |
| | 6.50 | 181.5 | |
| N-subchron | 6.70 | 182.1 | |
| | 6.78 | 183.8 | |
| | 6.85 | 184.8 | |
| Chron 7 (N) | | | |
| | 7.28 | 191.5 | |
| Chron 8 (R) | | | |
| N-subchron | 7.35 | 193.2–193.5 | |
| | 7.41 | 193.7–195.3 | |
| | 7.90 | 199.4–200.1 | |
| Chron 9 (N) | | | |
| | 8.21 | 204.9 | |
| Chron 10 (N) | | | |
| N-subchron | 8.41 | 207.2 | |
| | 8.50 | 209.2 | |
| N-subchron | 8.71 | 211.3 | |
| | 8.80 | 212.8 | |
| | 8.92 | 213.5 | |
| Chron 11 (N) | | | |

Note: The ages of Réunion Subchrons were taken from Harland et al. (1982); other ages are from Berggren et al. (1985a, 1985b). N = normal and R = reversed.

The magnetostratigraphic record in Hole 769B was determined from oriented APC cores and extends from the top of Hole 769B to Core 124-769B-24H. A continuous reversal sequence is seen in this hole with good reversal boundaries throughout most of the measured interval. Sedimentation rates were calculated and are shown in Figure 27. Depths and ages of reversal boundaries are given in Table 7.

Sedimentation rates determined from reversal stratigraphy were divided into five major trends. From the seafloor to the base of the Jaramillo Event (84.5 mbsf), sedimentation rates of 87 m/m.y. are very consistent.

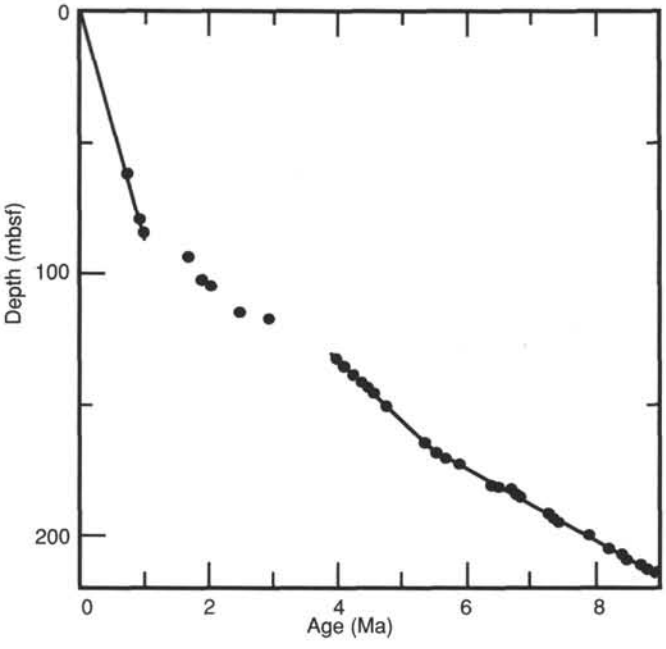


Figure 22. Plot of reversal depths vs. age for Cores 124-769B-1H to -24H.

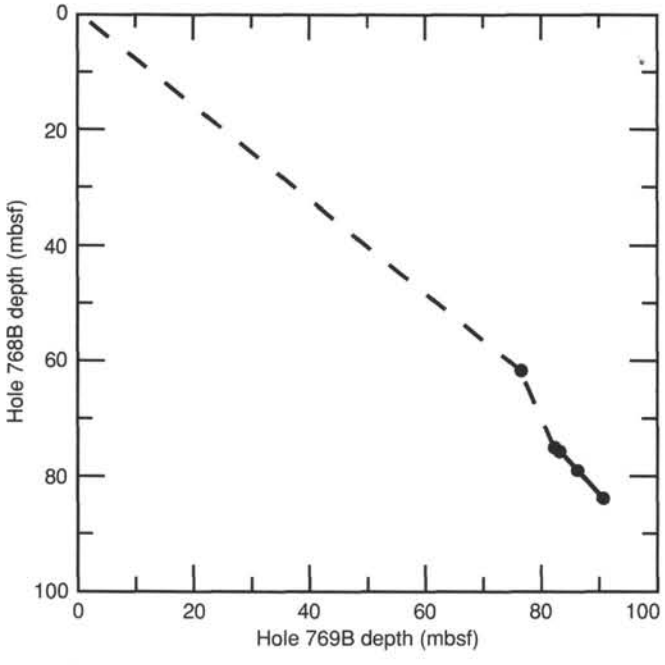


Figure 23. Correlation of reversal depths younger than Jaramillo Subchron between Holes 768B and 769B.

From the base of the Jaramillo Event to the base of the Cochiti Event (132.6 mbsf), sedimentation rates decrease dramatically compared with the previous interval, averaging 16 m/m.y. The magnetostratigraphic record is partially complicated throughout this interval because of some slumping and poor recovery in Core 124-769B-12H; however, the record has several reversals within the interval that constrain the magnetostratigraphy, enabling sedimentation rates to be determined with acceptable margins of error for segments within the disturbed interval.

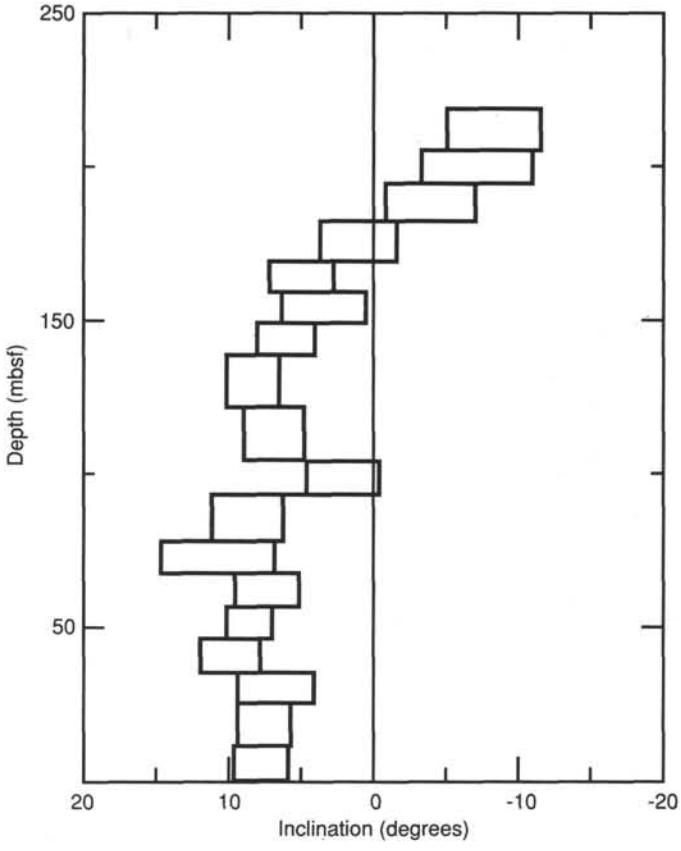


Figure 24. Inclination change vs. depth in Hole 769B. Boxes represent the mean and $\alpha_{95}$ of groups of 100 measurements. Before computing the mean, the sign of inclination values were reversed for areas of reversed polarity.

From the base of the Jaramillo Event (84.5 mbsf) to the top of the Olduvai (93.6 mbsf), sedimentation rates averaged 13 m/m.y. Throughout the Olduvai Event (93.6 to 102.3 mbsf), sedimentation rates increased to 40 m/m.y. From the base of the Olduvai Event (102.3 mbsf) to the Matuyama/Gauss boundary (114.5 mbsf), sedimentation rates averaged 20.7 m/m.y. From this point to the base of the Cochiti Event (132.6 mbsf), sedimentation rates averaged 12.1 m/m.y.

Sedimentation rates increased to 23 m/m.y throughout the following interval from the base of the Cochiti Event (132.6 mbsf) to the base of Chron 5 (172.6 mbsf). Sedimentation rates throughout this interval were very linear.

From the base of the Cochiti Event (132.6 mbsf) to the base of the second normal event in Chron 6 (182.1 mbsf), sedimentation rates declined from rates of 23 m/m.y. for the previous interval to 12 m/m.y. Rates of 20 m/m.y. were calculated from the base of the above interval down to the top of the first normal event in Chron 6 (180.6 mbsf), with rates of 5 m/m.y. below.

Sedimentation rates average 14 m/m.y. and are consistent from the base of the previous interval to the top of Chron 11 (213.5 mbsf). The magnetostratigraphy extends slightly below this depth but stays within Chron 11, making it impossible to determine sedimentation rates below this depth with magnetostratigraphy.

Sedimentation rates were also determined on the basis of biostratigraphic zones. Like other sites sampled during Leg 124, nannofossils were the predominant biostratigraphic marker used for determining sedimentation rates. Calcareous nannofossils

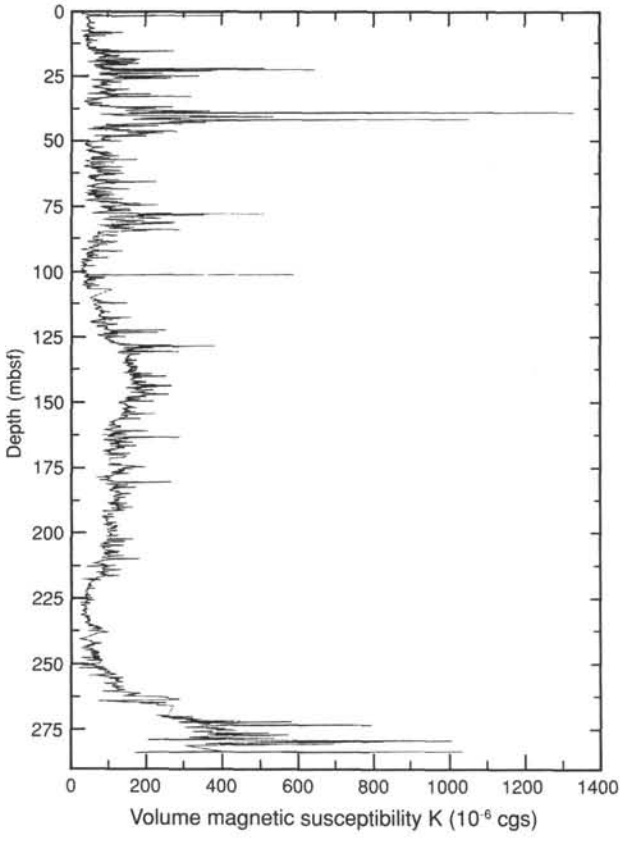


Figure 25. Magnetic susceptibility data, Hole 769B. Susceptibility data for Hole 769A is shown in Figure 26.

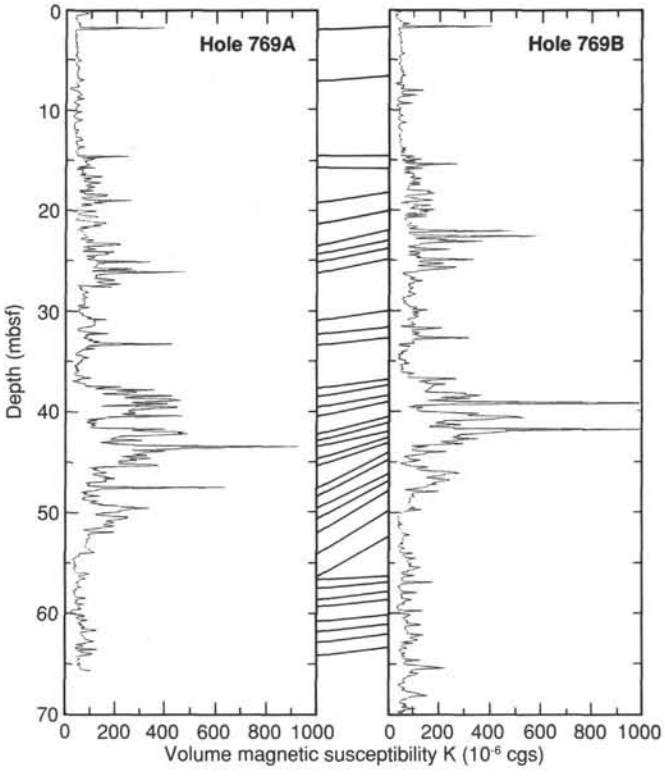


Figure 26. Magnetic susceptibility correlation of Holes 769A and 769B. Correlation was on the basis of the spacing of peaks and the trend of the curve.

were well preserved down to 93 mbsf. Below nannofossil Zone NN9, nannofossils were so poorly preserved that identification of biozones was difficult. Foraminifers were not definitive in sedimentation rate calculations, and radiolarian and diatom zones were only marginally useful where nannofossils were not observed.

Sedimentation rates calculated from biostratigraphic markers are shown in Figure 28. Age, depth, and sedimentation rates of individual biozones are given in Table 8.

High sedimentation rates were determined for the top 44 m of Site 769. Sedimentation rates for NN20/NN21 were calculated to be 78.5 m/m.y. Below NN20 sedimentation rates decrease dramatically, with only minor fluctuations in sedimentation rates with depth. For nannofossil Zone NN19, sedimentation rates averaged 37.9 m/m.y. The interval NN18–NN12 exhibits semilinear sedimentation rates with an average of 23.0 m/m.y. From NN11 to NN9, sedimentation rates fluctuate slightly with rates of 10.0, 23.0, and 10.3 m/m.y. for nannofossil Zones NN11, NN10, and NN9, respectively.

Specimens from the radiolarian *Diartus petterssoni* Zone were identified in Section 124-769B-25X-CC (230.4 mbsf), and the undifferentiated *Calocycletta costata/Sphenolithus wolffii* Zones were identified in Section 124-769B-29X-CC (269.0 mbsf). No diatom or radiolarian boundaries were identified within Site 769. Although there is inadequate control to establish a high degree of confidence in the sedimentation rate from the bottom of NN9 to 269 mbsf, an overall sedimentation rate of 6 m/m.y. was estimated.

No biozones were identified in the pyroclastic sediments observed at the base of Hole 769B and throughout Hole 769C; thus, sedimentation rates cannot be calculated for these sections.

## SEDIMENT INORGANIC GEOCHEMISTRY

This section summarizes the results of shipboard analysis of calcium carbonate and dissolved constituents in the interstitial water of the sediments drilled at Site 769. Dissolved sulfate and ammonium distributions are the result of the decomposition of organic carbon by sulfate reduction. Dissolved calcium, magnesium, pH, and silica profiles indicate the alteration of volcanic material and the formation of smectite between 100 and 150 mbsf. Calcium and magnesium distributions below 150 mbsf point to a source for these cations within the altered volcanic material below 250 mbsf. In general, the concentration gradients observed are of a smaller magnitude than those observed in previous sites.

### Calcium Carbonate

A total of 108 sediment samples were analyzed for their inorganic carbon content at Site 769 by means of the ODP shipboard standard method (see "Explanatory Notes" chapter, this volume). Results are given in Table 9, and the depth distribution is shown in Figure 29. The sediments in the uppermost 100 m are characterized by a carbonate content consistent with the observed calcareous marls of Unit I (see "Lithostratigraphy" section, this chapter) and are indicative of their deposition above carbonate compensation depth.

The sediments recovered below 115 mbsf are very low in carbonate components, as evidenced by the low $CaCO_3$ concentrations in these samples. The change in carbonate content is the result of a lowering of the CCD near the end of the Pliocene, which is concurrent with the observed drop in carbonate content

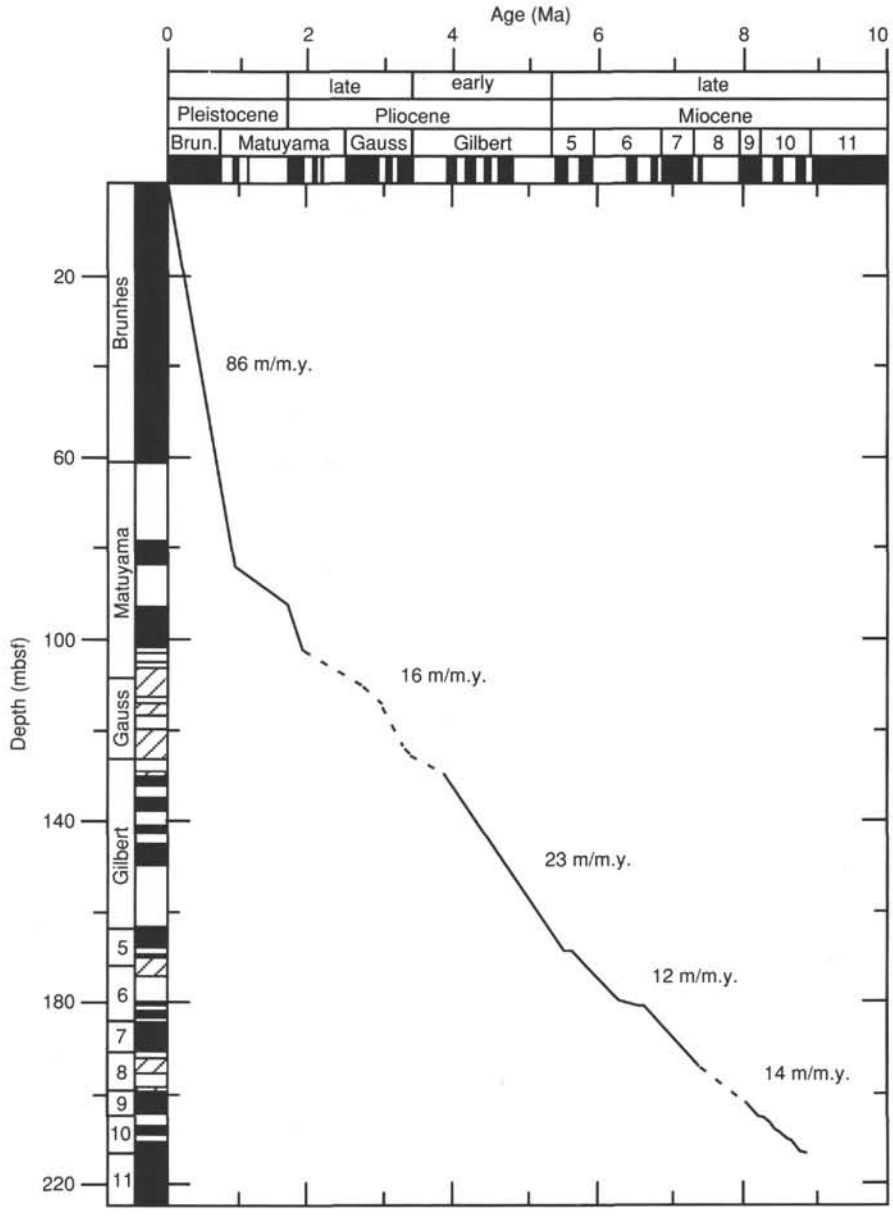


Figure 27. Sedimentation rates calculated from magnetostratigraphic data from Cores 124-769B-1H to -24H.

at Site 768. This implies that the drop in the CCD is the result of a tectonic mechanism that affects both sites simultaneously, and that there has been no relative movement between the sites since the Pliocene (see "Lithostratigraphy" section, this chapter).

## Interstitial Water Chemistry

A total of 20 interstitial water (IW) samples were collected for analysis at Site 769. They were retrieved from every core (approximately 10 m apart) in the uppermost 100 mbsf, by means of standard ODP squeezing techniques (see "Explanatory Notes" chapter, this volume). Below this depth, IW samples were taken every third core (about 30 m apart). With the exception of a few samples in the deeper sections of Hole 769B, whole-round core samples, 5–10 cm in length, provided sufficient IW ($>10$ cm$^3$) for shipboard chemical analysis. The results are summarized in Table 10, and the depth distributions are shown in Figure 30.

### *Salinity and Chloride*

With the exception of one data point at 117 mbsf, salinity in this site generally decreases with depth in the sediment column (Fig. 30). A similar decrease is observed in the chlorinity distribution.

### *pH*

The downcore pH distribution (Fig. 30) shows similar features to the ones observed at Sites 767 and 768. The pH values are generally less variable and lower in the uppermost 83 mbsf as compared with those in the deeper sections of the core. Below this depth, pH increases to a maximum value of 8.09 at about 200 mbsf, and then decreases again in the deepest sections of the hole. The higher pH values in the mid-section of the

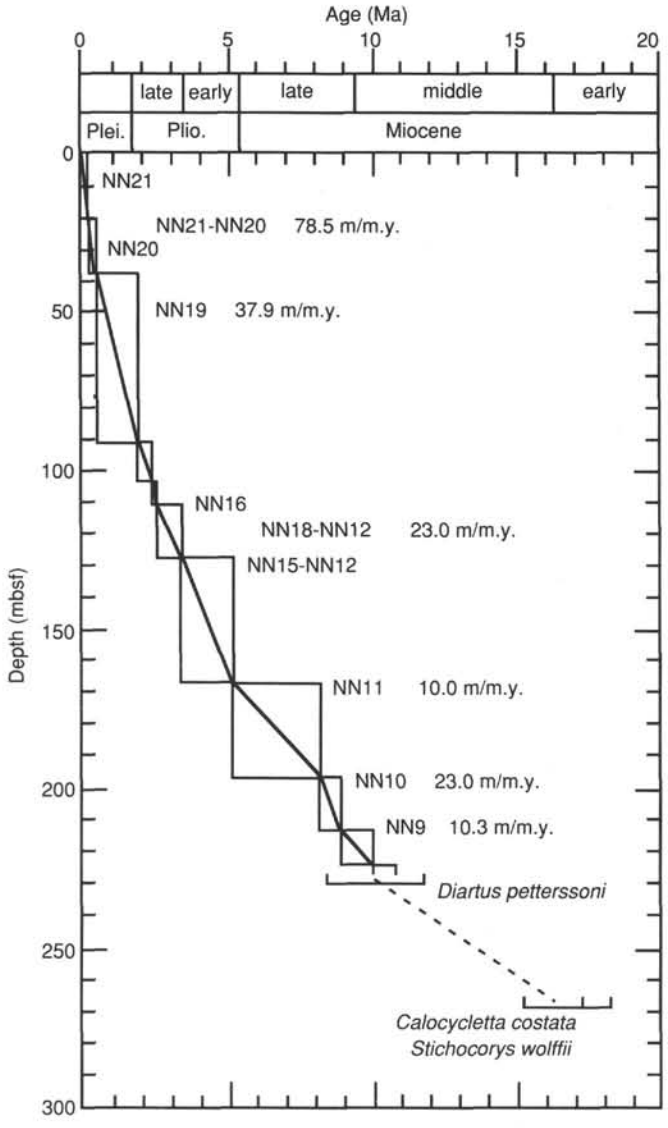


Figure 28. Sedimentation rates calculated from biostratigraphic data, Site 769.

**Table 8. Ages, depths, and sedimentation rates for the individual biozones identified at Site 769.**

| Biozone | Age (Ma) | Depth (mbsf) | Sed. rate (m/m.y.) |
|---|---|---|---|
| NN21 | 0–0.275 | 0–21.3 | 77.5 |
| NN20 | 0.275–0.474 | 21.3–37.2 | 79.9 |
| NN19 | 0.474–1.89 | 37.2–91.2 | 37.9 |
| NN18 | 1.89–2.35 | 91.2–105.2 | 28.3 |
| NN17 | 2.35–2.45 | 105.2–110.5 | 70.0 |
| NN16 | 2.45–3.40 | 110.5–127.7 | 16.8 |
| NN15–NN12 | 3.40–5.20 | 127.7–166.9 | 22.2 |
| NN11 | 5.20–8.20 | 166.9–197.0 | 10.0 |
| NN10 | 8.20–8.90 | 197.0–213.1 | 23.0 |
| NN9 | 8.90–10.0 | 213.1–224.4 | 10.3 |
| NN8 | 10.00–10.8 | 224.4–? | |
| *D. petterssoni* | 8.50–11.80 | 230.40 | |
| *C. costata/S. wolffii* | 15.30–18.2 | 269.00 | |

**Table 9. Results of calcium carbonate analysis, Site 769.**

| Core, section, interval (cm) | Depth (mbsf) | $CaCO_3$ (%) |
|---|---|---|
| 124-769A-1H-1, 62–64 | 0.62 | 37.2 |
| 124-769B-1H-1, 129–131 | 1.29 | 36.3 |
| 124-769B-1H-2, 44–46 | 1.94 | 41.8 |
| 124-769A-1H-2, 62–64 | 2.12 | 40.7 |
| 124-769B-1H-3, 52–54 | 3.52 | 40.0 |
| 124-769A-1H-3, 62–64 | 3.62 | 41.2 |
| 124-769B-1H-4, 47–49 | 4.97 | 26.2 |
| 124-769A-1H-4, 62–64 | 5.12 | 35.0 |
| 124-769B-2H-1, 101–103 | 6.41 | 34.9 |
| 124-769A-1H-5, 62–64 | 6.62 | 40.2 |
| 124-769A-2H-1, 70–72 | 9.10 | 46.1 |
| 124-769B-2H-3, 102–104 | 9.42 | 43.8 |
| 124-769B-2H-5, 0–3 | 11.40 | 37.3 |
| 124-769A-2H-3, 70–72 | 12.10 | 35.8 |
| 124-769B-2H-5, 98–100 | 12.38 | 38.3 |
| 124-769B-2H-7, 43–45 | 14.83 | 26.0 |
| 124-769A-2H-5, 70–72 | 15.10 | 31.8 |
| 124-769B-3H-1, 65–67 | 15.55 | 19.7 |
| 124-769B-3H-3, 64–66 | 18.54 | 41.2 |
| 124-769A-3H-2, 50–52 | 19.90 | 43.8 |
| 124-769B-3H-5, 0–3 | 20.90 | 25.7 |
| 124-769A-3H-4, 50–52 | 22.90 | 29.6 |
| 124-769B-3H-6, 50–52 | 22.90 | 32.2 |
| 124-769B-4H-1, 35–37 | 24.75 | 41.4 |
| 124-769A-3H-6, 50–52 | 25.90 | 30.8 |
| 124-769B-4H-4, 40–42 | 29.30 | 41.7 |
| 124-769A-4H-2, 70–72 | 29.60 | 40.3 |
| 124-769B-4H-6, 0–3 | 31.90 | 29.7 |
| 124-769B-4H-6, 70–72 | 32.60 | 45.3 |
| 124-769A-4H-4, 70–72 | 32.60 | 27.4 |
| 124-769B-4H-7, 39–41 | 33.79 | 32.6 |
| 124-769B-5H-1, 46–48 | 34.36 | 51.2 |
| 124-769B-5H-2, 75–77 | 36.15 | 19.4 |
| 124-769B-5H-4, 47–49 | 38.87 | 33.6 |
| 124-769B-5H-4, 75–77 | 39.15 | 12.3 |
| 124-769B-5H-5, 0–3 | 39.90 | 20.5 |
| 124-769B-5H-6, 75–77 | 42.15 | 30.3 |
| 124-769B-5H-7, 15–17 | 43.05 | 27.9 |
| 124-769B-6H-1, 56–58 | 43.96 | 29.3 |
| 124-769B-6H-2, 75–77 | 45.65 | 31.8 |
| 124-769B-6H-4, 53–55 | 48.43 | 30.3 |
| 124-769B-6H-4, 75–77 | 48.65 | 35.8 |
| 124-769B-6H-6, 0–3 | 50.90 | 34.5 |
| 124-769B-6H-6, 38–40 | 51.28 | 37.7 |
| 124-769B-6H-6, 75–77 | 51.65 | 41.0 |
| 124-769B-7H-1, 50–51 | 53.40 | 29.9 |
| 124-769B-7H-2, 92–94 | 55.32 | 37.6 |
| 124-769B-7H-3, 50–51 | 56.40 | 45.4 |
| 124-769B-7H-4, 105–107 | 58.45 | 25.5 |
| 124-769B-7H-5, 50–51 | 59.40 | 22.3 |
| 124-769B-7H-6, 0–3 | 60.40 | 50.5 |
| 124-769B-7H-6, 90–92 | 61.30 | 38.1 |
| 124-769B-7H-7, 50–51 | 62.40 | 32.7 |
| 124-769B-8H-2, 91–93 | 64.81 | 37.0 |
| 124-769B-8H-4, 91–93 | 67.81 | 30.2 |
| 124-769B-8H-6, 0–3 | 69.90 | 44.2 |
| 124-769B-8H-6, 91–93 | 70.81 | 47.5 |
| 124-769B-9H-2, 75–77 | 74.15 | 33.9 |
| 124-769B-9H-3, 0–3 | 74.90 | 48.4 |
| 124-769B-9H-4, 75–77 | 77.15 | 52.7 |
| 124-769B-9H-6, 75–77 | 80.15 | 35.4 |
| 124-769B-10H-1, 75–77 | 82.15 | 30.4 |
| 124-769B-10H-4, 0–3 | 85.90 | 35.1 |
| 124-769B-10H-4, 75–77 | 86.65 | 47.0 |
| 124-769B-10H-6, 75–77 | 89.65 | 39.5 |
| 124-769B-11H-1, 75–77 | 91.65 | 44.6 |
| 124-769B-11H-3, 0–3 | 93.90 | 40.7 |
| 124-769B-11H-4, 75–77 | 96.15 | 55.6 |
| 124-769B-11H-6, 75–77 | 99.15 | 35.2 |
| 124-769B-12H-1, 75–77 | 101.15 | 35.6 |
| 124-769B-12H-4, 0–3 | 104.90 | 42.1 |
| 124-769B-12H-4, 75–77 | 105.65 | 44.2 |
| 124-769B-13H-2, 70–72 | 112.10 | 22.7 |
| 124-769B-13H-4, 70–72 | 115.10 | 2.3 |
| 124-769B-13H-6, 0–3 | 117.40 | 0.8 |
| 124-769B-13H-6, 70–72 | 118.10 | 2.0 |
| 124-769B-14H-2, 65–67 | 121.55 | 2.4 |

**Table 9 (continued).**

| Core, section, interval (cm) | Depth (mbsf) | $CaCO_3$ (%) |
|---|---|---|
| 124-769B-14H-4, 66–68 | 124.56 | 3.8 |
| 124-769B-14H-6, 0–3 | 126.90 | 0.5 |
| 124-769B-14H-6, 70–72 | 127.60 | 3.7 |
| 124-769B-15H-2, 80–82 | 131.20 | 0.4 |
| 124-769B-15H-4, 80–82 | 134.20 | 0.2 |
| 124-769B-15H-6, 0–3 | 136.40 | 1.1 |
| 124-769B-15H-6, 80–82 | 137.20 | 0.3 |
| 124-769B-16H-1, 70–72 | 139.10 | 2.9 |
| 124-769B-16H-3, 70–72 | 142.10 | 3.9 |
| 124-769B-16H-5, 70–72 | 145.10 | 0.4 |
| 124-769B-16H-6, 0–3 | 145.90 | 0.2 |
| 124-769B-17H-1, 45–47 | 148.35 | 0.4 |
| 124-769B-17H-3, 95–97 | 151.85 | 1.7 |
| 124-769B-17H-5, 0–3 | 153.90 | 0.2 |
| 124-769B-17H-5, 95–97 | 154.85 | 0.5 |
| 124-769B-18H-1, 44–46 | 157.84 | 0.2 |
| 124-769B-18H-3, 44–46 | 160.84 | 0.2 |
| 124-769B-18H-5, 0–3 | 163.40 | 0.4 |
| 124-769B-18H-5, 44–46 | 163.84 | 0.2 |
| 124-769B-19H-4, 0–3 | 170.02 | 0.2 |
| 124-769B-20H-1, 111–113 | 174.41 | 0.3 |
| 124-769B-20H-3, 111–113 | 177.41 | 4.2 |
| 124-769B-20H-4, 0–3 | 177.80 | 0.5 |
| 124-769B-20H-6, 111–113 | 181.91 | 1.0 |
| 124-769B-21H-1, 100–102 | 183.80 | 0.2 |
| 124-769B-21H-3, 100–102 | 186.80 | 6.4 |
| 124-769B-21H-5, 0–3 | 188.80 | 2.8 |
| 124-769B-21H-5, 100–102 | 189.80 | 4.5 |
| 124-769B-22H-2, 70–72 | 194.50 | 1.2 |
| 124-769B-22H-4, 70–72 | 197.50 | 14.6 |
| 124-769B-22H-6, 0–3 | 199.80 | 0.5 |
| 124-769B-22H-6, 70–72 | 200.50 | 0.4 |
| 124-769B-23H-2, 70–72 | 204.00 | 0.7 |
| 124-769B-23H-4, 70–72 | 207.00 | 0.2 |
| 124-769B-23H-5, 0–3 | 207.80 | 0.2 |
| 124-769B-23H-6, 70–72 | 210.00 | 0.3 |
| 124-769B-24H-1, 80–82 | 212.10 | 0.5 |
| 124-769B-24H-4, 81–83 | 216.61 | 1.1 |
| 124-769B-24H-5, 0–3 | 217.30 | 0.3 |
| 124-769B-24H-6, 70–72 | 219.50 | 0.6 |
| 124-769B-25X-1, 80–82 | 221.60 | 1.2 |
| 124-769B-25X-3, 80–82 | 224.60 | 0.8 |
| 124-769B-25X-5, 80–82 | 227.60 | 0.6 |
| 124-769B-25X-6, 0–3 | 228.30 | 0.2 |
| 124-769B-26X-1, 80–82 | 231.20 | 0.7 |
| 124-769B-26X-3, 80–82 | 234.20 | 0.7 |
| 124-769B-26X-5, 0–3 | 236.40 | 0.2 |
| 124-769B-26X-5, 80–82 | 237.20 | 0.5 |
| 124-769B-27X-2, 70–72 | 242.30 | 0.5 |
| 124-769B-27X-4, 70–72 | 245.30 | 0.6 |
| 124-769B-27X-5, 0–3 | 246.10 | 0.2 |
| 124-769B-27X-6, 70–72 | 248.30 | 0.6 |
| 124-769B-28X-2, 70–72 | 251.90 | 0.5 |
| 124-769B-28X-4, 70–72 | 254.90 | 0.6 |
| 124-769B-28X-6, 0–3 | 257.20 | 0.1 |
| 124-769B-28X-6, 70–72 | 257.90 | 0.4 |
| 124-769B-29X-1, 26–28 | 259.66 | 0.4 |
| 124-769C-1R-1, 41–43 | 261.51 | 0.3 |
| 124-769C-1R-1, 131–133 | 262.41 | 0.2 |
| 124-769B-29X-3, 26–28 | 262.66 | 0.3 |
| 124-769B-29X-4, 0–3 | 263.90 | 0.1 |
| 124-769B-29X-5, 26–28 | 265.66 | 1.0 |
| 124-769B-30X-1, 95–97 | 269.95 | 1.4 |
| 124-769C-2R-1, 86–88 | 271.66 | 3.6 |
| 124-769B-30X-3, 95–97 | 272.95 | 0.9 |
| 124-769C-2R-3, 86–88 | 274.66 | 3.0 |
| 124-769B-30X-6, 0–3 | 276.50 | 1.7 |
| 124-769C-2R-5, 0–3 | 276.80 | 4.7 |
| 124-769B-30X-6, 95–97 | 277.45 | 1.5 |

hole (from 83 to 228 mbsf) are probably the result of the alteration of volcanic material (see "Silica" below).

### *Alkalinity, Sulfate, and Ammonium*

The depth distribution of alkalinity is shown in Figure 30. It increases from about 3 mM in the uppermost sample to a maximum value of 4.0 mM at 12 mbsf. Below this depth, the alkalinity decreases to the minimum value of 1.4 mM at 228 mbsf. The small increase in the last two samples may represent contamination with drilling fluid.

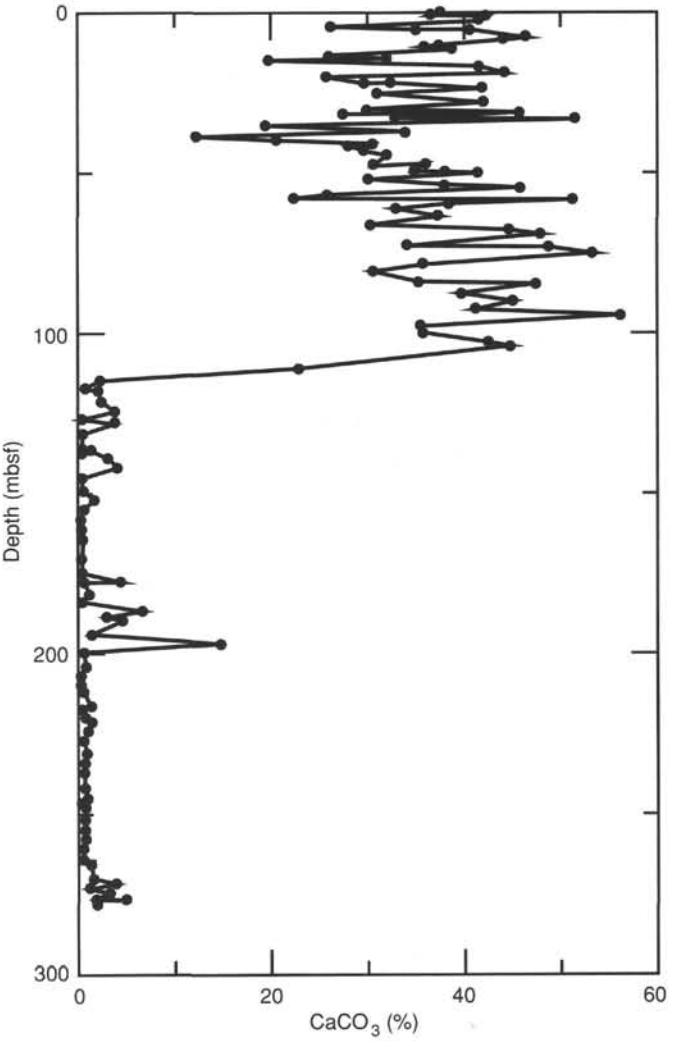


Figure 29. Downcore distribution of calcium carbonate, Site 769.

With the exception of one point at 12.85 mbsf, the sulfate concentration decreases with depth to a minimum value of 21.71 mM at 145.85 mbsf, resulting from the decomposition of organic matter by sulfate reduction. At this site and also at Site 768, the alkalinity distribution does not correspond to the observed decrease in dissolved sulfate (Fig. 31) in the uppermost carbonate-rich sediments. The alkalinity deficit implies that the pore water is saturated with respect to calcite and that bicarbonate has been removed from the pore water to form carbonates.

The downhole distribution of ammonium is also shown in Figure 30. Ammonium increases from 20 $\mu$M near the sediment surface to a maximum value of 92 $\mu$M at about 75 mbsf. The low levels of ammonium, as well as the lack of sulfate depletion, observed at this site are consistent with the low organic matter contents of the sediments (see "Organic Geochemistry" section, this chapter).

### *Silica*

Silica concentrations increase from 399 $\mu$M at 4.45 mbsf to 778 $\mu$M at 82.85 mbsf. They then drop sharply to values less than 300 $\mu$M, with a minimum value of 146 $\mu$M at 200 mbsf (Fig. 30). The variation in the dissolved silica profile in the up-

**Table 10. Interstitial water geochemical data, Site 769.**

| Core, section, interval (cm) | SBD (m) | Vol. ($cm^3$) | pH | Alk. (mM) | Sal. (g/kg) | $Mg^{2+}$ (mM) | $Ca^{2+}$ (mM) | $Cl^-$ (mM) | $SO_4^{2-}$ (mM) | $NH_4$ ($\mu$M) | $SiO_2$ ($\mu$M) | $Mg^{2+}/Ca^{2+}$ |
|---|---|---|---|---|---|---|---|---|---|---|---|---|
| 124-769B- | | | | | | | | | | | | |
| 1H-03, 145–150 | 4.45 | 50 | 7.67 | 2.951 | 35.5 | 52.07 | 10.66 | 550.00 | 26.59 | 20 | 399 | 4.88 |
| 2H-05, 145–150 | 12.85 | 56 | 7.57 | 4.001 | 35.5 | 49.70 | 11.07 | 548.00 | 29.36 | 24 | 520 | 4.49 |
| 3H-05, 145–150 | 22.35 | 67 | 7.53 | 3.443 | 35.5 | 47.42 | 11.70 | 552.00 | 26.38 | 50 | 638 | 4.05 |
| 4H-05, 145–150 | 31.85 | 59 | 7.39 | 3.927 | 35.3 | 47.16 | 11.96 | 544.00 | 26.15 | 55 | 694 | 3.94 |
| 5H-04, 145–150 | 39.85 | 65 | 7.52 | 3.895 | 35.5 | 45.21 | 12.90 | 542.00 | 25.67 | 71 | 709 | 3.50 |
| 6H-04, 145–150 | 49.35 | 45 | 7.52 | 3.448 | 35.0 | 44.14 | 13.33 | 547.00 | 25.71 | 60 | 737 | 3.31 |
| 7H-04, 145–150 | 58.85 | 50 | 7.54 | 2.815 | 35.0 | 43.32 | 13.61 | 542.00 | 24.87 | 89 | 778 | 3.18 |
| 8H-02, 145–150 | 65.35 | 47 | 7.46 | 3.013 | 35.2 | 42.99 | 14.88 | 547.00 | 24.72 | 91 | 735 | 2.89 |
| 9H-02, 145–150 | 74.85 | 58 | 7.39 | 3.000 | 35.0 | 41.78 | 15.61 | 549.00 | 23.44 | 92 | 765 | 2.68 |
| 10H-01, 145–150 | 82.85 | 48 | 7.38 | 2.894 | 35.0 | 40.38 | 16.78 | 548.00 | 23.58 | 73 | 778 | 2.41 |
| 13H-05, 145–150 | 117.35 | 54 | 7.97 | 2.826 | 33.0 | 36.55 | 21.40 | 543.00 | 21.71 | 51 | 305 | 1.71 |
| 16H-05, 145–150 | 145.85 | 35 | 7.85 | 1.784 | 34.5 | 33.03 | 24.60 | 539.00 | 21.84 | 32 | 191 | 1.34 |
| 19H-03, 140–150 | 169.92 | 30 | 7.99 | 1.897 | 34.8 | 32.11 | 29.14 | 547.00 | 22.88 | 41 | 178 | 1.10 |
| 22H-05, 140–150 | 199.70 | 20 | 8.09 | 1.354 | 34.8 | 31.40 | 32.20 | 543.00 | 23.02 | 36 | 146 | 0.98 |
| 25X-05, 140–150 | 228.20 | 8 | 7.71 | 1.381 | 34.5 | 34.61 | 33.54 | 538.00 | 23.98 | 29 | 193 | 1.03 |
| 28X-05, 140–150 | 257.10 | 11 | 7.33 | 1.587 | 34.5 | 40.32 | 31.13 | 544.00 | 26.71 | 34 | 264 | 1.30 |

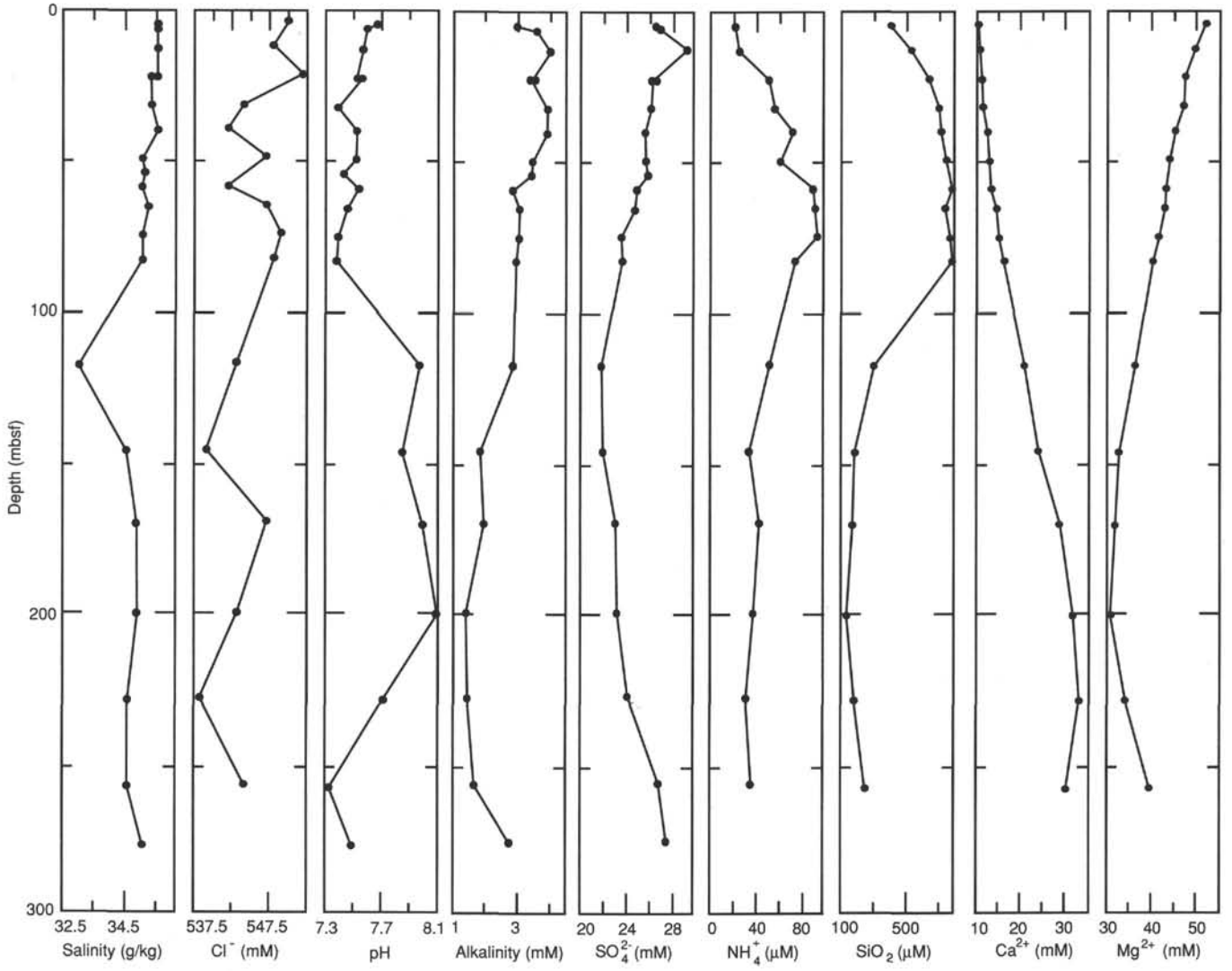


Figure 30. Summary of interstitial water analyses, Site 769, as a function of depth.

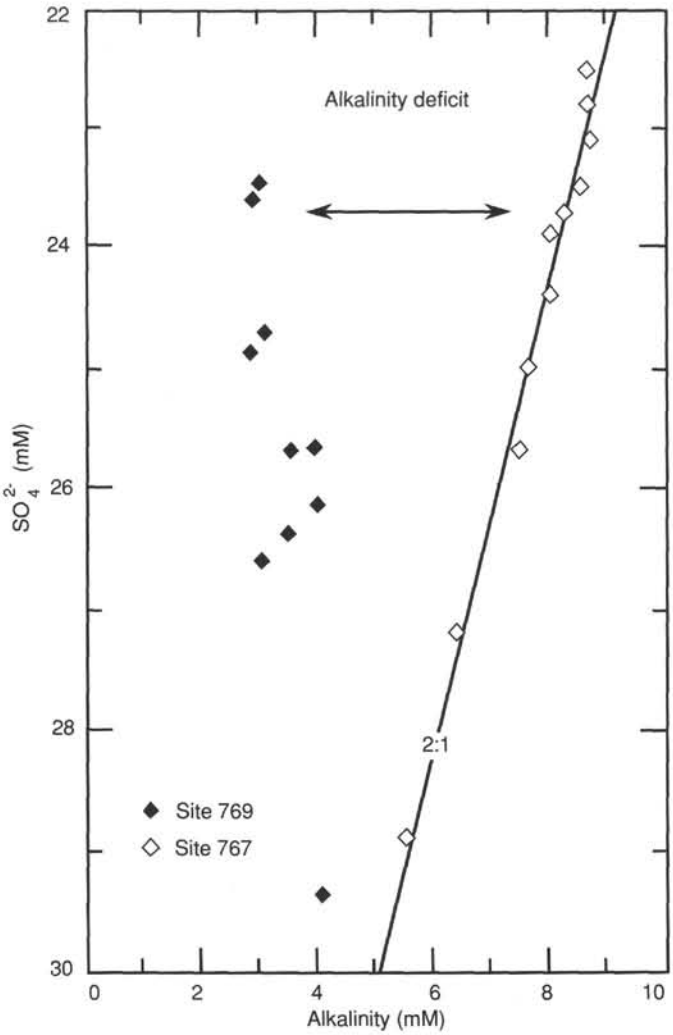


Figure 31. Relationship between alkalinity and dissolved sulfate in pore water from Sites 767 and 769. Note the deficit in dissolved alkalinity in Site 769 relative to the stoichiometric ratio for sulfate reduction shown by the pore-water samples from Site 767.

per 200 mbsf mirrors the pH distribution. Generally speaking, it is very similar to the variations found at Sites 767 and 768 and can be attributed to silicification reactions during the alteration of volcanic material (Kastner and Gieskes, 1976).

### *Calcium and Magnesium*

Dissolved calcium and magnesium distributions at Site 769 are shown in Figure 30. The observed increase in calcium concurrent with a magnesium decrease is a direct consequence of the alteration of volcanogenic material. The pH and silica distributions are also typical of the alteration of plagioclase and the formation of smectites (Kastner and Gieskes, 1976; Gieskes and Lawrence, 1981). These distributions were also observed within the sediment columns of Sites 767 and 768.

## ORGANIC GEOCHEMISTRY

The scientific purposes of Leg 124 shipboard organic geochemistry studies were outlined previously (see "Organic Geochemistry" section, "Site 767" chapter, this volume). The following summarizes the preliminary shipboard results for Site 769 (Cagayan Ridge and Sulu Sea).

### Samples

We collected 44 sediment samples from Site 769, 12 of which were obtained from Hole 769A, 31 from Hole 769B, and one sample from Hole 769C. We analyzed 29 of these sediments for their composition of light hydrocarbons by means of headspace gas analyses. Total organic carbon (TOC) content, hydrogen (HI) and oxygen (OI) indexes, and the maturity of the organic matter ($T_{max}$) were determined by Rock-Eval pyrolysis on all samples. Details of the analytical methods used are given in the "Explanatory Notes" chapter (this volume).

### Results and Discussion

#### *Amount, Type, and Maturity of Organic Matter*

The TOC values are below 0.5%. Given the amount of organic matter, three zones can be distinguished in the sedimentary column of Site 769 (Tables 11 and 12 and Fig. 32):

1. From 0 to 120 mbsf, TOC values are generally below 0.1%, corresponding to hemipelagic, carbonate-rich sediments. Olive-colored layers, rich in diatoms, are encountered in this zone sometimes; they display TOC values slightly higher (0.15%–0.20%) than in the surrounding sediments. The organic matter of these sediments was identified as marine amorphous on the basis of smear slide observation.
2. From 120 to 246 mbsf, TOC values range from 0.15% to 0.30%, corresponding to clayey sediments (see "Lithostratigraphy" section, this chapter). A maximum TOC value of 0.5% was observed at 170 mbsf.
3. Red clays between 246 and 277 mbsf are characterized by lower TOC values than in the zone above.

#### *Hydrocarbon Gases*

Background concentrations of methane were observed in all headspace gas samples (Table 12), indicating that no biogenic or thermogenic gas production is present in the sediments of Site 769.

### Conclusions

The sediments contain only low amounts of organic matter. Variations in the content of organic matter parallel the changes in lithology. No gas generation was observed in the sediments at Site 769.

## PHYSICAL PROPERTIES

### Introduction

The physical properties measured at Site 769 include wet-bulk density, grain density, porosity, water content, void ratio, and compressional wave velocities determined from discrete samples; continuous GRAPE (gamma ray attenuation porosity evaluation) and compressional wave velocities, as well as thermal conductivity and vane shear strength. Descriptions of the measurement procedures can be found in the "Explanatory Notes" chapter (this volume). The lithostratigraphic units used in this section are those described in the "Lithostratigraphy" section (this chapter).

Seismic velocities and index properties were measured on nearly all of the cores. The GRAPE bulk density measurements were made to a depth of 55 mbsf in Hole 769A and to 260 mbsf in Hole 769B. Thermal conductivity measurements were made on competent material in Holes 769A, 769B, and 769C. Vane shear strength measurements from Hole 769A were obtained to a depth of 55 mbsf. Tables 13–16 tabulate the various physical properties data. The variations of these properties with depth are illustrated in Figures 33–38.

**Table 11. Rock-Eval data, Site 769.**

| Core, section, interval (cm) | Depth (mbsf) | $S_1$ (mg/g) | $S_2$ (mg/g) | $S_3$ (mg/g) | TOC (%) | %C | HI | OI | $T_{max}$ (°C) | PI | $S_2/S_3$ |
|---|---|---|---|---|---|---|---|---|---|---|---|
| 124-769B-1H-1, 67-69 | 0.67 | 0.11 | 0.41 | 6.12 | 0.04 | 0.04 | 1025 | 15300 | 352 | 0.21 | 0.06 |
| 124-769A-1H-5, 0-3 | 6.00 | 0.14 | 0.76 | 4.56 | 0.10 | 0.07 | 760 | 4560 | 528 | 0.16 | 0.16 |
| 124-769A-2H-5, 0-3 | 14.40 | 0.15 | 0.71 | 4.32 | 0.09 | 0.07 | 788 | 4800 | 357 | 0.17 | 0.16 |
| 124-769B-3H-1, 19-22 | 15.09 | 0.04 | 0.23 | 2.88 | 0.02 | 0.02 | 1150 | 14400 | 304 | 0.15 | 0.07 |
| 124-769A-3H-5, 0-3 | 23.90 | 0.06 | 0.24 | 3.68 | 0.02 | 0.02 | 1200 | 18400 | 307 | 0.20 | 0.06 |
| 124-796B-4H-2, 111-115 | 27.01 | 0.19 | 0.92 | 4.52 | 0.17 | 0.09 | 541 | 2658 | 382 | 0.17 | 0.20 |
| 124-769B-4H-CC, 13-15 | 34.26 | 0.08 | 0.29 | 4.28 | 0.02 | 0.03 | 1450 | 21400 | 361 | 0.22 | 0.06 |
| 124-769A-4H-6, 0-3 | 34.90 | 0.12 | 0.45 | 4.02 | 0.06 | 0.04 | 750 | 6700 | 427 | 0.21 | 0.11 |
| 124-769A-5H-5, 0-3 | 42.90 | 0.05 | 0.32 | 3.07 | 0.03 | 0.03 | 1066 | 10233 | 307 | 0.14 | 0.10 |
| 124-769A-5H-5, 24-25 | 43.14 | 0.07 | 0.29 | 3.50 | 0.02 | 0.03 | 1450 | 17500 | 287 | 0.19 | 0.08 |
| 124-769A-5H-5, 29-30 | 43.19 | 0.10 | 0.49 | 3.84 | 0.14 | 0.04 | 350 | 2742 | 327 | 0.17 | 0.12 |
| 124-769A-5H-5, 31-32 | 43.21 | 0.12 | 0.40 | 4.30 | 0.15 | 0.04 | 266 | 2866 | 337 | 0.23 | 0.09 |
| 124-769A-5H-5, 32-33 | 43.22 | 0.13 | 0.39 | 4.52 | 0.17 | 0.04 | 229 | 2658 | 339 | 0.25 | 0.08 |
| 124-769A-5H-5, 35-36 | 43.25 | 0.17 | 0.58 | 3.72 | 0.06 | 0.06 | 966 | 6200 | 282 | 0.23 | 0.15 |
| 124-769B-6H-1, 140-144 | 44.80 | 0.10 | 0.57 | 3.19 | 0.11 | 0.05 | 518 | 2900 | 362 | 0.15 | 0.17 |
| 124-769A-6H-6, 0-3 | 53.90 | 0.12 | 0.49 | 3.98 | 0.06 | 0.05 | 816 | 6633 | 339 | 0.20 | 0.12 |
| 124-769A-7H-6, 0-3 | 63.40 | 0.11 | 0.35 | 3.70 | 0.05 | 0.03 | 700 | 7400 | 307 | 0.24 | 0.09 |
| 124-769B-8H-6, 0-3 | 69.90 | 0.07 | 0.22 | 4.16 | 0.03 | 0.02 | 733 | 13866 | 352 | 0.25 | 0.05 |
| 124-769B-9H-3, 0-3 | 74.90 | 0.13 | 0.57 | 3.54 | 0.06 | 0.05 | 950 | 5900 | 345 | 0.19 | 0.16 |
| 124-769B-10H-4, 0-3 | 85.90 | 0.07 | 0.51 | 3.17 | 0.07 | 0.04 | 728 | 4528 | 307 | 0.12 | 0.16 |
| 124-769B-11H-3, 0-3 | 93.90 | 0.05 | 0.44 | 4.00 | 0.05 | 0.04 | 880 | 8000 | 345 | 0.10 | 0.11 |
| 124-769B-11H-5, 79-83 | 97.69 | 0.07 | 0.41 | 4.48 | 0.03 | 0.04 | 1366 | 14933 | 349 | 0.15 | 0.09 |
| 124-769B-12H-4, 0-3 | 104.90 | 0.06 | 0.33 | 4.06 | 0.10 | 0.03 | 330 | 4060 | 343 | 0.16 | 0.08 |
| 124-769B-13H-6, 0-3 | 117.40 | 0.07 | 2.63 | 0.96 | 0.32 | 0.22 | 821 | 300 | 518 | 0.03 | 2.73 |
| 124-769B-14H-6, 0-3 | 126.90 | 0.02 | 1.73 | 0.50 | 0.24 | 0.14 | 720 | 208 | 484 | 0.01 | 3.46 |
| 124-769B-15H-6, 0-3 | 136.40 | 0.18 | 2.38 | 0.98 | 0.27 | 0.21 | 881 | 362 | 475 | 0.07 | 2.42 |
| 124-769B-16H-4, 31-33 | 143.21 | 0.05 | 1.83 | 0.66 | 0.20 | 0.15 | 915 | 330 | 457 | 0.03 | 2.77 |
| 124-769B-16H-6, 0-3 | 145.90 | 0.06 | 2.05 | 0.42 | 0.23 | 0.17 | 891 | 182 | 504 | 0.03 | 4.88 |
| 124-769B-17H-5, 0-3 | 153.90 | 0.05 | 1.42 | 0.45 | 0.19 | 0.12 | 747 | 236 | 477 | 0.03 | 3.15 |
| 124-769B-18H-5, 0-3 | 163.40 | 0.05 | 1.67 | 0.58 | 0.20 | 0.14 | 835 | 290 | 475 | 0.03 | 2.87 |
| 124-769B-19H-4, 0-3 | 170.02 | 0.12 | 1.81 | 0.49 | 0.50 | 0.16 | 362 | 98 | 474 | 0.06 | 3.69 |
| 124-769B-20H-4, 0-3 | 177.80 | 0.04 | 1.38 | 0.51 | 0.20 | 0.11 | 690 | 255 | 525 | 0.03 | 2.70 |
| 124-769B-20H-6, 31-35 | 181.11 | 0.08 | 1.21 | 1.16 | 0.22 | 0.10 | 550 | 527 | 561 | 0.06 | 1.04 |
| 124-769B-21H-5, 0-3 | 188.80 | 0.06 | 0.71 | 1.47 | 0.15 | 0.06 | 473 | 980 | 579 | 0.08 | 0.48 |
| 124-769B-22H-6, 0-3 | 199.80 | 0.05 | 1.46 | 0.31 | 0.22 | 0.12 | 663 | 140 | 487 | 0.03 | 4.70 |
| 124-769B-23H-5, 0-3 | 207.80 | 0.04 | 2.05 | 0.06 | 0.22 | 0.17 | 931 | 27 | 470 | 0.02 | 34.16 |
| 124-769B-24H-5, 0-3 | 217.30 | 0.03 | 1.41 | 0.27 | 0.19 | 0.12 | 742 | 142 | 468 | 0.02 | 5.22 |
| 124-769B-25X-6, 0-3 | 228.30 | 0.05 | 1.15 | 0.24 | 0.22 | 0.10 | 522 | 109 | 478 | 0.04 | 4.79 |
| 124-769B-26X-5, 0-3 | 236.40 | 0.08 | 2.79 | 0.23 | 0.29 | 0.23 | 962 | 79 | 453 | 0.03 | 12.13 |
| 124-769B-27X-5, 0-3 | 246.10 | 0.01 | 1.25 | 0.32 | 0.15 | 0.10 | 833 | 213 | 476 | 0.01 | 3.90 |
| 124-769B-28X-6, 0-3 | 257.20 | 0.07 | 0.87 | 0.23 | 0.09 | 0.07 | 966 | 255 | 450 | 0.07 | 3.78 |
| 124-769B-29X-4, 0-3 | 263.90 | 0.30 | 1.44 | 0.19 | 0.14 | 0.14 | 1028 | 135 | 449 | 0.17 | 7.57 |
| 124-769B-30X-6, 0-3 | 276.50 | 0.25 | 1.05 | 0.69 | 0.10 | 0.10 | 1050 | 690 | 460 | 0.19 | 1.52 |
| 124-769C-2R-5, 0-3 | 276.80 | 0.57 | 2.39 | 2.51 | 0.24 | 0.24 | 995 | 1045 | 582 | 0.19 | 0.95 |

Note: TOC = total organic carbon, HI = hydrogen index, OI = oxygen index, and PI = production index.

## Results

### *Index Properties*

Wet-bulk density, grain (or matrix) density, porosity, and water content (dry basis) of discrete samples from Site 769 are listed in Table 13. Bulk density data obtained from index property tests are compared with the bulk density values determined with the GRAPE technique (measurements were made every 5 cm on APC cores from Holes 769A and 769B) in Figure 33.

Samples were as representative as possible of the sediment section as a whole; however, several samples were taken from thinner layers of markedly different rock types that may represent only a minor part of the overall stratigraphic sequence drilled. Sample selection and the frequency of sampling depended on the relative thickness and homogeneity of a particular sequence.

Index properties are influenced by drilling and sampling disturbance and by the testing procedures used in the laboratory. For example, the water content of a particular sample could be increased by the drilling fluid (seawater) that often surrounded a disturbed core for many hours prior to a sample being removed from the core for analysis.

The variation of bulk density obtained from discrete sample measurements shows a pattern that closely reflects the lithostratigraphy at Site 769 (Fig. 33) (see "Lithostratigraphy" section, this chapter). The bulk densities measured in Unit I, a sequence of thin- to thick-bedded pelagic marls, range from about 1.40 g/cm$^3$ at the seafloor to about 1.50 g/cm$^3$ at the base of the unit (102 mbsf). The gradient of bulk density increase in Unit I is about 1 g/cm$^3$/km.

Bulk density in Unit II shows a linear increase with depth in Subunit IIA, increasing to about 1.85 g/cm$^3$ at the base of the unit (262 mbsf). The gradient observed in Subunit IIA is about 2.5 g/cm$^3$/km. Subunit IIB, composed of brown hemipelagic clay, shows a steep gradient of decreasing bulk density with depth, dropping from approximately 1.85 g/cm$^3$ at the top of the unit to about 1.5 g/cm$^3$ at the base of the unit. The bulk density of the volcaniclastic lapillistone of Unit III (278-377 mbsf) is generally invariant with depth, being approximately 2.10 g/cm$^3$ for the entire drilled interval.

Continuous GRAPE bulk density measurements were made in Holes 769A and 769B to a maximum depth of 260 mbsf (Fig. 34). Although the bulk densities cluster within a rather narrow range, which agrees closely with the discrete bulk density measurements (Fig. 33), the detailed pattern of GRAPE data shows a periodic variation downhole with an amplitude of roughly 0.15 g/cm$^3$ and a frequency of 25-30 m. This pattern may be the result of drilling disturbance.

**Table 12. Total organic carbon content and methane concentration of headspace gases from sediments of Site 769 (Carle GC).**

| Core, section, interval (cm) | Depth (mbsf) | TOC (%) | Methane (ppm) |
|---|---|---|---|
| 124-769A- | | | |
| 1H-5, 0–3 | 6.00 | 0.10 | 2.20 |
| 2H-5, 0–3 | 14.40 | 0.09 | 2.30 |
| 3H-5, 0–3 | 23.90 | 0.02 | 2.10 |
| 4H-2, 111–115 | 30.03 | | |
| 4H-6, 0–3 | 34.90 | 0.06 | 2.30 |
| 5H-5, 0–3 | 42.90 | 0.03 | 2.30 |
| 5H-5, 24–25 | 43.14 | 0.02 | |
| 5H-5, 29–30 | 43.19 | 0.14 | |
| 5H-5, 31–32 | 43.21 | 0.15 | |
| 5H-5, 32–33 | 43.22 | 0.17 | |
| 5H-5, 35–36 | 43.25 | 0.06 | |
| 6H-6, 0–3 | 53.90 | 0.06 | 2.00 |
| 7H-6, 0–3 | 63.40 | 0.05 | 2.40 |
| 124-769B- | | | |
| 1H-1, 67–69 | 0.68 | 0.04 | |
| 3H-1, 19–22 | 15.09 | 0.02 | |
| 4H-CC, 13–15 | 33.53 | 0.02 | |
| 6H-1, 140–144 | 43.80 | 0.11 | |
| 8H-6, 0–3 | 69.90 | 0.03 | 2.10 |
| 9H-3, 0–3 | 74.90 | 0.06 | 2.10 |
| 10H-4, 0–3 | 85.90 | 0.07 | 2.20 |
| 11H-3, 0–3 | 93.90 | 0.05 | 2.40 |
| 11H-5, 79–83 | 97.70 | 0.03 | |
| 12H-4, 0–3 | 104.90 | 0.10 | 2.20 |
| 13H-6, 0–3 | 117.40 | 0.32 | 2.10 |
| 14H-6, 0–3 | 126.90 | 0.24 | 2.20 |
| 15H-6, 0–3 | 136.40 | 0.27 | 2.00 |
| 16H-4, 31–33 | 133.40 | 0.20 | |
| 16H-6, 0–3 | 145.90 | 0.23 | 2.10 |
| 17H-5, 0–3 | 153.90 | 0.19 | 2.20 |
| 18H-5, 0–3 | 163.40 | 0.20 | 2.30 |
| 19H-4, 0–3 | 170.40 | 0.50 | 2.20 |
| 20H-4, 0–3 | 177.80 | 0.20 | 2.60 |
| 20H-6, 31–35 | 179.61 | 0.22 | |
| 21H-5, 0–3 | 188.80 | 0.15 | 2.50 |
| 22H-6, 0–3 | 199.80 | 0.22 | 2.30 |
| 23H-5, 0–3 | 207.80 | 0.22 | 2.40 |
| 24H-5, 0–3 | 217.30 | 0.19 | 2.30 |
| 25X-6, 0–3 | 228.30 | 0.22 | 2.20 |
| 26X-5, 0–3 | 236.40 | 0.29 | 2.40 |
| 27X-5, 0–3 | 246.10 | 0.15 | 1.80 |
| 28X-6, 0–3 | 247.60 | 0.09 | |
| 29X-4, 0–3 | 263.90 | 0.14 | 2.50 |
| 30X-6, 0–3 | 276.50 | 0.10 | 2.20 |

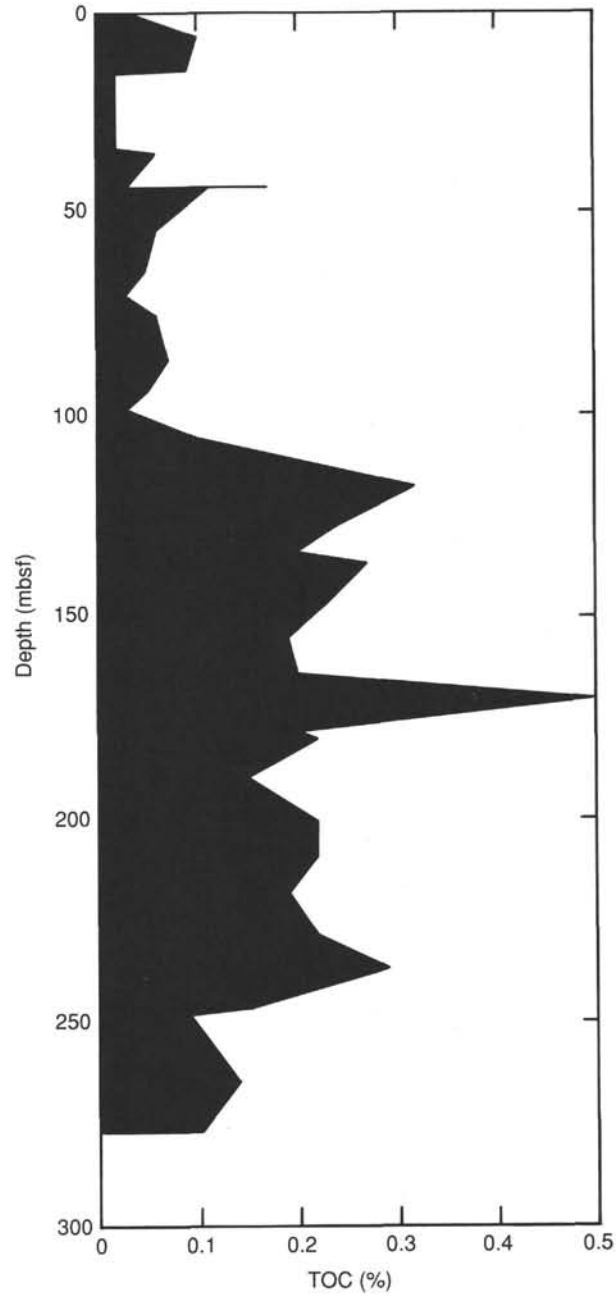


Figure 32. Total organic carbon (TOC) content of sediment samples from Cagayan Ridge, Site 769.

Grain densities at Site 769 accurately reflect the main lithologic units drilled. The pelagic marl of Unit I shows variable grain densities between 2.35 and 2.75 g/cm$^3$. The grain density of Unit II is fairly constant at about 2.72 g/cm$^3$. Subunit IIB, however, exhibits a marked decrease in grain density with depth, reaching roughly 2.55–2.60 g/cm$^3$ at the top of Unit III. Unit III grain density is variable around a mean value of about 2.50 g/cm$^3$, significantly lower than that of overlying Unit II.

The porosity of Unit I is uniform at 80%–85% (Fig. 33). Together with Unit II, porosity shows an overall decrease with depth. Superimposed on this trend, however, are periodic oscillations similar to those observed in the GRAPE bulk density data. Subunit IIB shows a rapid increase of porosity with depth. Porosity values reach a high of nearly 80% at 278 mbsf, at the top of Unit III. The porosity of the Unit III lapillistone is 30%–40% and exhibits no consistent variability with depth.

Water content at Site 769 shows a nonlinear decrease as a function of depth, with the greatest rate of change occurring near the seafloor. The water content of the sediment near the seafloor ranges from 150% to 215% and decreases to roughly 50% at the base of Subunit IIA (Fig. 33). However, as seen in the bulk density and porosity data, a strong reversal of trend occurs in Subunit IIB. Water content increases rapidly from near 50% to as much as 125% downward through Subunit IIB, despite the effects of gravitational loading from the overlying sedimentary section. The water content of the lapillistone of Unit III is consistently less than 25%.

Figure 33 shows that the void ratio (the ratio of voids to solids) follows a pattern similar to that of water content. This is to be expected for material completely saturated with fluid.

### *Velocity*

The compressional wave velocities of discrete samples from Holes 769B and 769C are tabulated in Table 14 and plotted in Figure 35. The velocity plot shows a near-constant velocity of

**Table 13. Index property data, Site 769.**

| Core, section, interval (cm) | Depth (mbsf) | Wet-bulk density (%) | Grain density (%) | Porosity (%) | Water content (%) | Void ratio |
|---|---|---|---|---|---|---|
| 124-769A- | | | | | | |
| 1H-1, 62-64 | 0.62 | 1.31 | 2.43 | 84.2 | 192.4 | 5.33 |
| 1H-2, 62-64 | 2.12 | 1.35 | 2.76 | 85.2 | 183.9 | 5.77 |
| 1H-3, 62-64 | 3.62 | 1.37 | 2.66 | 83.0 | 162.6 | 4.88 |
| 1H-4, 62-64 | 5.12 | 1.42 | 2.72 | 82.2 | 144.6 | 4.60 |
| 1H-5, 62-64 | 6.62 | 1.37 | 2.61 | 82.6 | 162.4 | 4.74 |
| 2H-1, 70-72 | 9.10 | 1.39 | 2.71 | 82.2 | 152.8 | 4.60 |
| 2H-5, 70-72 | 15.10 | 1.37 | 2.68 | 83.7 | 167.6 | 5.14 |
| 3H-2, 50-52 | 19.90 | 1.39 | 2.56 | 79.8 | 142.5 | 3.94 |
| 3H-4, 50-52 | 22.90 | 1.35 | 2.64 | 84.0 | 176.6 | 5.25 |
| 3H-6, 50-52 | 25.90 | 1.42 | 2.60 | 79.2 | 134.1 | 3.80 |
| 4H-2, 70-72 | 29.60 | 1.33 | 2.54 | 83.5 | 179.0 | 5.05 |
| 4H-4, 70-72 | 32.60 | 1.33 | 2.64 | 85.1 | 188.6 | 5.69 |
| 4H-6, 70-72 | 35.60 | 1.39 | 2.80 | 82.3 | 153.2 | 4.65 |
| 5H-2, 75-77 | 39.15 | 1.45 | 3.12 | 67.2 | 90.6 | 2.05 |
| 5H-4, 75-77 | 42.15 | 1.44 | 2.59 | 78.2 | 124.8 | 3.58 |
| 6H-2, 75-77 | 48.65 | 1.38 | 2.70 | 83.3 | 163.3 | 5.00 |
| 6H-4, 75-77 | 51.65 | 1.41 | 2.57 | 80.8 | 142.9 | 4.20 |
| 6H-6, 75-77 | 54.65 | 1.39 | 2.73 | 83.4 | 158.6 | 5.01 |
| 7H-1, 50-51 | 56.40 | 1.38 | 2.50 | 80.8 | 149.0 | 4.20 |
| 7H-3, 50-51 | 59.40 | 1.39 | 2.57 | 80.6 | 145.5 | 4.17 |
| 7H-5, 50-51 | 62.40 | 1.39 | 2.57 | 81.2 | 148.8 | 4.32 |
| 7H-7, 50-51 | 65.40 | 1.39 | 2.50 | 80.6 | 146.9 | 4.16 |
| 124-769B- | | | | | | |
| 1H-1, 129-131 | 1.29 | 1.39 | 2.64 | 82.5 | 156.1 | 4.73 |
| 1H-2, 44-46 | 1.94 | 1.36 | 2.84 | 88.1 | 196.2 | 7.38 |
| 1H-3, 52-54 | 3.52 | 1.34 | 2.52 | 82.6 | 170.4 | 4.73 |
| 1H-4, 47-49 | 4.97 | 1.33 | 2.76 | 85.5 | 192.1 | 5.88 |
| 2H-1, 101-103 | 6.41 | 1.35 | 2.67 | 83.6 | 173.7 | 5.11 |
| 2H-3, 102-104 | 9.42 | 1.35 | 2.49 | 84.4 | 178.3 | 5.39 |
| 2H-5, 98-100 | 12.38 | 1.35 | 2.61 | 83.9 | 176.6 | 5.21 |
| 2H-7, 43-45 | 14.83 | 1.34 | 2.49 | 83.6 | 176.9 | 5.09 |
| 3H-1, 65-67 | 15.55 | 1.52 | 2.58 | 71.3 | 92.8 | 2.48 |
| 3H-3, 64-66 | 18.54 | 1.44 | 2.72 | 80.0 | 131.8 | 3.99 |
| 3H-6, 50-52 | 22.90 | 1.45 | 2.63 | 77.1 | 118.7 | 3.36 |
| 4H-1, 35-37 | 24.75 | 1.38 | 2.59 | 81.4 | 153.9 | 4.38 |
| 4H-4, 40-42 | 29.30 | 1.38 | 2.62 | 81.3 | 151.4 | 4.35 |
| 4H-7, 39-41 | 33.79 | 1.33 | 2.56 | 83.5 | 179.3 | 5.08 |
| 5H-1, 46-48 | 34.36 | 1.35 | 2.65 | 83.5 | 172.9 | 5.07 |
| 5H-4, 47-49 | 38.87 | 1.44 | 2.61 | 77.6 | 124.0 | 3.47 |
| 5H-7, 15-17 | 43.05 | 1.41 | 2.71 | 80.2 | 139.6 | 4.05 |
| 6H-1, 56-58 | 43.96 | 1.38 | 2.53 | 79.9 | 146.2 | 3.97 |
| 6H-4, 53-55 | 48.43 | 1.44 | 2.62 | 77.2 | 121.9 | 3.38 |
| 6H-6, 38-40 | 51.28 | 1.38 | 2.60 | 80.3 | 146.7 | 4.09 |
| 7H-2, 92-94 | 55.32 | 1.44 | 2.69 | 77.9 | 125.1 | 3.53 |
| 7H-4, 105-107 | 58.45 | 1.39 | 2.51 | 78.9 | 140.1 | 3.75 |
| 7H-6, 90-92 | 61.30 | 1.28 | 2.43 | 86.1 | 219.4 | 6.19 |
| 8H-2, 91-93 | 64.81 | 1.37 | 2.52 | 80.5 | 150.5 | 4.13 |
| 8H-4, 91-93 | 67.81 | 1.43 | 2.63 | 79.7 | 134.3 | 3.94 |
| 8H-6, 91-93 | 70.81 | 1.41 | 2.61 | 80.4 | 141.2 | 4.09 |
| 9H-2, 75-77 | 74.15 | 1.44 | 2.66 | 78.2 | 124.5 | 3.59 |
| 9H-4, 75-77 | 77.15 | 1.45 | 2.60 | 76.7 | 117.9 | 3.30 |
| 9H-6, 75-77 | 80.15 | 1.47 | 2.66 | 76.6 | 114.2 | 3.28 |
| 10H-1, 75-77 | 82.15 | 1.52 | 2.67 | 73.9 | 99.3 | 2.83 |
| 10H-4, 75-77 | 86.65 | 1.42 | 2.64 | 80.1 | 136.8 | 4.02 |
| 10H-6, 75-77 | 89.65 | 1.50 | 2.65 | 76.1 | 107.4 | 3.18 |
| 11H-1, 75-77 | 91.65 | 1.35 | 2.35 | 80.7 | 157.2 | 4.18 |
| 11H-4, 75-77 | 96.15 | 1.42 | 2.62 | 79.2 | 134.0 | 3.81 |
| 11H-6, 75-77 | 99.15 | 1.38 | 2.65 | 82.8 | 158.7 | 4.80 |
| 12H-1, 75-77 | 101.15 | 1.40 | 2.71 | 81.8 | 149.3 | 4.51 |
| 12H-4, 75-77 | 105.65 | 1.38 | 2.54 | 79.9 | 144.8 | 3.99 |
| 13H-2, 70-72 | 112.10 | 1.50 | 2.63 | 74.9 | 104.6 | 2.98 |
| 13H-4, 70-72 | 115.10 | 1.47 | 2.69 | 76.9 | 115.6 | 3.33 |
| 13H-6, 70-72 | 118.10 | 1.50 | 2.65 | 75.8 | 106.7 | 3.13 |
| 14H-2, 65-67 | 121.55 | 1.48 | 2.71 | 77.7 | 116.6 | 3.48 |
| 14H-4, 66-68 | 124.56 | 1.52 | 2.67 | 75.3 | 103.0 | 3.04 |
| 14H-6, 70-72 | 127.60 | 1.64 | 2.69 | 68.7 | 75.5 | 2.20 |
| 15H-2, 80-82 | 131.20 | 1.50 | 2.63 | 72.3 | 97.7 | 2.62 |
| 15H-4, 80-82 | 134.20 | 1.60 | 2.80 | 71.2 | 83.5 | 2.47 |
| 15H-6, 80-82 | 137.20 | 1.54 | 2.67 | 67.0 | 80.0 | 2.03 |
| 16H-1, 70-72 | 139.10 | 1.61 | 2.78 | 69.6 | 79.3 | 2.29 |
| 16H-3, 70-72 | 142.10 | 1.67 | 2.69 | 64.0 | 64.3 | 1.78 |
| 16H-5, 70-72 | 145.10 | 1.61 | 2.65 | 67.5 | 75.1 | 2.08 |
| 17H-1, 45-47 | 148.35 | 1.55 | 2.73 | 72.3 | 91.0 | 2.61 |
| 17H-3, 95-97 | 151.85 | 1.65 | 2.79 | 68.2 | 73.1 | 2.14 |
| 17H-5, 95-97 | 154.85 | 1.69 | 2.70 | 65.2 | 65.5 | 1.87 |
| 18H-1, 44-46 | 157.84 | 1.65 | 2.70 | 64.6 | 66.7 | 1.82 |
| 18H-3, 44-46 | 160.84 | 1.59 | 2.75 | 69.6 | 81.4 | 2.29 |
| 18H-5, 44-46 | 163.84 | 1.65 | 2.67 | 65.7 | 69.3 | 1.92 |
| 20H-1, 111-113 | 174.41 | 1.63 | 2.73 | 67.3 | 73.1 | 2.06 |
| 20H-3, 111-113 | 177.41 | 1.61 | 2.80 | 69.5 | 79.0 | 2.28 |
| 20H-6, 111-113 | 181.91 | 1.65 | 2.81 | 69.4 | 75.6 | 2.27 |
| 21H-1, 100-102 | 183.80 | 1.60 | 2.65 | 68.1 | 77.5 | 2.13 |
| 21H-3, 100-102 | 186.80 | 1.56 | 2.63 | 71.0 | 87.1 | 2.45 |
| 21H-5, 100-102 | 189.80 | 1.65 | 2.66 | 67.1 | 71.7 | 2.04 |
| 22H-2, 70-72 | 194.50 | 1.65 | 2.72 | 67.1 | 71.3 | 2.04 |
| 22H-4, 70-72 | 197.50 | 1.63 | 2.72 | 68.3 | 74.9 | 2.16 |
| 22H-6, 70-72 | 200.50 | 1.66 | 2.71 | 67.7 | 72.1 | 2.10 |
| 23H-2, 70-72 | 204.00 | 1.66 | 2.65 | 65.9 | 68.3 | 1.94 |
| 23H-4, 70-72 | 207.00 | 1.59 | 2.76 | 71.9 | 86.6 | 2.56 |
| 23H-6, 70-72 | 210.00 | 1.67 | 2.68 | 67.2 | 69.9 | 2.05 |
| 24H-4, 81-83 | 216.61 | 1.80 | 2.76 | 78.4 | 80.7 | 3.63 |
| 24H-6, 70-72 | 219.50 | 1.83 | 2.69 | 74.9 | 72.3 | 2.98 |
| 25X-3, 80-82 | 224.60 | 1.79 | 2.76 | 80.7 | 85.8 | 4.17 |
| 25X-5, 80-82 | 227.60 | 1.72 | 2.69 | 63.0 | 60.3 | 1.70 |
| 26X-1, 80-82 | 231.20 | 1.86 | 2.69 | 79.2 | 77.3 | 3.80 |
| 26X-3, 80-82 | 234.20 | 1.82 | 2.68 | 57.8 | 48.4 | 1.37 |
| 26X-5, 80-82 | 237.20 | 1.87 | 2.64 | 52.9 | 40.9 | 1.12 |
| 27X-2, 70-72 | 242.30 | 1.78 | 2.65 | 57.9 | 49.8 | 1.38 |
| 27X-4, 70-72 | 245.30 | 1.82 | 2.70 | 58.2 | 48.7 | 1.39 |
| 27X-6, 70-72 | 248.30 | 1.85 | 2.70 | 56.5 | 45.6 | 1.30 |
| 28X-2, 70-72 | 251.90 | 1.75 | 2.66 | 59.9 | 54.0 | 1.49 |
| 28X-4, 70-72 | 254.90 | 1.74 | 2.65 | 61.1 | 56.3 | 1.57 |
| 28X-6, 70-72 | 257.90 | 1.82 | 2.72 | 59.2 | 50.1 | 1.45 |
| 29X-1, 26-28 | 259.66 | 1.70 | 2.68 | 64.3 | 63.2 | 1.80 |
| 29X-3, 26-28 | 262.66 | 1.88 | 2.62 | 74.9 | 69.1 | 2.99 |
| 29X-5, 26-28 | 265.66 | 1.62 | 2.55 | 68.3 | 75.8 | 2.16 |
| 30X-1, 95-97 | 269.95 | 1.53 | 2.78 | 75.3 | 101.3 | 3.06 |
| 30X-3, 95-97 | 272.95 | 1.44 | 2.64 | 78.5 | 126.2 | 3.65 |
| 30X-6, 95-97 | 277.45 | 1.45 | 2.52 | 76.5 | 118.5 | 3.26 |
| 31X-1, 80-82 | 279.50 | 2.20 | 2.57 | 38.0 | 21.5 | 0.61 |
| 31X-CC, 33-35 | 281.32 | 2.58 | 2.64 | 20.5 | 8.9 | 0.26 |
| 124-769C- | | | | | | |
| 1R-1, 41-43 | 261.51 | 1.80 | 2.76 | 59.7 | 51.4 | 1.48 |
| 1R-1, 131-133 | 262.41 | 1.74 | 2.61 | 63.5 | 59.6 | 1.74 |
| 2R-1, 86-88 | 271.66 | 1.50 | 2.59 | 76.5 | 109.8 | 3.25 |
| 2R-3, 86-88 | 274.66 | 1.50 | 2.75 | 78.1 | 114.6 | 3.56 |
| 2R-5, 86-88 | 277.66 | 1.51 | 2.66 | 76.1 | 106.4 | 3.19 |
| 3R-1, 122-124 | 281.72 | 2.15 | 2.53 | 35.3 | 20.3 | 0.55 |
| 4R-1, 74-76 | 290.94 | 2.21 | 2.48 | 24.3 | 12.7 | 0.32 |
| 4R-2, 80-82 | 292.5 | 2.57 | 2.53 | 15.5 | 6.6 | 0.18 |
| 4R-3, 56-58 | 293.41 | 2.68 | 2.68 | 5.1 | 2.0 | 0.05 |
| 5R-1, 37-37 | 300.07 | 2.00 | 2.51 | 41.8 | 27.2 | 0.72 |
| 5R-2, 29-31 | 301.28 | 2.04 | 2.44 | 35.0 | 21.3 | 0.54 |
| 5R-3, 116-118 | 303.37 | 2.17 | 2.43 | 42.1 | 24.8 | 0.73 |
| 6R-1, 76-78 | 310.06 | 2.06 | 2.45 | 35.7 | 21.6 | 0.56 |
| 6R-2, 56-58 | 311.34 | 2.03 | 2.48 | 39.1 | 24.5 | 0.64 |
| 7R-1, 66-68 | 319.66 | 2.08 | 2.61 | 40.7 | 25.2 | 0.69 |
| 8R-1, 54-56 | 329.14 | 2.08 | 2.49 | 29.1 | 16.7 | 0.41 |
| 8R-3, 65-67 | 331.75 | 2.13 | 2.43 | 38.0 | 22.3 | 0.61 |
| 9R-2, 52-54 | 340.19 | 2.11 | 2.49 | 33.0 | 19.1 | 0.49 |
| 10R-2, 51-53 | 349.81 | 2.05 | 2.58 | 41.5 | 26.3 | 0.71 |
| 11R-2, 118-120 | 360.28 | 2.11 | 2.53 | 36.0 | 21.2 | 0.56 |
| 12R-1, 8-10 | 367.28 | 2.08 | 2.46 | 32.4 | 18.9 | 0.48 |
| 12R-2, 134-136 | 370.04 | 2.03 | 2.48 | 37.5 | 23.3 | 0.60 |
| 12R-6, 8-10 | 374.64 | 2.11 | 2.49 | 31.1 | 17.7 | 0.45 |

about 1.55 km/s in Unit I (1 point in Unit I) and Unit II. No velocity measurements were made in Subunit IIB. The contact between the hemipelagic sediments and the lapillistone is reflected in an abrupt increase in velocity from approximately 1.55 km/s in the hemipelagic clay to roughly 3.0 km/s in the lapillistone.

We acquired the *P*-wave logger data from the upper 260 m of sediment at Site 769 (Fig. 36). These data show a gradual increase in velocity through Unit I, with a well-defined reversal of velocity gradient at the Units I/II contact, followed by a distinct increase in velocity to the base of Subunit IIA.

### *Thermal Conductivity*

Thermal conductivities of cores from Holes 769A, 769B, and 769C are given in Table 15 and are graphically presented in Fig-

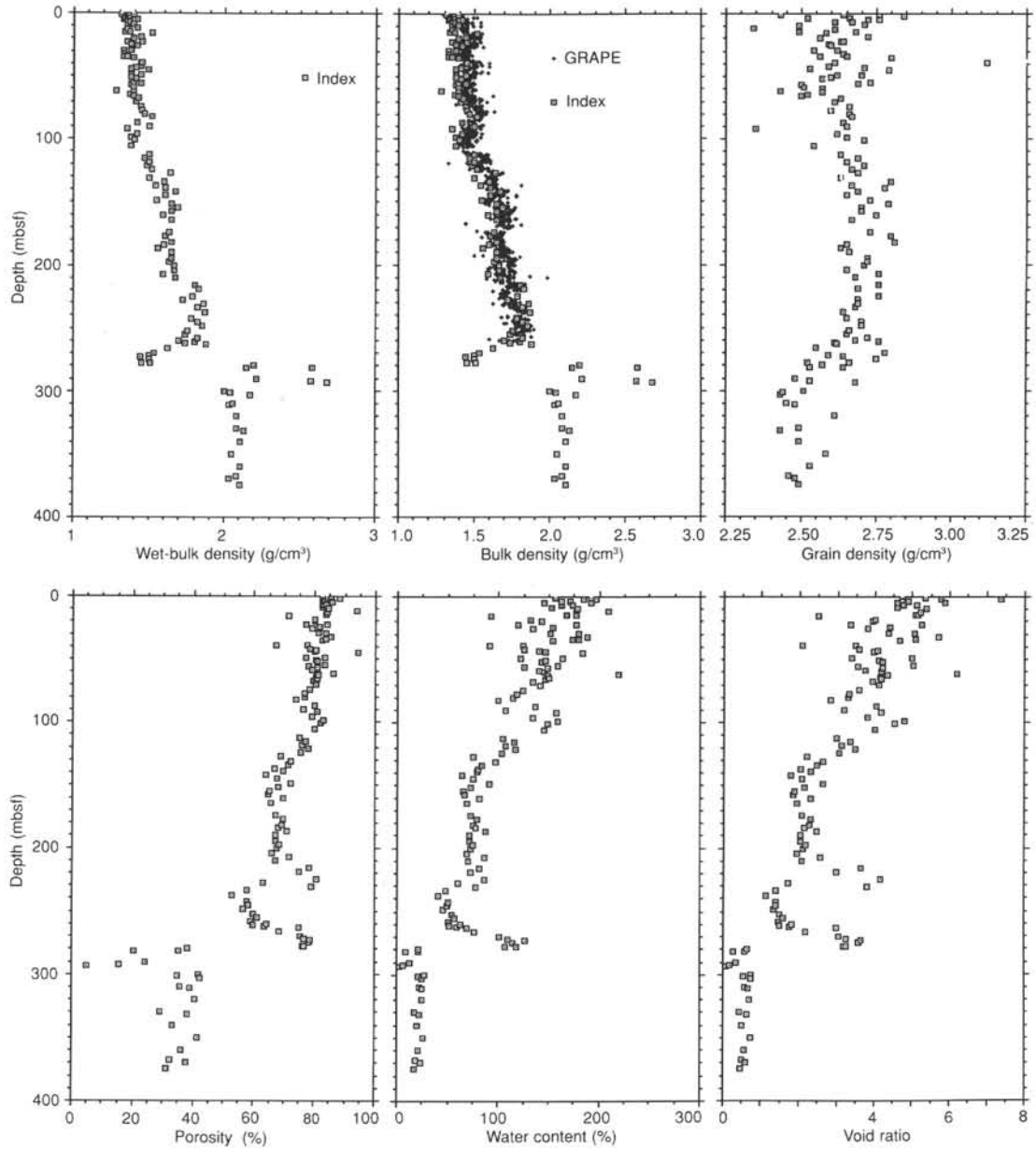


Figure 33. Downhole changes in index properties (wet-bulk density, GRAPE bulk density, grain density, porosity, water content, and void ratios), Site 769.

ure 37. All values measured in Units I and II were obtained by means of probes inserted through the core liners into full core sections. An attempt was made to insert the probes at locations along each core section that appeared to be the least disturbed. However, an annulus of disturbed sediment and drill fluid was often present along the inside of the liner, preventing visual identification of the more intact segments of the core. The core sections were allowed to reach thermal equilibrium in the laboratory (about 24°C), which usually required between 2 and 3 hr. Conductivity measurements were then obtained over a 9–12-min period.

The thermal conductivity of the lapillistone of Unit III was determined with the half-space technique using polished segments 8–15 cm long taken from the split core. Core samples were placed in a saltwater bath at room temperature and allowed to reach thermal equilibrium prior to taking readings over a 9-min period with a single thermal probe.

Thermal conductivity at Site 769 ranges from ~0.9 to 1.0 W/m·K at the seafloor and increases with depth to ~260 mbsf, the base of Subunit IIA, where it reaches ~1.35 W/m·K. Below 260 mbsf, thermal conductivity rapidly decreases through Subunit IIB to the top of Unit III, dropping to roughly 0.95 W/m·K. Thermal conductivity in Unit III is ~1.15 W/m·K, with one measurement of nearly 1.40 W/m·K.

### *Vane Shear Strength*

Values of undrained shear strength were obtained with a four-bladed motorized vane shear apparatus on samples taken from APC cores from Hole 769A. The hydraulic piston cores displayed evidence of sample disturbance; thus, the measured shear strengths may vary significantly from those *in situ*. The resulting peak and remolded shear strengths are given in Table 16 and plotted as a function of depth in Figure 38. The vane was set to rotate at about 90°/min, which generally resulted in 8°–14° of

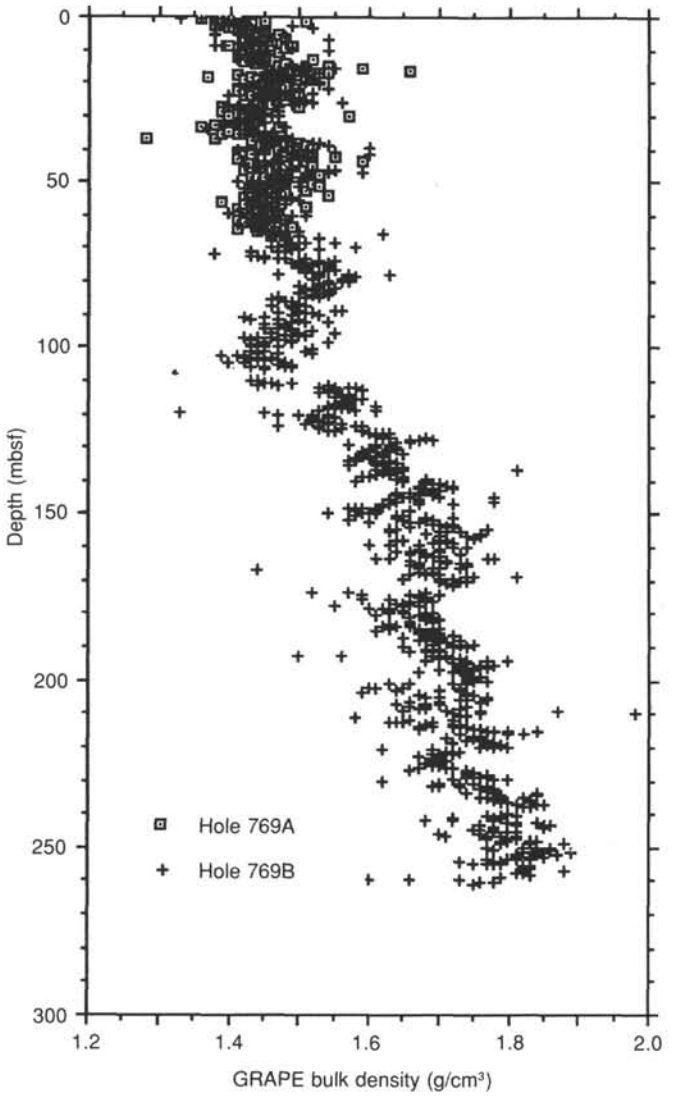


Figure 34. Detailed plot of GRAPE bulk density vs. depth to 300 mbsf, Holes 769A and 769B.

rotation before peak shear strength was achieved. The vane was permitted to continue rotation for at least 120°, allowing the shear strength to drop to a constant value for determination of the remolded shear strength.

Undrained peak shear strength increases rapidly with increasing depth below seafloor until a depth of approximately 18 mbsf is reached. Below this depth, the rate of increase in undrained peak shear strength gradually drops. Shear strength extrapolates to zero at the seafloor and increases to about 30 kPa at 18 mbsf. By 55 mbsf, shear strength increased to approximately 50 kPa. Below about 55 mbsf, we ended shear vane testing because the failure mechanism around the vane became dominated by cracks that propagated away from the ends of the vane. Given the cylindrical failure surface around the vane, the equations for shear strength determination were no longer valid. The remolded shear strength displayed a similar increase with depth over the interval from 0 to 55 mbsf, with typical sensitivities ranging from 2 to 4.

## Conclusions

In general, all physical properties measured at Site 769 displayed depth-dependent variations. Bulk density increased with depth in Units I and II, almost certainly a result of compaction caused by gravitational loading, but bulk density values were constant in Unit III. This observation is corroborated by the porosities, water contents, and void ratios, which decreased with depth in Units I and II but showed little variation in Unit III. Grain densities showed a slight increase with depth in Unit I and were essentially constant in Unit II; in Unit III, however, they were lower than in Unit II. Subunit IIB is a zone of high inverse gradient for most of the properties measured. The contrast in physical properties at the boundary between the hemipelagic sediments and the volcaniclastic Unit III is well-defined. Compressional wave velocity provides an unambiguous indicator of the contacts between the hemipelagic and volcaniclastic rocks. Thermal conductivities were variable but showed an increase with depth in the upper 260 m at Site 769. The volcaniclastic rocks yielded low values of thermal conductivity, and peak shear strength displayed a strong increase with depth over the interval from 0 to 55 mbsf.

**Table 14. Compressional wave velocity data, Site 769.**

| Core, section, interval (cm) | Depth (mbsf) | Velocity (km/s) |
|---|---|---|
| 124-769B- | | |
| 9H-2, 84–86 | 74.24 | 1.51 |
| 14H-7, 8–10 | 128.48 | 1.61 |
| 14H-7, 38–40 | 128.78 | 1.67 |
| 15H-5, 39–41 | 135.29 | 1.55 |
| 16H-2, 61–63 | 140.51 | 1.62 |
| 19H-1, 112–114 | 168.02 | 1.52 |
| 20H-6, 96–98 | 181.76 | 1.53 |
| 22H-1, 103–105 | 193.33 | 1.52 |
| 22H-4, 100–102 | 197.80 | 1.52 |
| 23H-6, 82–84 | 210.12 | 1.56 |
| 25X-1, 83–85 | 221.63 | 1.55 |
| 25X-7, 22–24 | 230.02 | 1.57 |
| 26X-1, 76–79 | 231.16 | 1.58 |
| 26X-5, 83–85 | 237.23 | 1.61 |
| 27X-2, 68–70 | 242.28 | 1.59 |
| 28X-1, 60–63 | 250.30 | 1.58 |
| 31X-CC, 33–35 | 281.32 | 4.46 |
| 124-769C- | | |
| 3R-1, 122–124 | 281.72 | 3.27 |
| 3R-2, 41–43 | 282.41 | 4.67 |
| 4R-1, 74–76 | 290.94 | 3.90 |
| 4R-2, 80–82 | 292.50 | 4.72 |
| 4R-3, 56–58 | 293.41 | 5.52 |
| 5R-1, 37–39 | 300.07 | 2.96 |
| 5R-2, 29–31 | 301.28 | 3.14 |
| 5R-3, 116–118 | 303.37 | 3.18 |
| 6R-1, 76–78 | 310.06 | 3.40 |
| 6R-2, 56–58 | 311.34 | 2.95 |
| 7R-1, 66–68 | 319.66 | 2.81 |
| 8R-1, 54–56 | 329.14 | 3.24 |
| 8R-3, 65–67 | 331.75 | 3.29 |
| 9R-2, 52–54 | 340.19 | 3.30 |
| 10R-2, 51–53 | 349.81 | 2.91 |
| 11R-2, 118–120 | 360.28 | 3.18 |
| 12R-1, 8–10 | 367.28 | 3.00 |
| 12R-2, 134–136 | 370.04 | 2.85 |
| 12R-6, 8–10 | 374.64 | 3.17 |

## SEISMIC STRATIGRAPHY

Site 769 is located on multichannel seismic Line SO49-07 acquired on board the *Sonne* in April 1987 and processed by the Bundesanstalt für Geowissenschaften und Rohstoffe (BGR) in February 1988 (see Hinz and Block, this volume, and backpocket figure). In addition, pre-site single-channel seismic reflection data were shot on board the *JOIDES Resolution* prior to drilling on 13 December 1988 (see "Underway Geophysics" chapter, this volume). *Sonne* navigation was obtained with tran-

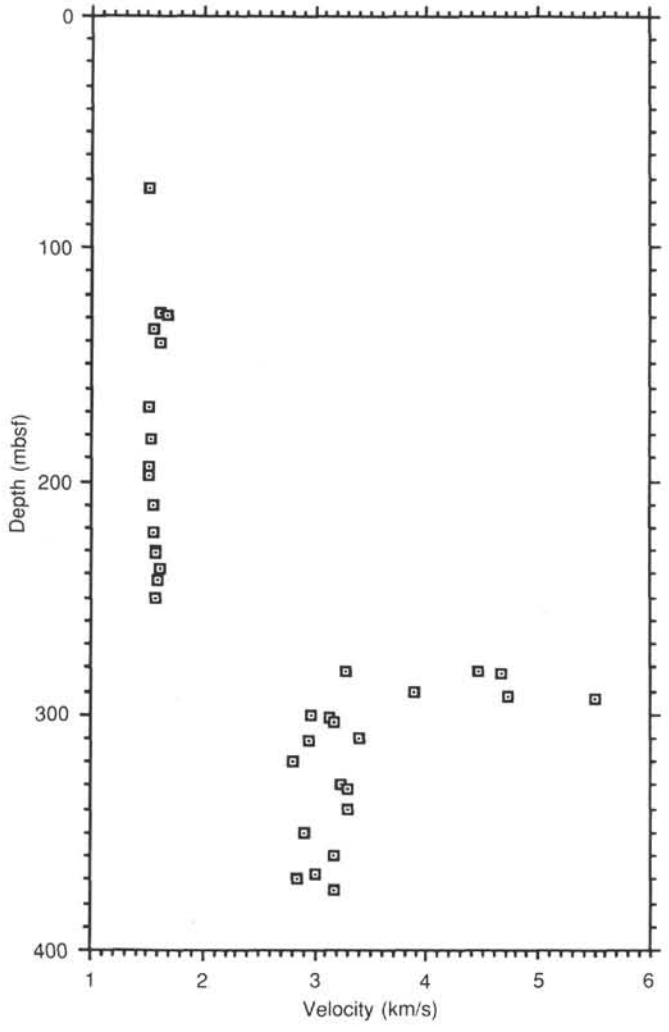


Figure 35. Hamilton Frame compressional velocity vs. depth, Site 769.

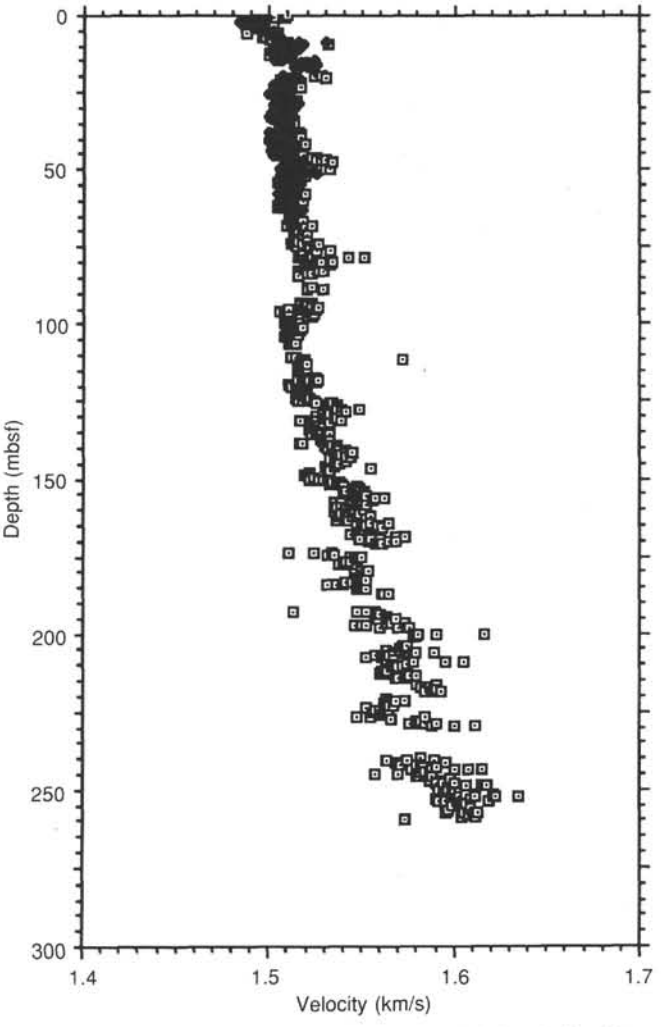


Figure 36. Comparison of compressional wave velocities obtained from the Hamilton Frame and *P*-wave logger, 0–300 mbsf.

sit satellites, Loran C, and doppler sonar. The *JOIDES Resolution* used the global positioning system (GPS) for the entire survey.

More regional data include a small detailed bathymetric map provided to the scientific party by Scripps Institution of Oceanography (SIO). A multichannel seismic line, CEPM 15 (Mascle and Biscarrat, 1978), and a single-channel seismic line collected by *J. Charcot* in 1984 (DJAMAN cruise) complete the data base for this area.

The site is located along the southeastern edge of the Cagayan Ridge and is flanked by the southeast Sulu Sea abyssal plain. The SeaBeam map shows that the site is located on the flank of an elongated ridge that can be interpreted as volcanic because of the presence of several conical peaks. Seismic surveying with the *JOIDES Resolution* has confirmed the general south-directed slope. Seismic Line SO49-07 cuts obliquely across what seems to be the apron of the volcano. This volcanic edifice apparently is separated from the higher parts of the Cagayan Ridge by another fault scarp (CEPM 15 and shot point 2200) and a small depression identified at the intersection of Lines SO49-06 and SO49-07 (Fig. 39).

Site 769 is located on a gentle (2.5°) slope in a position similar to that of shot point 624 on Line SO49-07 (Figs. 40 and 41). The mud line is marked by numerous channels and levees, indicating important bottom-current activity. The site is located ex- (Fig. 42). Line SO49-07 is a migrated depth section and shows the following seismic stratigraphy:

1. Seismic Sequence 1 is 130 m thick and shows discontinuous low-energy reflectors, interrupted by numerous small normal faults.

2. Seismic Sequence 2, 130–140 m thick, shows the same characteristics as Sequence 1 but is truncated by the overlying unit. The faults are synthetic with the slope, shallow dipping, and interpreted as the result of gravity sliding. Identified slumps within the section at this depth support this hypothesis.

3. Seismic Sequence 3, 20–30 m thick, is marked by a thin, transparent layer above a high-amplitude reflector. This sequence could represent the brown clay unit drilled just above Sequence 4 or the altered upper part of this sequence. Discrepancies between the depth of this seismic sequence and the depth of the unit drilled at Site 769 may be explained by the offset of the drilled site from Line SO49-07.

4. Seismic Sequence 4 is separated from the overlying sequence by the high-amplitude reflector mentioned above. Most of the faults observed in the sequences above do not affect Seismic Sequence 4. Consequently, the reflector separating Se-

**Table 15. Thermal conductivity data, Site 769.**

| Core, section, interval (cm) | Depth (mbsf) | Thermal conductivity (W/m·K) |
|---|---|---|
| 124-769A- | | |
| 1H-1, 78–79 | 0.78 | 0.8939 |
| 1H-4, 23–24 | 4.73 | 0.9881 |
| 1H-6, 29–30 | 7.79 | 0.9247 |
| 2H-1, 70–71 | 9.10 | 0.9509 |
| 2H-3, 70–71 | 12.10 | 0.9026 |
| 2H-4, 70–71 | 13.60 | 0.9288 |
| 2H-6, 70–71 | 16.60 | 0.9653 |
| 3H-1, 50–51 | 18.40 | 0.8952 |
| 3H-3, 50–51 | 21.40 | 0.9231 |
| 3H-4, 50–51 | 22.90 | 0.9433 |
| 3H-6, 50–51 | 25.90 | 0.9632 |
| 4H-2, 75–76 | 29.65 | 0.9290 |
| 4H-5, 75–76 | 34.15 | 0.9600 |
| 5H-2, 75–76 | 39.15 | 0.9980 |
| 5H-5, 75–76 | 43.65 | 0.9280 |
| 6H-2, 50–51 | 48.40 | 0.9030 |
| 6H-5, 50–51 | 52.90 | 0.9920 |
| 7H-2, 50–51 | 57.90 | 0.9420 |
| 7H-5, 50–51 | 62.40 | 0.9170 |
| 124-769B- | | |
| 1H-1, 120–121 | 1.20 | 0.9731 |
| 1H-2, 75–76 | 2.25 | 0.8865 |
| 1H-3, 75–76 | 3.75 | 0.9583 |
| 1H-4, 40–41 | 4.90 | 0.9401 |
| 2H-1, 75–76 | 6.15 | 0.9601 |
| 2H-3, 75–76 | 9.15 | 0.9382 |
| 2H-5, 75–76 | 12.15 | 0.9349 |
| 2H-7, 40–41 | 14.80 | 0.9129 |
| 3H-1, 75–76 | 15.65 | 0.9778 |
| 3H-3, 75–76 | 18.65 | 0.9465 |
| 3H-5, 75–76 | 21.65 | 0.9534 |
| 3H-7, 30–31 | 24.20 | 0.9200 |
| 4H-1, 75–76 | 25.15 | 0.9924 |
| 4H-3, 75–76 | 28.15 | 0.8989 |
| 4H-5, 75–76 | 31.15 | 0.9283 |
| 4H-7, 40–41 | 33.80 | 0.9361 |
| 5H-1, 75–76 | 34.65 | 0.9411 |
| 5H-3, 75–76 | 37.65 | 0.9550 |
| 5H-5, 75–76 | 40.65 | 0.9774 |
| 5H-7, 35–36 | 43.25 | 0.9450 |
| 6H-1, 75–76 | 44.15 | 0.9521 |
| 6H-3, 75–76 | 47.15 | 0.9974 |
| 6H-5, 75–76 | 50.15 | 0.9908 |
| 6H-7, 40–41 | 52.80 | 0.9634 |
| 7H-1, 75–76 | 53.65 | 0.9564 |
| 7H-3, 75–76 | 56.65 | 0.9834 |
| 7H-5, 75–76 | 59.65 | 0.9808 |
| 7H-7, 35–36 | 62.25 | 0.9945 |
| 8H-1, 75–76 | 63.15 | 0.9462 |
| 8H-3, 75–76 | 66.15 | 0.9849 |
| 8H-5, 75–76 | 69.15 | 0.9912 |
| 8H-7, 40–41 | 71.80 | 0.9669 |
| 9H-1, 75–76 | 72.65 | 0.9353 |
| 9H-3, 75–76 | 75.65 | 0.9807 |
| 9H-5, 75–76 | 78.65 | 1.0060 |
| 9H-7, 40–41 | 81.30 | 0.9934 |
| 10H-1, 75–76 | 82.15 | 1.0230 |
| 10H-3, 75–76 | 85.15 | 0.9498 |
| 10H-5, 75–76 | 88.15 | 1.0236 |
| 10H-7, 40–41 | 90.80 | 1.0092 |
| 11H-1, 75–76 | 91.65 | 0.9688 |
| 11H-3, 75–76 | 94.65 | 0.9718 |
| 11H-5, 75–76 | 97.65 | 1.0193 |
| 11H-7, 40–41 | 100.30 | 0.9498 |
| 12H-1, 75–76 | 101.15 | 0.9391 |
| 12H-3, 75–76 | 104.15 | 0.9367 |
| 12H-4, 75–76 | 105.65 | 0.9981 |
| 12H-5, 25–26 | 106.65 | 0.9299 |
| 13H-2, 70–71 | 112.10 | 1.0503 |
| 13H-5, 70–71 | 116.60 | 1.0061 |
| 14H-2, 70–71 | 121.60 | 0.9998 |
| 14H-5, 70–71 | 126.10 | 1.0541 |
| 15H-2, 80–81 | 131.20 | 1.0520 |

**Table 15 (continued).**

| Core, section, interval (cm) | Depth (mbsf) | Thermal conductivity (W/m·K) |
|---|---|---|
| 124-769B- | | |
| 15H-5, 80–81 | 135.70 | 1.1329 |
| 16H-2, 80–81 | 140.70 | 1.1664 |
| 16H-5, 80–81 | 145.20 | 1.2157 |
| 17H-2, 70–71 | 150.10 | 1.0717 |
| 17H-5, 70–71 | 154.60 | 1.0898 |
| 18H-2, 70–71 | 159.60 | 1.1519 |
| 18H-5, 70–71 | 164.10 | 1.1772 |
| 19H-1, 80–81 | 167.70 | 1.1602 |
| 19H-4, 80–81 | 170.82 | 1.1905 |
| 20H-2, 80–81 | 175.60 | 1.0933 |
| 20H-5, 80–81 | 180.10 | 1.1725 |
| 21H-1, 75–76 | 183.55 | 1.1599 |
| 21H-3, 75–76 | 186.55 | 1.1420 |
| 21H-5, 75–76 | 189.55 | 1.1208 |
| 21H-6, 75–76 | 191.05 | 0.9217 |
| 22H-1, 75–76 | 193.05 | 1.2617 |
| 22H-3, 75–76 | 196.05 | 1.3258 |
| 22H-5, 75–76 | 199.05 | 1.3444 |
| 22H-6, 75–76 | 200.55 | 1.2494 |
| 23H-1, 75–76 | 202.55 | 1.1677 |
| 23H-3, 75–76 | 205.55 | 1.1211 |
| 23H-5, 75–76 | 208.55 | 1.0765 |
| 23H-7, 25–26 | 211.05 | 1.2680 |
| 24H-1, 75–76 | 212.05 | 1.1477 |
| 24H-3, 75–76 | 215.05 | 1.1943 |
| 24H-5, 75–76 | 218.05 | 1.1822 |
| 24H-6, 75–76 | 219.55 | 1.2386 |
| 27X-1, 75–76 | 240.85 | 1.2962 |
| 27X-3, 75–76 | 243.85 | 1.2341 |
| 27X-5, 75–76 | 246.85 | 1.2890 |
| 27X-6, 75–76 | 248.35 | 1.3385 |
| 29X-1, 75–76 | 260.15 | 1.1615 |
| 29X-2, 75–76 | 261.65 | 1.1391 |
| 29X-4, 75–76 | 264.65 | 1.3341 |
| 29X-5, 35–36 | 265.75 | 1.1509 |
| 30X-1, 75–76 | 269.75 | 1.0189 |
| 30X-3, 75–76 | 272.75 | 0.9834 |
| 30X-5, 75–76 | 275.75 | 0.9367 |
| 30X-7, 25–26 | 278.25 | 0.9810 |
| 1R-1, 75–76 | 261.85 | 1.0580 |
| 1R-2, 25–26 | 262.85 | 1.0690 |
| 2R-1, 75–76 | 271.55 | 1.0350 |
| 2R-3, 75–76 | 274.55 | 0.9930 |
| 2R-4, 75–76 | 276.05 | 0.9830 |
| 2R-5, 75–76 | 277.50 | 0.9740 |
| 4R-3, 48–56 | 293.33 | 1.3870 |
| 5R-2, 21–28 | 301.20 | 1.1420 |
| 7R-1, 92–96 | 319.92 | 1.1410 |

quences 3 and 4 can be interpreted as a decollement surface for the slumps above.

On Figure 41, Seismic Sequence 4 is 75–100 m thick, on the basis of an assumed stacking velocity of 1751 m/s. However, measurements of compressional velocities made on board the *JOIDES Resolution* give average velocities of 4600 m/s for the cores in Seismic Sequence 4. Consequently, this sequence is more than 250 m thick. It corresponds to the massive and poorly stratified coarse tuff and lapillistone drilled at the base of Hole 769C. This sequence shows discontinuous reflectors in a fairly transparent zone. Seismic Sequence 4 is continuous in the seismic records across the surveyed topographic high.

5. The underlying Seismic Sequence 5 is poorly reflective and can also be traced across the ridge. Many discontinuous, moderate-amplitude reflectors indicate the presence of rough stratification, probably disrupted by faults. Normal faults are identified at the top of the sequence where they are sealed by Sequence 4. Some of these faults are antithetic and can be conjugate with normal faults controlling the main escarpment.

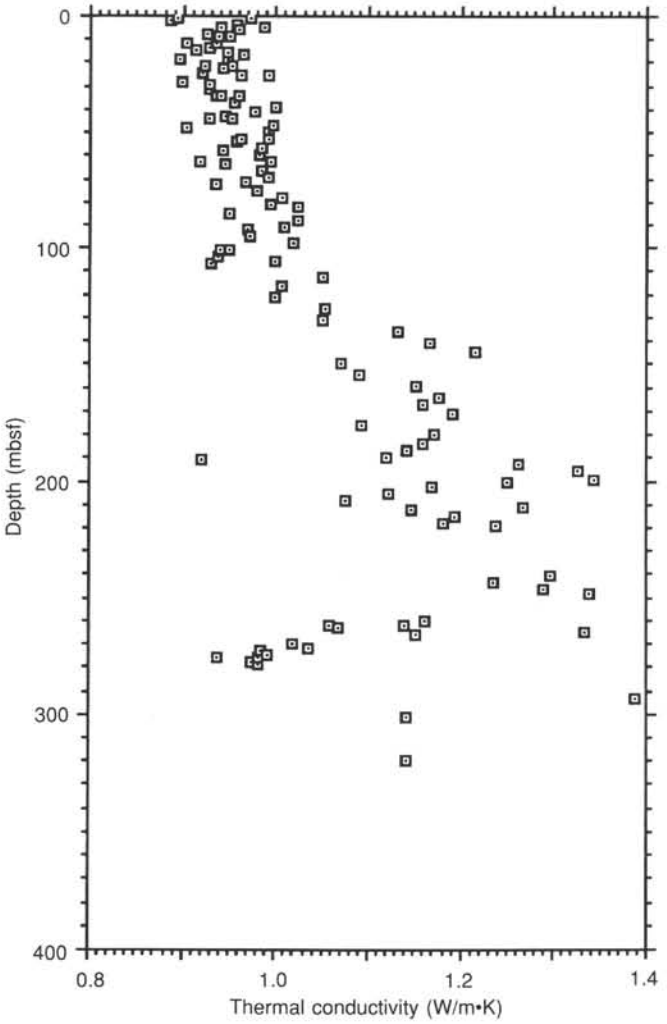


Figure 37. Thermal conductivity vs. depth, Site 769.

The base of Seismic Sequence 5 possibly occurs as deep as 650 mbsf on Line SO49-07 (Fig. 40), at which point the reflectors lose coherency. This thick seismic sequence, not reached by drilling at Site 769, may be stratified volcaniclastic and volcanic rocks. The layers within the sequence dip toward the southeast when present and may indicate a large amount of volcanic material erupted along the southeast flank of the Cagayan Ridge.

## SUMMARY AND CONCLUSIONS

Site 769 was located on the southeast flank of the Cagayan Ridge, in 3643.6 mbsl of water. The purpose of the site was to determine the Neogene paleoceanographic history of the enclosed Sulu Sea basin, at a site that was thought to lie above the CCD and to be protected from turbidite deposition. A secondary objective was to determine the nature of the basement of the Cagayan Ridge and to relate the basement and stratigraphic information to the results of Site 768 within the Sulu Sea.

Hole 769A was spudded in on 14 December 1988, and we recovered the first core at 1745 (UTC). We recovered seven APC cores at Hole 769A and then drilled Hole 769B, which re-cored the same interval with a 3-m offset to obtain duplicate cores and to avoid gaps in the uppermost part of the record. Hole 769B reached a depth of 290.2 mbsf with the APC and XCB, at which point volcanic tuff was encountered. We then switched to RCB coring. Hole 769C began at depth 261.1 mbsf to re-core the lower 30 m of sediment, which was thought to be very important for dating purposes, and continued to a total depth of 376.9 mbsf. We reached volcaniclastic material at 278 mbsf and cored Hole 769C continuously to 376.9 mbsf.

The following synthetic succession was obtained in these three holes:

Unit I (0–102.1 mbsf) is late Pliocene to Holocene in age. The dominant lithology is thin- to thick-bedded nannofossil marl with foraminifers, interpreted as a mixture of pelagic biogenic

**Table 16. Shear strength data, Site 769.**

| Core, section, interval (cm) | Depth (mbsf) | Shear strength (kPa) | | Sensitivity |
|---|---|---|---|---|
| | | Peak | Remolded | |
| 124-769A- | | | | |
| 1H-1, 116–117 | 1.16 | 2.1 | 0.9 | 2.3 |
| 1H-2, 51–52 | 2.01 | 2.3 | 1.1 | 2.1 |
| 1H-2, 126–127 | 2.76 | 4.3 | 2.7 | 1.6 |
| 1H-3, 23–24 | 3.23 | 3.6 | 2.3 | 1.6 |
| 1H-3, 99–100 | 3.99 | 7.6 | 4.5 | 1.7 |
| 1H-4, 20–21 | 4.70 | 7.0 | 4.1 | 1.7 |
| 1H-4, 95–96 | 5.45 | 10.4 | 5.0 | 2.1 |
| 1H-5, 47–48 | 6.47 | 16.2 | 8.5 | 1.9 |
| 1H-5, 128–129 | 7.28 | 9.0 | 5.2 | 1.7 |
| 2H-1, 36–37 | 8.76 | 19.8 | 9.0 | 2.2 |
| 2H-1, 98–99 | 9.38 | 16.2 | 9.0 | 1.8 |
| 2H-2, 30–31 | 10.20 | 15.3 | 7.2 | 2.1 |
| 2H-2, 129–130 | 11.19 | 14.0 | 6.3 | 2.2 |
| 2H-3, 125–126 | 12.65 | 16.7 | 9.0 | 1.9 |
| 2H-4, 53–54 | 13.43 | 20.5 | 9.4 | 2.2 |
| 2H-4, 132–133 | 14.22 | 21.6 | 7.9 | 2.7 |
| 2H-5, 10–11 | 14.50 | 22.1 | 13.1 | 1.7 |
| 2H-6, 38–39 | 16.28 | 44.1 | 14.9 | 3.0 |
| 2H-6, 130–131 | 17.20 | 34.0 | 19.4 | 1.8 |
| 3H-2, 16–17 | 19.56 | 25.7 | 9.4 | 2.7 |
| 3H-2, 96–97 | 20.36 | 27.5 | 12.6 | 2.2 |
| 3H-3, 50–51 | 21.40 | 18.9 | 8.5 | 2.2 |
| 3H-3, 73–74 | 21.63 | 19.4 | 8.5 | 2.3 |
| 3H-4, 26–27 | 22.66 | 25.7 | 9.4 | 2.7 |
| 3H-4, 125–126 | 23.65 | 23.9 | | |
| 3H-5, 62–63 | 24.52 | 23.9 | 9.0 | 2.7 |
| 3H-5, 92–93 | 24.82 | 18.0 | 9.0 | 2.0 |
| 3H-6, 43–44 | 25.83 | 36.9 | 18.0 | 2.1 |
| 3H-6, 136–137 | 26.76 | 24.8 | 9.1 | 2.7 |
| 4H-1, 97–98 | 28.37 | 19.4 | 9.0 | 2.2 |
| 4H-2, 41–42 | 29.31 | 25.2 | 12.6 | 2.0 |
| 4H-2, 94–95 | 29.84 | 18.2 | | |
| 4H-3, 63–64 | 31.03 | 31.7 | 13.1 | 2.4 |
| 4H-3, 120–121 | 31.60 | 39.2 | | |
| 4H-4, 51–52 | 32.41 | 27.9 | 13.5 | 2.1 |
| 4H-4, 101–102 | 32.91 | 31.5 | 13.5 | 2.3 |
| 4H-5, 42–43 | 33.82 | 30.6 | 11.3 | 2.7 |
| 4H-5, 122–123 | 34.62 | 25.0 | 11.3 | 2.2 |
| 4H-6, 45–46 | 35.35 | 28.8 | | |
| 4H-6, 136–137 | 36.26 | 30.2 | 13.1 | 2.3 |
| 5H-1, 44–45 | 37.34 | 32.9 | 13.5 | 2.4 |
| 5H-1, 111–112 | 38.01 | 30.6 | 13.5 | 2.3 |
| 5H-2, 41–42 | 38.81 | 32.4 | 13.7 | 2.4 |
| 5H-2, 117–118 | 39.57 | 43.7 | 13.5 | 3.2 |
| 5H-3, 12–13 | 40.02 | 26.1 | | |
| 5H-3, 98–99 | 40.88 | 31.5 | 10.8 | 2.9 |
| 5H-4, 45–46 | 41.85 | 38.7 | 16.7 | 2.3 |
| 5H-4, 136–137 | 42.76 | 36.0 | 17.5 | 2.1 |
| 5H-5, 46–47 | 43.36 | 43.0 | | |
| 5H-5, 99–100 | 43.89 | 32.4 | | |
| 5H-6, 41–42 | 44.81 | 34.0 | | |
| 5H-6, 117–118 | 45.57 | 46.8 | 16.7 | 2.8 |
| 5H-7, 67–68 | 46.57 | 35.1 | 13.1 | 2.7 |
| 6H-1, 81–82 | 47.21 | 39.4 | 15.8 | 2.5 |
| 6H-2, 54–55 | 48.44 | 47.3 | 15.8 | 3.0 |
| 6H-3, 97–98 | 50.37 | 36.2 | | |
| 6H-4, 113–114 | 52.03 | 37.4 | 15.3 | 2.4 |
| 6H-5, 87–88 | 53.27 | 38.3 | 14.5 | 2.6 |
| 6H-6, 15–16 | 54.05 | 40.5 | | |
| 6H-6, 50–51 | 54.40 | 52.2 | 19.4 | 2.7 |
| 6H-6, 125–126 | 55.15 | 48.6 | 18.9 | 2.6 |

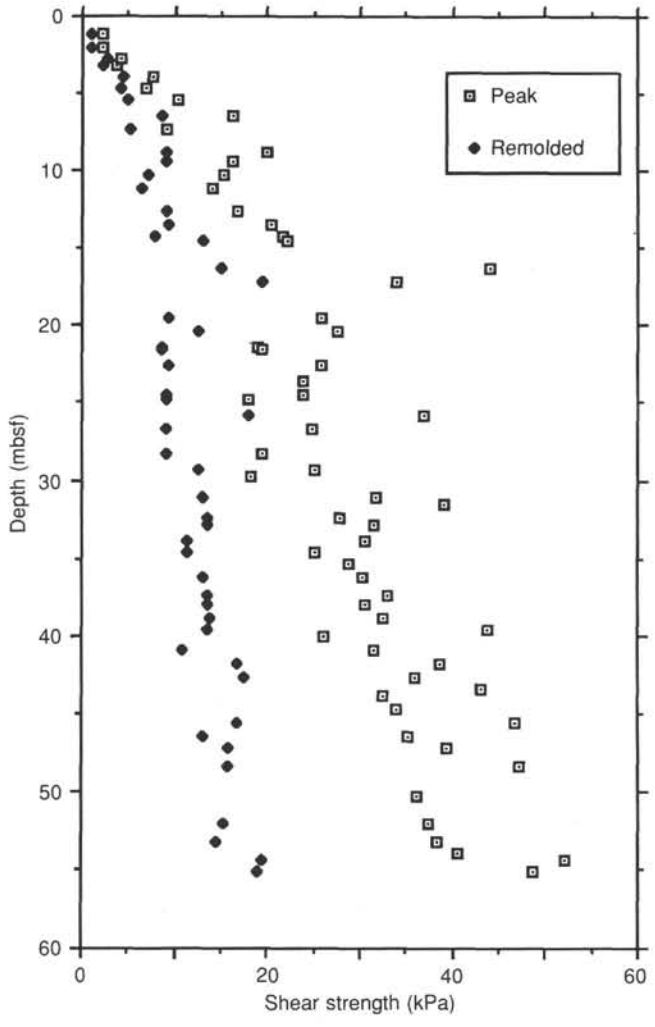


Figure 38. Peak and remolded shear strength vs. depth, Site 769.

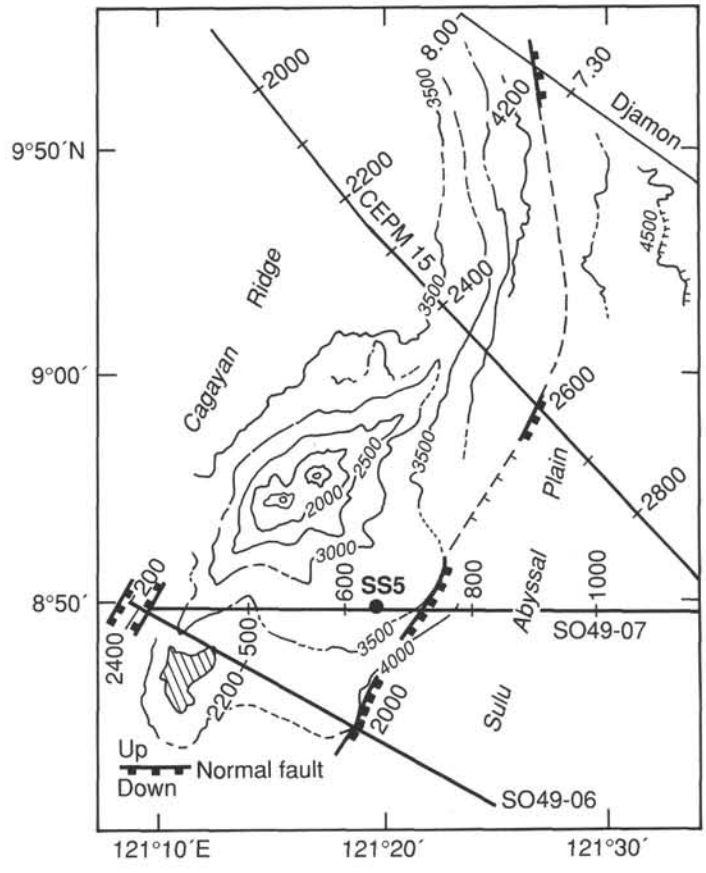


Figure 39. Location of multichannel seismic lines in the drilling area. Proposed Site SS5 is on Line SO49-07. Simplified bathymetric map from unpublished SEABEAM map (PaPaTua Leg 8, SIO, April 1986).

carbonate sediment and hemipelagic clay. Minor thin beds of volcanic ash and turbidites of foraminiferal ooze are also present within the unit. Slump structures appear to increase with depth in the section. The Pliocene/Pleistocene boundary was determined near 93 mbsf, which corresponds to the top of the Olduvai paleomagnetic event. Below this interval carbonate concentration is greatly reduced, with the replacement of marls by noncalcareous clay. The increase in carbonate content at the end of the Pliocene indicates a rapid drop of the CCD at that time.

Unit II (102.1–278.5 mbsf) is late early Miocene to late Pliocene in age and composed mainly of clays, interpreted to be hemipelagic in origin. Two subunits were distinguished on the basis of a color change from grayish green to brown. Subunit IIA (102.1–262.3 mbsf), late middle Miocene to late Pliocene in age, is composed mainly of clay, with thin turbidite interlayers consisting of minor marl, calcareous clay, and silty clays. Thin ash layers are present. The lower contact is gradational to Subunit IIB (262.3–278.5 mbsf), which is late early Miocene to early middle Miocene in age, and consists of grayish brown to brown massive clay, with very rare silty layers. No evidence of bedding is seen except for rare, thin laminae. The brown clay is commonly soft and water rich, with harder angular clasts of brown clay. Subunit IIB is marked by a major contrast in physical properties, with a significant increase in porosity and water content and a decrease in density.

Unit III (278.5–376.9 mbsf) is a massive, unstratified, dark green coarse tuff and lapillistone of andesitic to basaltic composition, with no intermixed or interbedded sedimentary material. Volcanic glass makes up over 70% of the material in the tuff and fine lapillistone. The glass is highly vesicular but rarely pumiceous. The tuff is not dated, but from superposition it is late early Miocene (the same age as the base of Unit IIB) or older.

The paleomagnetics are good from the surface to the Gilbert Epoch and show an excellent and remarkably continuous record from the Gilbert through Chron 11. Very precise correlation can be done between Holes 769A and 769B by means of the susceptibility record, and evidence of block faulting within the site was made with the record of inclination in the cores, in excellent agreement with the seismic record.

The major increase in carbonate content of the cores in Sites 768 and 769 observed near the top of the Pliocene indicates a rapid drop in the CCD. The low carbonate content (representing a high CCD) in the upper Miocene and lower Pliocene may be the result of the closing off of the basin because of collisions. The drop of the CCD seen in the Pliocene-Pleistocene section may indicate variations in the depth of the sills present between Mindoro and North Palawan or along the Sulu Archipelago where a recent volcanic arc has been built. In addition, this corresponds to a global deepening of the CCD recognized in all the major oceans at that time.

The eruption of the tuffs and lapillistones corresponds closely in time with the opening of the Sulu Sea, as shown by the formation of crust at Site 768 in the late early Miocene. The radiolarian assemblage overlying the pyroclastic rocks at Site 768 is

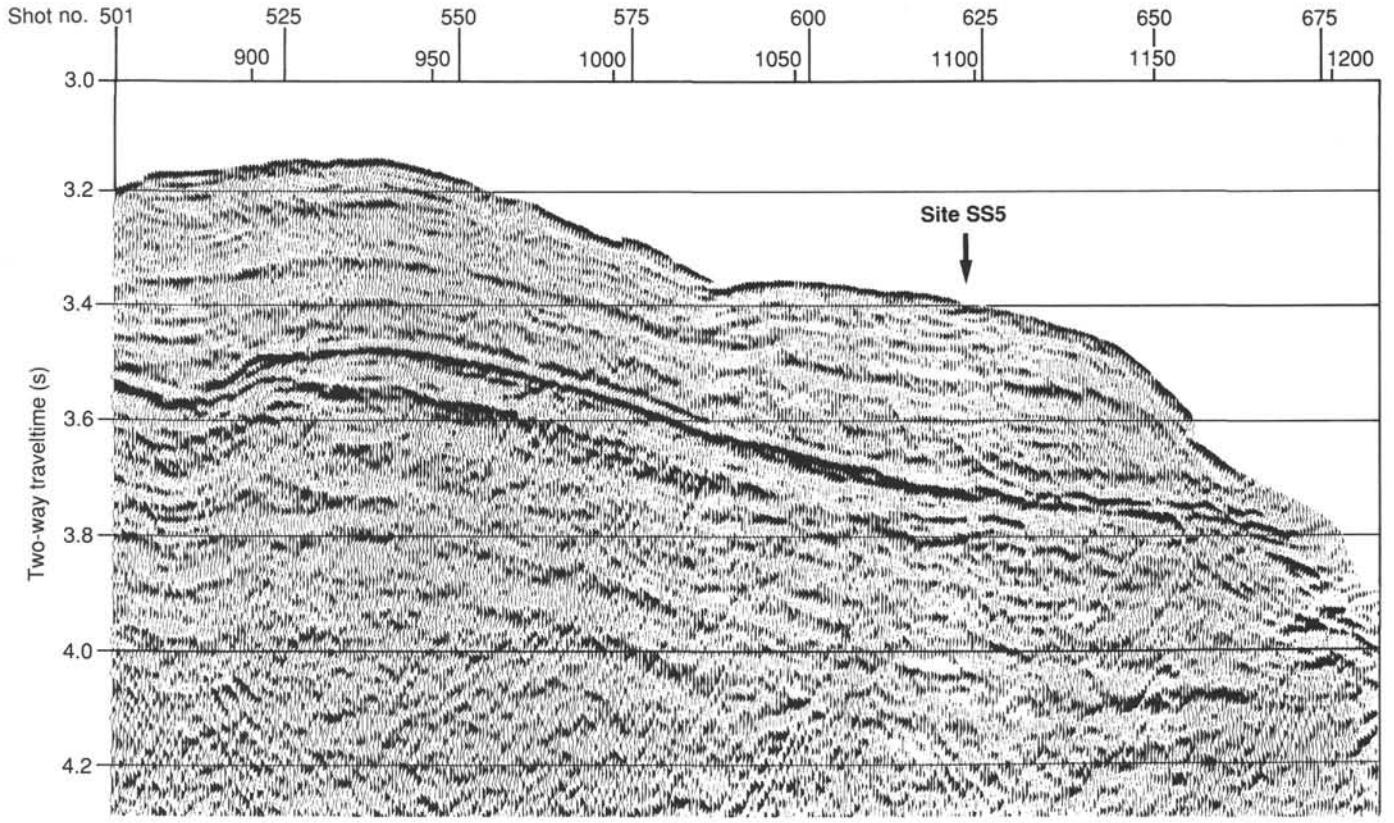


Figure 40. Multichannel seismic profile of Line SO49-07 (depth section, vertical exaggeration = 4) from BGR (unpubl. rept. 104.463, 1988), with position of proposed Site SS5.

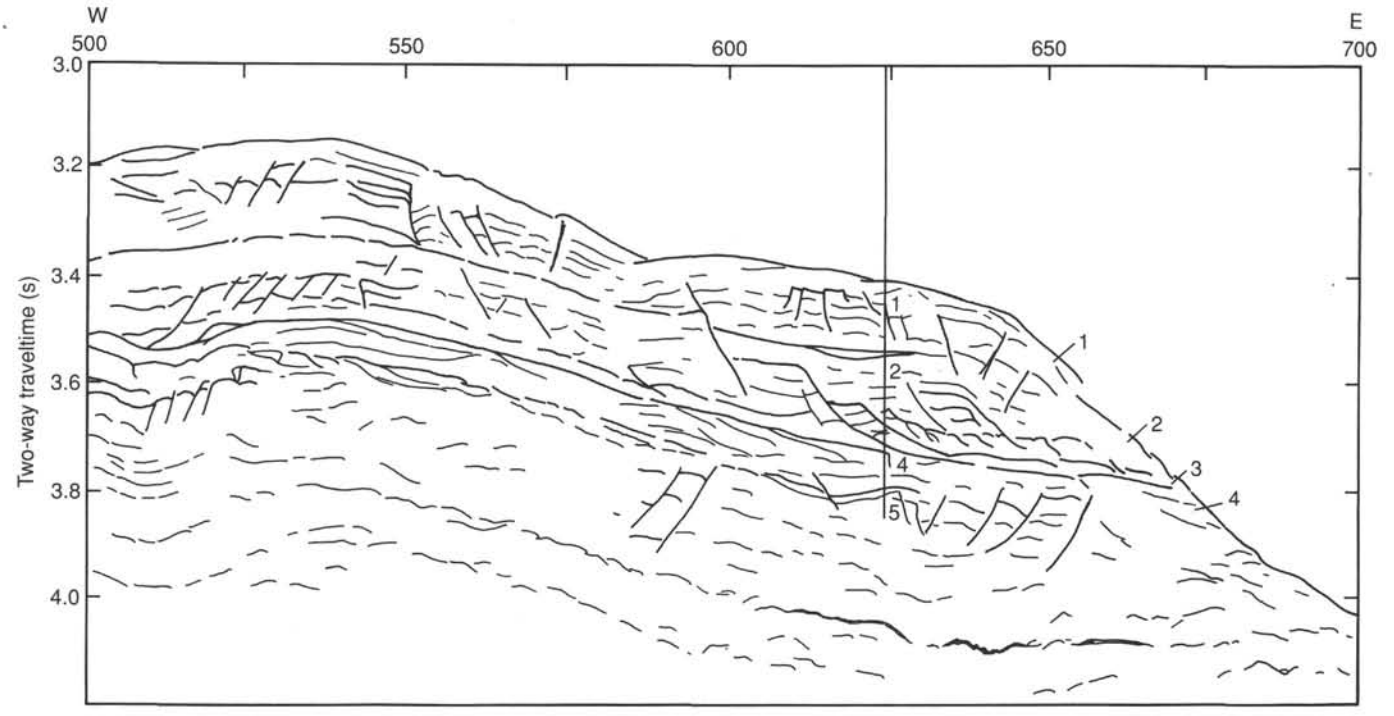


Figure 41. Line drawing of seismic Line SO49-07 (Fig. 40), showing Seismic Sequences 1–5. See text for details.

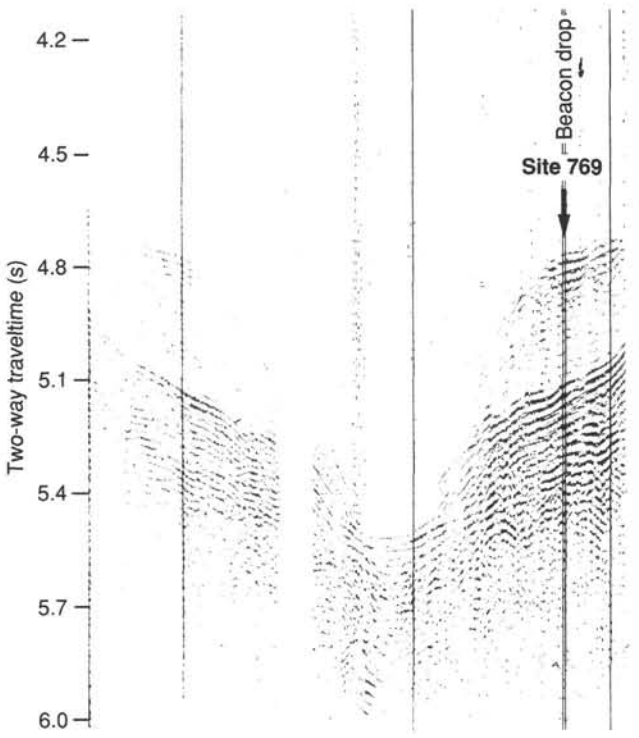


Figure 42. Single-channel seismic profile recorded on board *JOIDES Resolution* during the location of Site 769, which is shown on the profile.

about the same age as that found overlying tuffs at Site 769. However, the gross composition of the volcanic material differs (rhyolitic vs. andesitic), so we are not sure of the parentage of the Site 768 pyroclastic rocks.

The tuffs on the Cagayan may represent the last stage of arc volcanism for the Cagayan Ridge, or they may correspond to a short volcanic event that resulted from passive margin rifting (analogous to that observed on the Vøring Plateau). On the basis of a roughly similar seismic reflection signature and visual descriptions of the drilled material, neither hypothesis can yet be disregarded. Compared with Site 768, the sediments overlying the brown clay are characterized by the lack of turbidites, illustrating that the present elevated position of the Cagayan Ridge was similarly elevated during all of the Neogene.

## REFERENCES


Backman, J., 1979. Pliocene biostratigraphy of DSDP Sites 111 and 116 from the North Atlantic Ocean and the age of the Northern Hemisphere glaciation. *Stockholm Contrib. Geol.*, 32:115–137.

Barron, J. A., 1985a. Late Eocene to Holocene diatom biostratigraphy of the equatorial Pacific Ocean, Deep Sea Drilling Project Leg 85. *In* Mayer, L., Theyer, F., et al., *Init. Repts. DSDP*, 85: Washington (U.S. Govt. Printing Office), 413–456.

_____, 1985b. Miocene to Holocene planktic diatoms. *In* Bolli, H. M., Saunders, J. B., and Perch-Nielsen, K. (Eds.), *Plankton Stratigraphy*: Cambridge (Cambridge Univ. Press), 763–810.

Berger, W. H., Adelseck, C., and Mayer, L., 1976. Distribution of carbonate in surface sediments of the Pacific Ocean. *J. Geophys. Res.*, 81:2617–2627.

Berggren, W. A., Kent, D. V., Flynn, J. J., and Van Couvering, J. A., 1985a. Cenozoic geochronology. *Geol. Soc. Am. Bull.*, 96:1407–1418.

Berggren, W. A., Kent, D. V., and Van Couvering, J. A., 1985b. The Neogene: Part 2, Neogene geochronology and chronostratigraphy. *In* Snelling, N. J. (Ed.), *The Chronology of the Geological Record*. Geol. Soc. Mem. (London), 10:211–260.

Bowler, J. M., Hope, G. S., Jennings, J. N., Singh, G., and Walker, D., 1976. Late Quaternary climates of Australia and New Guinea. *Quat. Res.*, 6:359–399.

Burckle, L. H., 1977. Late Cenozoic planktonic diatom datum levels from the equatorial Pacific. *Quat. Res.*, 7:330–40.

Burckle, L. H., and Trainer, J., 1979. Middle and late Pliocene diatom datum levels from the central Pacific. *Micropaleontology*, 25:281–293.

Eldholm, O., Thiede, J., et al., 1987. *Proc. ODP, Init. Repts.*, 104: College Station, TX (Ocean Drilling Program).

Ewart, A., 1979. A review of the mineralogy and chemistry of Tertiary-Recent dacitic, latitic, rhyolitic and related salic volcanic rocks. *In* Barker, F. (Ed.), *Trondhjemites, Dacites, and Related Rocks*: Amsterdam (Elsevier), 13–121.

_____, 1982. Classification, petrology, and mineralogy of orogenic volcanic rocks. The mineralogy and petrology of Tertiary-Recent volcanic rocks: with special reference to the andesite-basaltic compositional range. *In* Thorpe, R. S. (Ed.), *Andesites: Orogenic Andesites and Related Rocks*: New York (Wiley-Interscience), 25–95.

Exon, N. F., Haake, F.-W., Hartmann, M., Kölger, F.-C., Müller, P. J., and Whiticar, M. J., 1981. Morphology, water characteristics and sedimentation in the silled Sulu Sea, Southeast Asia. *Mar. Geol.*, 39: 165–195.

Fisher, R. V., 1984. Submarine volcaniclastic rocks. *In* Kokelaar, B. P., and Howells, M. F. (Eds.), *Marginal Basin Geology*. Geol. Soc. Spec. Publ. (London), 16:5–27.

Fisher, R. V., and Schmincke, H.-U., 1984. *Pyroclastic Rocks*: Berlin-Heidelberg-New York (Springer-Verlag).

Gartner, S., Jr., 1977. Calcareous nannofossil biostratigraphy and revised zonation of the Pleistocene. *Mar. Micropaleontol.*, 2:1–25.

Gieskes, J. M., and Lawrence, J. R., 1981. Alteration of volcanic matter in deep sea sediments: evidence from the chemical composition of interstitial waters from deep sea drilling cores. *Geochim. Cosmochim. Acta*, 45:1687–1703.

Hamilton, W., 1979. Tectonics of the Indonesian region. *Geol. Surv. Prof. Paper U.S.*, No. 1078.

Harland, W. B., Cox, A. V., Llewellyn, P. G., Pickton, C.A.G., Smith, A. G., and Walters, R., 1982. *A Geologic Time Scale*: Cambridge (Cambridge Univ. Press).

Holloway, N. H., 1981. The North Palawan Block, Philippines: its relation to the Asian Mainland and its role in the evolution of the South China Sea. *Bull. Geol. Soc. Malays.*, 14:19–58.

Jakes, P., and Gill, J., 1970. Rare earth elements and the island-arc tholeiitic series. *Earth Planet. Sci. Lett.*, 9:17–28.

Jakes, P., and White, A.J.R., 1972. Major and trace element abundances in volcanic rocks of orogenic areas. *Geol. Soc. Am. Bull.*, 83:29–40.

Karig, D. E., 1983. Accreted terrains in the northern part of the Philippine Archipelago. *Tectonics*, 2:211–236.

Kastner, M., and Gieskes, J. M., 1976. Interstitial water profiles and sites of diagenetic reactions, Leg 35, DSDP, Bellingshausen Abyssal Plain. *Earth Planet. Sci. Lett.*, 33:11–20.

Kudrass, H. R., Wiedicke, M., Čepek, P., Kreuzer, H., and Müller, P., 1985. Mesozoic and Cainozoic rocks dredged from the South China Sea (Reed Bank area) and Sulu Sea and their significance for plate-tectonic reconstructions. *Mar. Pet. Geol.*, 3:19–30.

Linsley, B. K., Thunell, R. C., Morgan, C., and Williams, D. F., 1985. Oxygen minimum expansion in the Sulu Sea, western equatorial Pacific, during the last glacial low stand of sea level. *Mar. Micropaleontol.*, 9:395–418.

Martini, E., 1971. Standard Tertiary and Quaternary calcareous nannoplankton zonation. *In* Farinacci, A. (Ed.), *Proceedings of the Second International Conference on Planktonic Microfossils, Roma, 1970*: Rome (Tecnoscienza), 739–785.

Martini, E., and Müller, C., 1986. Current Tertiary and Quaternary calcareous nannoplankton stratigraphy and correlation. *Newsl. Stratigr.*, 16:99–112.

Mascle, A., and Biscarrat, P. A., 1978. The Sulu Sea: a marginal basin in Southeast Asia. *In* Watkins, J. S., Montadert, L., and Dickerson, P. W. (Eds.), *Geological and Geophysical Investigations of the Continental Margins*. AAPG Mem., 29:373–381.

Miyashiro, A., 1974. Volcanic rock series in island arcs and active continental margins. *Am. J. Sci.*, 274:321–355.

Quinn, W. H., 1974. Late Quaternary meteorological and oceanographic developments in the equatorial Pacific. *Nature*, 229:330–331.

Riedel, W. R., and Sanfilippo, A., 1978. Stratigraphy and evolution of tropical Cenozoic radiolarians. *Micropaleontology*, 23:81–96.

Rottman, M. L., 1979. Dissolution of planktonic foraminifera and pteropods in the South China Sea sediments. *J. Foram. Res.*, 9:41–49.

Ruddiman, W. F., Kidd, R. B., Thomas, E., et al., 1986. *Init. Repts. DSDP*, 94, Pts. 1 and 2: Washington (U.S. Govt. Printing Office).

Shackleton, N. J., Backman, J., Baldauf, J. G., Desprairies, A., Homrighausen, R., Huddlestun, P., Keene, J. B., Kaltenback, A. J., Krumisek, K.A.O., Morton, A. C., Murray, J. W.., and Westberg-Smith, J., 1984. Oxygen isotope calibration of the onset of ice rafting in DSDP Site 552A: history of glaciation in the North Atlantic region. *Nature*, 307:620–623.

Srivastava, S. P., Arthur, M., et al., 1987. *Proc. ODP, Init. Repts.*, 105: College Station, TX (Ocean Drilling Program).

Valencia, M. J., 1973. Calcium carbonate and gross size analysis of surface sediments, western equatorial Pacific. *Pac. Sci.*, 3:290–303.

Van Riel, P. M., 1943. *The Snellius Expedition 1929–1930: Oceanographic results. Part V, The Bottom Water: Introductory Remarks and Oxygen Content* (Vol. 2): Leiden (Brill), 1–76.

Watts, A., 1975. Gravity field of the northwest Pacific ocean basin and its margin: Philippine Sea. *Geol. Soc. Am., Map and Chart Ser.*, MC-12.

Webster, P. J., and Streten, N. A., 1978. Quaternary ice age climates of tropical Australia: interpretations and reconstructions. *Quat. Res.*, 10279–10309.

Zimmerman, H., Shackleton, N. J., Backman, J., Kent, D. V., Baldauf, J. G., Kaltenback, A. J., and Morton, A. C., 1985. History of Plio-Pleistocene climate in the northeastern Atlantic, Deep Sea Drilling Project Hole 552A. *In* Roberts, D, Schnitker, D., et al., *Init. Repts. DSDP*, 81: Washington (U.S. Govt. Printing Office), 861–875.

**Ms 124A-112**

**NOTE: All core description forms ("barrel sheets") and core photographs have been printed on coated paper and bound as Section 3, near the back of the book, beginning on page 423.**